# Discharge mechanism in $CO_2$

## A study on possible occurrence of secondary discharges caused by field distortion during propagation of streamer or leader

Suhaib Kappadan

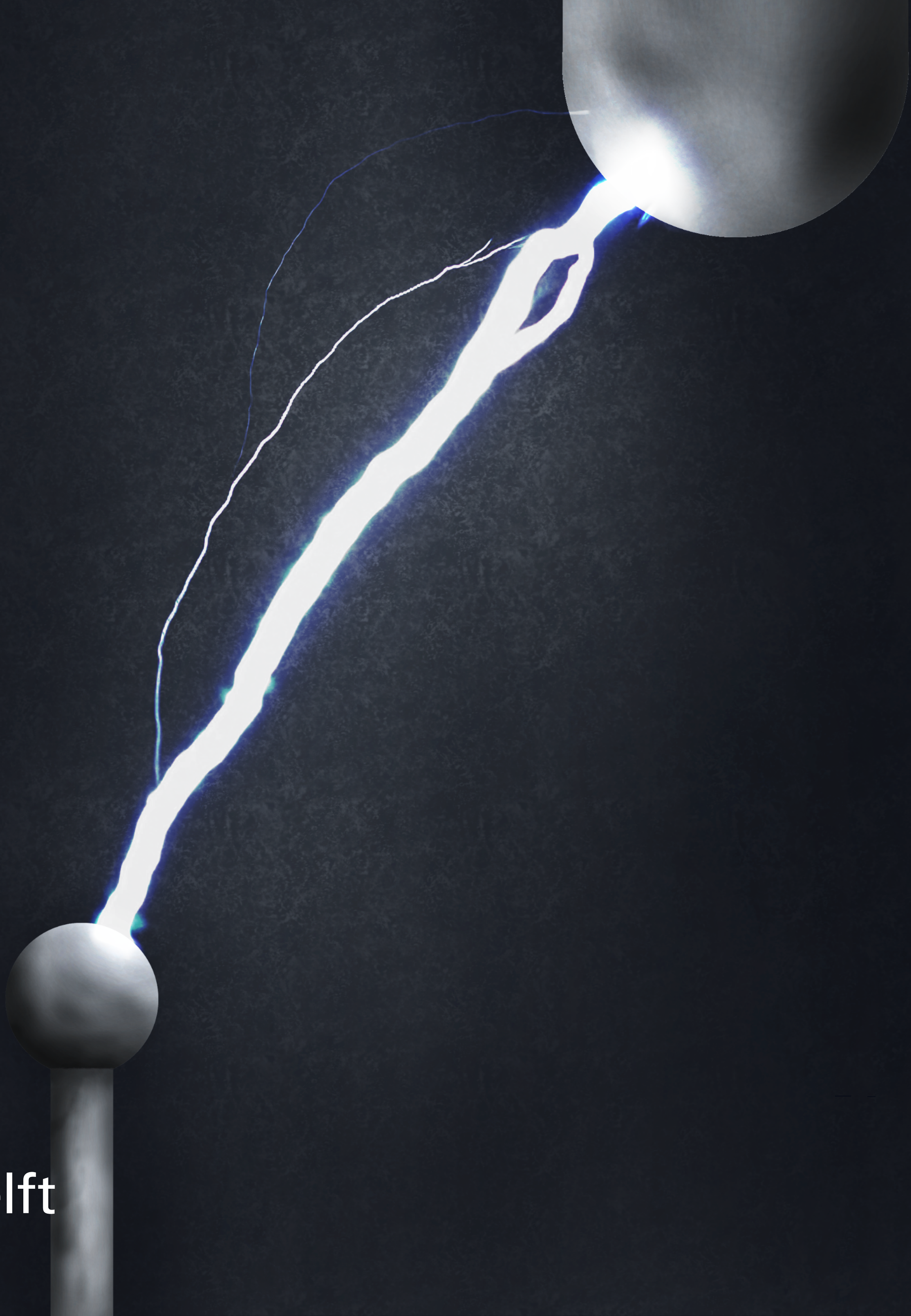

Technische Universiteit Delft

# Discharge mechanisms in CO2

## A study on possible occurrence of secondary discharges caused by field distortion during streamer or leader propagation

by

Suhaib Kappadan

to obtain the degree of Master of Science
at the Delft University of Technology,
to be defended publicly on Friday November 26, 2021 at 01:00 PM.

| | | |
|---|---|---|
| Student number: | 4922069 | |
| Project duration: | December 1, 2020 – June 30, 2021 | |
| Thesis committee: | Prof. Dr. R. Ross, | Professor, TU Delft (DCE&S) |
| | Dr. J. Cremer, | Assistant Professor, TU Delft (IEPG) |
| | Dr. M. Ghaffarian, | Assistant Professor, TU Delft (DCE&S) |
| | Dr. M. Seeger, | Sr. Principal Scientist, Hitachi ABB Power Grids |

*This thesis is confidential and cannot be made public until November 26, 2022.*

# Summary

Since the introduction of $SF_6$ in the 1950s, gas-insulated high voltage circuit breakers and Gas insulated switchgear (GIS) have improved considerably, in particular concerning required drive energy for operation, compactness, and reliability. Nevertheless, high voltage insulation design has become increasingly challenging in recent years. Customer demands for reducing the physical footprint of HV equipment has led to an increase in operational field stress and therefore, much higher pressure on tolerances and an increased susceptibility to defects. Dielectric design is based on how electrostatic fields are distributed and how much stress they can generate. In the course of conducting the intensive theoretical and experimental investigations on the dielectric design of insulation systems applied to high voltage power and pulsed power applications, it is becoming necessary to consider the influence of phenomena that have not been considered before. On top of that, as $SF_6$ is one of the greenhouse gases listed in the *Kyoto Protocol*, $SF_6$ usage regulations have been implemented in many industries. In Europe, $SF_6$ is regulated under the *F-Gas* directive, which bans or restricts its use for several purposes. Several studies have indicated that $CO_2$ is a viable alternative to $SF_6$ for the transmission and distribution of electricity.

In this context, this project aims to investigate a potential new phenomenon, the occurrence of secondary discharges caused by propagating streamer or leader discharges in HV gas insulation. Learning more about such phenomena can help us improve the dielectric design or perhaps explain the occurrence of breakdowns reported in high voltage equipment for which no obvious cause could be found. Specifically, $CO_2/O_2$ mixtures will be studied, and its results compared to $SF_6$. Breakdown in gaseous insulation is caused by propagating discharges which are external in ambient air, e.g. on a bushing, or inside high-pressure insulation, e.g. across the surface of a GIS insulator. During the propagation of such discharges and flashovers (streamer or leader), transient electric field enhancement may occur, leading the local fields to exceed the inception fields at other locations. This can result in *secondary discharges*.

Dielectric experiments using *Image Intensifier* and *Photomultiplier tubes (PMT)* have been conducted at three different pressure ranges; $SF_6$ and $CO_2/O_2$ were selected as the insulation mediums. A *negative* polarity electric field is expected to trigger the secondary discharge. An analysis of images obtained from optical investigations and time lag records obtained from *PMT* signals suggested that secondary discharges can occur at low pressures (0.2MPa) in both $SF_6$ and $CO_2/O_2$. At higher pressures (0.4 to 0.6MPa), no secondary discharges were detected. The reason for this is that, at higher pressures, breakdown field is higher leading to a faster propagation of discharge across that gap. Hence, the formative time lag of the discharge is very short (some $100ns$ or less) and this short time is not sufficient for secondary discharge inception.

# Preface

While pursuing a graduate degree in Electrical Power Engineering at the *Technische Universiteit Delft (TU Delft), The Netherlands*, I completed my master thesis project at the *Hitachi ABB Power Grids Research Center, Baden-Dättwil, Switzerland*. It was a seven-month project starting on *January 1st, 2020*.

*Hitachi ABB Power Grids* is a market leader that provides a variety of equipment for power transmission and distribution. With a long history of inventions along with many patents in this field, the *Research Center* at *Baden-Dättwil* combines continuous product development and order-related engineering research. I learned great deal during my time with *Hitachi ABB Power Grids* and it was an important step towards my professional aspiration as a researcher in my field of study. Therefore, I view myself as a very lucky individual as I was given the opportunity to take part in the ongoing work there. During this time, I also met many wonderful people and professionals who helped guide me.

The deepest sense of gratitude goes out to *Dr. Martin Seeger, Senior Principal Scientist*, for his thoughtful and valuable guidance that has been extremely valuable for my study both theoretically and practically. I have the greatest privilege of working under him, as he is the most senior scientist in the *CB Research group*. Despite the restrictions imposed by the *COVID-19* pandemic, he has taught me more than I could have described in this report in this short period of time. I express my sincere gratitude to *Ing. Daniel Over* for supporting me to prepare all laboratory works and all other support. My sincere thanks also go out to everyone at *CB Research*. They provide me with a friendly work environment and were always supportive when I had questions.

As my direct supervisor at the university, I would like to thank *Assistant Professor Dr. Mohamad Ghaffarian Niasar* for his continuous assistance . I would like to thank *Professor Dr. Rob Ross* and *Assistant Professor Dr. Jochen Cremer* for evaluating my thesis by being the committee members.

Last but not least, I would like to take this opportunity to thank my wife *Hiba*, daughter *Zehn* and my parents for their immense support and motivation throughout this program.

*Suhaib Kappadan*
*Delft, November 2021*

# Contents

# List of Figures

# List of Tables

# 1

# Introduction

Gaseous insulation usually means components other than air and above atmospheric pressure, which are being used in electrical equipment to prevent discharges to occur. The use of gases as an electrical insulator in high-voltage equipment has many advantages over liquid and solid insulation. Insulation gases features relatively low weight, low costs, a simple manufacturing process of equipment, full recovery of insulation performance after partial discharge, and the ability to insulate moving parts. Air is an obvious first choice and is being used for many outdoor installations. However, since space is a major concern and ionization is of air is easier across short distances, there was the necessity to look for non-air gases to serve this purpose.

In 1889, K. Natterer found that gaseous substances such as *Carbon tetrachloride ($CCl_4$)*, *Methyl trichloride ($CHCl_3$)* and *Silicon tetrachloride ($SiCl_4$)* exhibit higher electric strengths compared to that of air or nitrogen ($N_2$)[1]. Later in the early 1930s, M.T Rodine and R.G. Herb[2] intentionally used $CCl_4$ in their *Van de Graaf* generator and proved that the dielectric strength has been significantly improved compared to pressurized air. He also observed that the mixing of air with $CCl_4$ further increased the dielectric performance. Most halocarbons are found to have higher electric field strength than air and nitrogen and in the 1930s, E. E. Charlton and F. S. Cooper[1] proposed *Dichlorodifluoromethane ($CCl_2F_2$)* as a potential insulation gas. $CCl_2F_2$ is also known as the refrigerant *CFC-12*. Later in the 1980s, *CFC-12* was widely banned after introduction of *Montreal Protocol*[1] due to its role in ozone depletion. K. Natterer also observed from his experiments that the dielectric strength of gases containing the *cyano (−CN)* functional group, namely *cyanogen ($C_2N_2$)* are nearly two times that of nitrogen. Despite their toxicity, some of the nitrile gases are still used as insulation gases after being categorized as “acceptable toxicity”[3, 4].

F. S. Cooper from *General Electric* patented $SF_6$ as insulation for higher voltage application in 1937. However, the exceptional arc quenching ability, specific high heat capacity, its dissociation during arcing, and the subsequent recombination of

[1] More information can be accessed on https://treaties.un.org/doc/publication/unts/volume%201522/volume-1522-i-26369-english.pdf

the dissociation products etc. are proved by V. Grosse from AEG in 1938[2][1]. In the 1930s and 1940s, the dielectric properties of various potential insulation gases including $SF_6$ were experimentally determined. Since various independent studies by J Townsend, H. Raether, J. M. Meek, L. B. Loeb etc. gave light to the discharge mechanism in gases and superior dielectric strength of $SF_6$ due to its high electron affinity or attachment[1, 5, 6]. Among all halogenated substances, $SF_6$ turned out to be the best insulation gas in terms of stability, toxicity, and liquefaction temperature, although other gases revealed higher electric strengths. Since the invention of $SF_6$ circuit breakers in the 1950s[7], industrial production of $SF_6$ has grown rapidly. The first $SF_6$ based *gas-insulated switchgear (GIS)* is produced in Europe in the 1960s and since then manufacturers began to replace oil with $SF_6$ because of its superior arc quenching and insulation properties. On the transmission level, *air insulated substations(AIS)* were more and more replaced by *GIS*. Also on the distribution level, *AIS* has been gradually replaced by *GIS*, the latter being more compact, reliable, and safe in operation.

Since the introduction of $SF_6$ in the 1950s, gas-insulated high voltage circuit breakers and *GIS* have improved considerably, in particular concerning required drive energy for operation, compactness and reliability. However, in recent years, high voltage insulation design has become very challenging due to two major reasons. The first major reason is the requirements from the industry to further reduce the size of equipment in order to reduce the physical footprint of the substation. A further size reduction implies increasing operational field stress and, thus, a reduction in built-in safety margins[8]. If the design comes closer to its physical limits, the dielectric coordination of the contact systems in various components becomes more and more challenging. Requirements from industry for higher voltage and current rating along with improved reliability substantiate the difficult design challenge. The first $SF_6$ circuit breaker introduced in 1959 by *Westinghouse Electric Company* was rated for $138kV$ and $41kA$ interruption capacity[9]. Since then *GIS* and gas circuit breaker capacities have continuously evolved. Currently, $SF_6$ circuit breakers up to $1200kV/80kA$ ratings are available in the market.

The second major reason is, after being classified as one of the greenhouse gases in the *Kyoto Protocol*[3], regulative measures for $SF_6$ usage have been implemented in various industries. Since 2006, In Europe, $SF_6$ falls under the F-Gas directive which bans or control its use for several applications. Though the electrical industry as the largest contributor to reported $SF_6$ emissions has been excluded from any $SF_6$ ban so far, intense researches and many initiatives are underway to replace $SF_6$ with alternatives. Though gases such as $CO_2$ and fluorine based gas mixtures are emerging as promising candidates, none of them is expected to reach the qualities of $SF_6$ as an insulation gas, particularly in terms of excellent arc-quenching ability. This means that, when replacing $SF_6$, electrical insulation design will face a new set of challenges[1, 8, 10, 11].

[2]The details can be accessed on https://en.wikipedia.org/wiki/Sulfur_hexafluoride_circuit_breaker

[3]The details can be accessed on http://unfccc.int/resource/docs/convkp/kpeng.pdf

## 1.1. Problem background

A gas-insulated system is designed to withstand all possible operational stresses for a longer period, usually 30 years atleast. As well as being stressed by the nominal voltage (AC or DC), electric insulation systems are also stressed by impulse voltages (switching impulses, lightning impulses, and pulsed voltages) and fast transients. All high voltage insulation designs account for the aforementioned operational stresses by means of an additional safety margin. An intensive testing process according to international standards ensures that the product is designed and manufactured in such a way that it can withstand all possible operational stresses. Due to two major reasons explained in the previous section, the design of gas-insulated systems has become more challenging during recent years.

Dielectric designs are primarily based on the distribution of electrostatic fields and the maximum stress they can generate. As part of the intensive theoretical and experimental investigations of the dielectric design of insulation systems applied to high voltage power and pulsed power applications, it becomes necessary to consider the influence of phenomena not previously considered. Simka et al.[12] investigated the effect of *Overlapping of the breakdown probability distribution* of two contacts (main and arcing contact of CB interrupter) and the frequent occurrence of *Very Fast Transients (VFT)* on dielectric failures in the circuit breaker design context. The field enhancement caused by propagating discharges is another such phenomenon that might be studied in depth.

As as example, **Figure 1.1** shows two high field regions embedded in a parallel plate set up with a background field $E_{bg}$. The *pin* shaped region $(A)$ and the *plug* shaped region $(B)$ in the opposite electrode. $A$ and $B$ are separated by a solid insulator (usually *PTFE*), so there can be no breakdown between $A$ and $B$. In $A$, the local field is higher than local field in $B$, while the applied background $E_{bg}$ is strong enough to cause a breakdown from $A$, but is not yet high enough to cause any inception from $B$. Due to its high concentration of charges, the discharge from $A$ can distort the surrounding field when propagating across the gap. This distortion can cause the field to enhance locally on the surface of $B$. The enhanced field is greater than the local inception field at $B$, so inception might occur at $B$.

Numerous studies have explained the discharge process in electronegative gases, such as $SF_6$[13–18], and some recent investigations have examined how the discharge propagates in $CO_2$[19]. However, there is still a significant absence in the literature in understanding the transient field distortion during propagation of a discharge across a gap (breakdown) between two electrodes in a gas medium. Such field distortion can further enhance the stress in the nearby high field area and trigger a so-called secondary discharge from another area or direction. It could be even dangerous if the first discharge would not bridge the gap but trigger the other discharge which could then bridge the gap. It is also possible that leftover charges can influence insulation. This scenario is not easy to understand and many parameters, such as statistical and formative time lags, play a role.

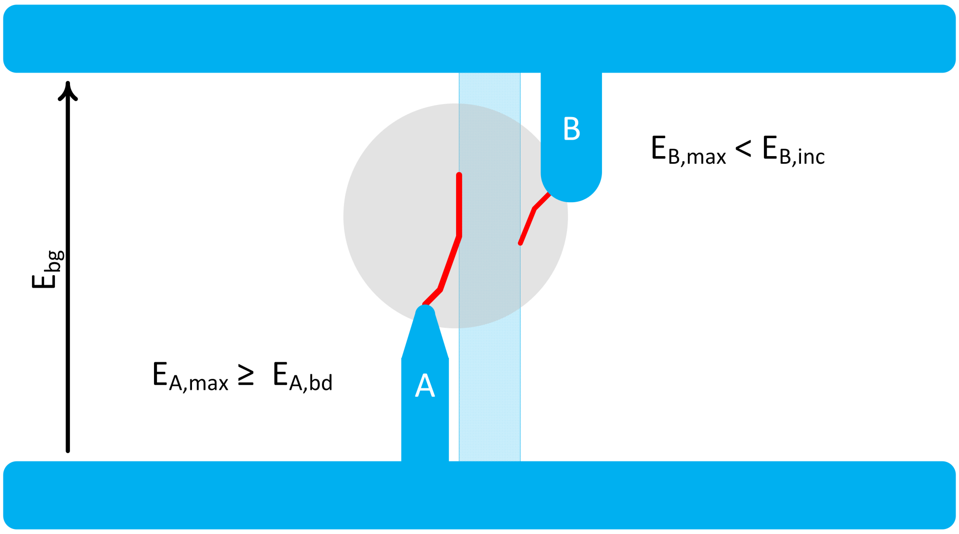


Figure 1.1: Simple illustration explaining secondary discharge caused by field enhancement due to propagating discharge. The red line extending from $A$ is the primary discharge causing the main breakdown. The red line from $B$ is the possible secondary discharge inception caused by local field enhancement at $B$. In order to prevent breakdown in between, a PTFE separation is provided between $A$ and $B$.

## 1.2. Objective of the thesis

This project aims to investigate the possible occurrence of secondary discharges triggered by propagating *streamer* or *leader* discharges in HV gas insulations. Specifically, $CO_2$ will be studied, and its results compared to $SF_6$. Gaseous insulation is used in many applications in high voltage equipment, e.g. Gas Insulated switchgear (GIS) or HV Circuit breakers (HVCB). Breakdown in gaseous insulation results from propagating discharges, which can be external in ambient air on a bushing for example, or also inside of the high-pressure insulation, e.g. at a GIS insulator. During the propagation of such discharges and flashovers (*streamer* or *leader*), transient electric field enhancement may occur, leading the local fields to exceed the inception fields at other locations. This can result in *"secondary discharges"*.

This project shall investigate the conditions under which such secondary discharges occur including the pressure, the gaseous medium etc. Due to $SF_6$'s strong greenhouse gas properties, the search for alternatives has greatly intensified in recent years. $CO_2$ shows promise in replacing $SF_6$ in HV switchgear. In insulation applications, $CO_2$ is not used in its pure form. It is always mixed with other gases, mainly $O_2$. Consequently, this thesis examines discharge in both $SF_6$ and $CO_2/O_2$ and compares the differences within the above-mentioned framework. The breakdown process in $CO_2$ (or $CO_2/O_2$) is an area where little is known.

This project aims to deliver the following;-

- Optically investigate possible impact of propagating discharges in $CO_2$ on the inception from other areas.

- Compare the results with similar experiments in $SF_6$.
- Discuss the findings by extrapolating them to other operating conditions.

The main research questions are the following;-

1. When $CO_2$ is used as an insulation medium, can a transient field enhancement caused by propagating streamers or leaders initiate secondary discharges?
2. Can a transient field enhancement caused by propagating streamers or leaders result in secondary discharge inception when $SF_6$ is used as an insulation medium?
3. For different pressures, how does the phenomenon behave differently?

## 1.3. Structure of the report

This report is structured as follows. this first chapter introduces the reader to the evolution of gaseous insulation from the 1800s to the present day, which is $SF_6$. Throughout the chapter, the problem that is addressed in this project is introduced and its goal is described clearly. The literature review is the focus of **Chapter 2**. To conduct this research review, previously published papers on discharge in $CO_2$ are presented.

**Chapter 3** provides a comprehensive treatment of the principles involved in the physics of a discharge mechanism. $SF_6$ and $CO_2$ are also outlined as insulation gases with their special features. This project's methodology is fully explained in **Chapter 4**. In a separate section, the setup, procedures, and statistical analysis of experimental data are explained in detail.

Each of the results gathered from the field calculation, the analytical calculation, the breakdown experiments, the inception measurements, and the optical diagnostics in **Chapter 5** are presented in its own section. **Chapter 6** is for discussion of results. This chapter discusses the results obtained and uses the results of the experiment to extrapolate further. The thesis ends by concluding the findings in **Chapter 7**.

# 2 Literature review

The use of gases as insulation mediums in high voltage applications is widespread, including transformers, gas insulated switchgears, and gas circuit breakers. A number of literary works have been published that explain the breakdown mechanism of $SF_6$ gas under varying conditions ever since it was used as insulation gas in the $1950$s. Thanks to its excellent insulation capacity and arc quenching ability. The performance of $SF_6$ as an insulation medium in gas-insulated high voltage circuit breakers and GIS has improved considerably in recent years, especially in terms of power requirement, compactness, and reliability.

As early as the late $1970$s, researchers began looking for alternatives to $SF_6$. These studies were motivated by the desire to find a gas or gas mixture that has a low production cost, a low boiling point, and a dielectric strength that is higher and less sensitive to surface roughness and particles[9]. After understanding the global warming potential (GWP) of $SF_6$, research in this area has been intensified in the past two decades. $SF_6$ is an extremely potent greenhouse gas, and it is estimated to have a global GWP of approximately $23500$ times greater than $CO_2$ over a $100$-year horizon[20]. $SF_6$ also has a number of unfavourable properties, such as forming harmful by-products after electric discharges and being highly prone to condensation on the insulator surface[21].

The investigation of gases encompasses three categories. In the first category are natural single gases like $CO_2$, $N_2$ and dry air; the later two having been successfully used for medium voltage switches. GCBs up to $145kV$ have been manufactured using $CO_2$. However, there is no known gas whose performance is comparable to $SF_6$ across the whole range of required properties. The second category is $SF_6$ based gas mixtures. Research has shown that $SF_6$ mixed with $N_2$ or $CF_4$ can reduce the amount of $SF_6$ used in GIL's or GCBs, or prevent the liquefaction of the insulating or arc-quenching medium in cold areas. The issue of $SF_6$-related global warming can, however, not be resolved fully with these measures[10]. Recent attention has been drawn to one of the third categories; organic macro-molecular gases that exhibit significantly higher insulation strength than $SF_6$. Some of the possible alternative gas mixtures include fluorinated gases (e.g. $CF_3I$, c-$C_4F_8$), perfluoroketones (PFK) and perfluoronitriles (PFN)[10, 11]. As base gases $CO_2/O_2$ or $N_2/O_2$ mixtures are usually

| Chemical name | Pure gas | GWP | ODP |
|---|---|---|---|
| Sulfur hexafluride | $SF_6$ | 23500 | 0 |
| Carbon dioxide | $CO_2$ | 1 | 0 |
| Trifluoroiodomethane | $CF_3I$ | 0.4 | Very low |
| Hexafluoroethane | $C_2F_6$ | 11100 | 0 |
| Octafluoropropane | $C_3F_8$ | 8900 | 0 |
| Octafluorocyclobutane | c-$C_4F_8$ | 9540 | 0 |
| C4 fluoronitrile | $C_4F_7N$ | 2100 | 0 |
| C5 fluoroketone | $C_5F_10_O$ | < 1 | 0 |
| C6 fluoroketone | $C_6F_12_O$ | < 1 | 0 |
| Hydrofluoroolefin | $C_3H_2F_4$ | < 1 | 0 |
| Hydrochlorofluoroolefin | $C_3H_2ClF_3$ | 1 | Very low |

Table 2.1: Chemical names and environmental properties of potential alternative gases[11].

employed.

A comprehensive investigation of the $SF_6$ alternatives has been conducted by the IEEE Alternative Gas Task Force. **Table 2.1** lists candidate gases that scored well on features such as low GWP, low toxicity levels, and low ozone depletion potential (ODP) as well as compliance with technical requirements[11].

A number of studies have suggested that $CO_2$ is a viable replacement for $SF_6$ in the transmission and distribution of electricity[8, 22]. Typically, these applications will be between $0.1MPa$ and $1MPa$[19]. Insulating and interrupting characteristics of $CO_2$ are satisfactory, as it recomposes after arcing to its original state. One of the first high-voltage circuit breakers using $CO_2$ has recently been introduced to the market by major OEM's such as ABB, Hiatchi ABB Power Grids and GE grid. New eco-friendly gas mixed-gas switchgear (GIS) prototypes from *Hitachi ABB Power Grids* and *GE grid* are using a $CO_2$ based gas mixture for the replacement of $SF_6$. GE grid (former Alstom) and Hitachi ABB Power Grids (former ABB High Voltage Products division)focus on a gas mixture of *Fluoronitrile ($C_4F_7N$)* and $CO_2$/$O_2$ as an arc-quenching medium. ABB uses mixture of *Fluoroketone ($C_5F_{10}O$)* and air (known as *AirPlus*) as insulation medium for their medium voltage (MV) switchgears.

There has been a great deal of research done on $SF_6$ and we know a lot about its breakdown mechanism, but there has been little study on the details of electrical breakdown in $CO_2$ so far. Being decisive criteria for the breakdown in gases, knowledge about the critical field, streamer inception, streamer stability field, streamer propagation, streamer-to-leader transition, statistical time lag, formative time lag etc. (details of the theory of gas discharges are given in **Chapter 3** are essential for its application in the field[19]).

This literature review highlights relevant researches on $CO_2$ that helps us understand the breakdown process in it. All of these pieces of information will be useful for the project presented in this thesis.

# 2.1. $CO_2$ as insulation gas

An early investigation of $CO_2$ breakdown was performed in 1950 by Young [24]. He studied $CO_2$ breakdown at low pressures into liquid form. For low pressures, $Paschen$'s similarity law was verified, but there was a deviation for high pressures and short gap distances. Using pre-breakdown current measurements, Young determined $Townsend$'s first coefficient in $CO_2$ and field emission constants. A study by Brand and Kopainsky [25] examined the breakdown field strength of unitary attaching gases and mixtures with non-attaching gases. $CO_2$ was one of the attaching gases they studied. Within admissible error, they created a breakdown model that accurately predicted the critical field strength of gases and gas mixtures. The experimental critical field used by Brand and Kopainsky [25] was $15kV$ at $p = 0.66atm$ ($1atm = 0.1MPa$) and $pd = 4.6atm.mm$ [30], which results in $E = 21.5kV/cm.bar$ for pressure reduced conditions.

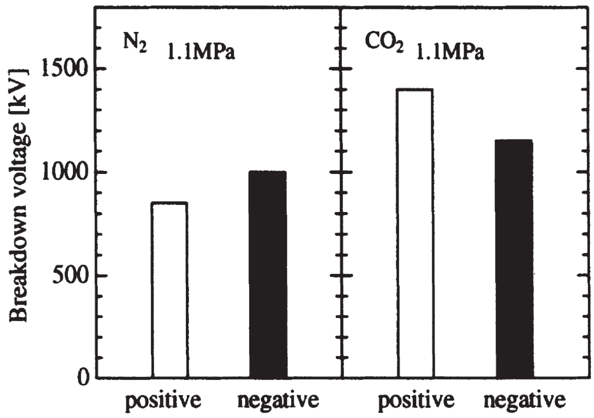


Figure 2.1: Comparison of breakdown level of $CO_2$ and $N_2$ as presented in [23].

Shiiki et al. [23] investigated dielectric performance of $CO_2$ and compared with that of $N_2$. At a pressure of $1.1MPa$, they tested both gases with a lightning impulse voltage on a cylindrical coaxial setup with inner and outer radii of $6cm$ and $15cm$, respectively. Based on the results of their experiment, presented in **Figure 2.1**, he called for further investigation to understand the effect of the polarity difference between the two gases. $CO_2$'s negative polarity outperformed $N_2$'s positive polarity by $35\%$, which was the polarity with the lowest breakdown voltage, respectively. Shiiki et al. [23]'s breakdown voltages for $CO_2$ reached $70\%$ of those for $SF_6$ at $0.5MPa$ pressure.

A study by Uchii et al. [26] investigated the arc-quenching behaviour of $CO_2$ used as the insulation and interruption medium in a gas circuit breaker for a rating of $72.5kV$ and $31.5kA$. A circuit breaker with an operating pressure of $0.8MPa$ was designed on the basis of that fundamental research. The circuit breaker performed satisfactorily in all tests conducted by them. The life cycle analysis of the $CO_2$ circuit breaker showed that it would have a global warming impact which was reduced by $45\%$ when compared to the latest $SF_6$ breakers. Kynast and Juhre [27] assessed the performance of $CO_2$, $N_2$, and an $80/20$ mixture of $N_2$ and $CO_2$ in GIS applications. The GIS system allowed them to test gas from $0.6MPa$ to $1.8MPa$ with coaxial cylindrical electrodes. According to **Figure 2.2**, the $CO_2$ and the mixture outperformed pure $N_2$ in terms of withstanding electric field strengths. However, neither could provide comparable performance to $SF_6$ at $0.4MPa$, the typical pressure in a $SF_6$ GIS system..

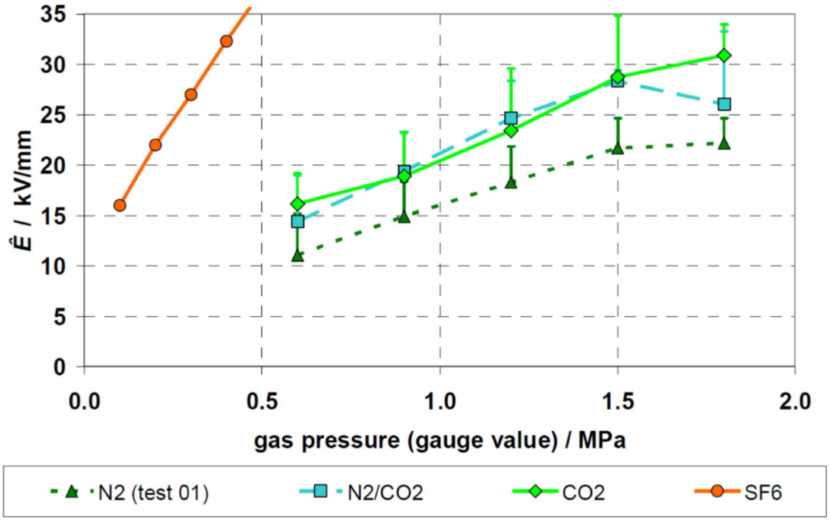


Figure 2.2: Comparison of breakdown level of $CO_2$,$N_2$, $N_2/CO_2$ and $SF_6$ as presented in[27] for lightning impulse voltage applied.

| Gas | Calculated breakdown value (kV/cm.bar) | Experimental value (kV/cm.bar) |
|---|---|---|
| $N_2$ | 32.9 | 20±0.3 |
| $CO_2$ | 30.1 | 22±0.1 |
| $SF_6$ | 89.0 | 79±0.5 |

Table 2.2: Comparison of experimentally obtained breakdown values of $SF_6$, $CO_2$ and $N_2$ and their calculated breakdown values[28].

Meijer et al. [28] compared the breakdown strength of $CO_2$, $N_2$ and $SF_6$. Their experiments were conducted with two smooth Rogowski electrodes at gas pressures of $7$, $9$ and $11 bar$ absolute. The setup was tested for AC, lightning impulse, and switching impulse voltages. **Table 2.2** shows their average breakdown values. It was found that $CO_2$ had the better insulation properties due to the small amount of scattering, even though $N_2$ and $CO_2$ had similar results. In addition, they concluded that the pressure reduced electric field strength was nearly constant, indicating an almost linear increase in break-down strength with increased pressure in that pressure range.

Liu et al. [29] examined the characteristics of the field-time breakdown of air, $N_2$, $CO_2$, and $SF_6$ using simulation models based on kinetic and fluid drift-diffusion. Their kinetic approach relies on the avalanche-to-streamer threshold criterion ([6]). For the fluid drift-diffusion model, self-consistent numerical solutions for the continuity equations of charged species and the Poisson equation for the electric field, are used. The time to breakdown as a function of the applied field was obtained for all investigated gases. This study relied on the fact that statistical time lag is stochastic, making it difficult to model and hence, the breakdown time was only based on formative time. They presented time to breakdown as a function of $E/N$[1]. Photoionization and background radiation are also not included in the model.

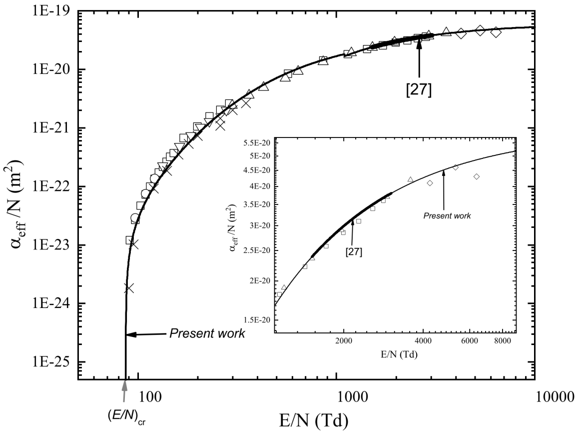


(a) Plot of $(\alpha_{eff}/N)$ as a function of $(E/N)$; dots represents experimental data from previous works. The Fitting curves obtained for $CO_2$ from [29] are also shown

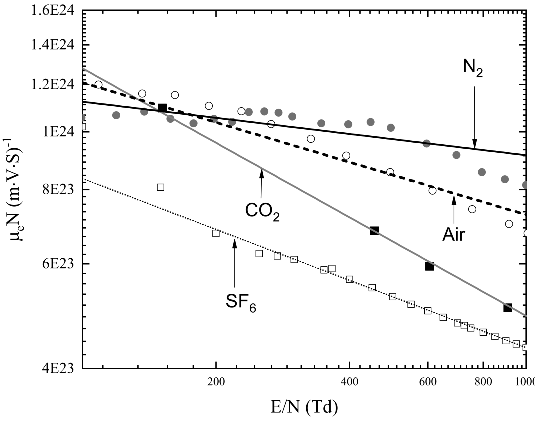


(b) Plot of $(\mu_e.N)$ as a function of $(E/N)$; dots represents experimental data from previous works. The Fitting curves obtained from [29] are also shown.

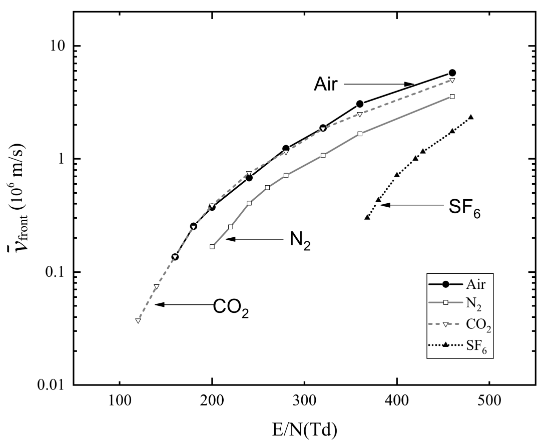


(c) Nominal average velocity of the ionization front, $\bar{v}_{front}$, as a function of $(E/N)$[29].

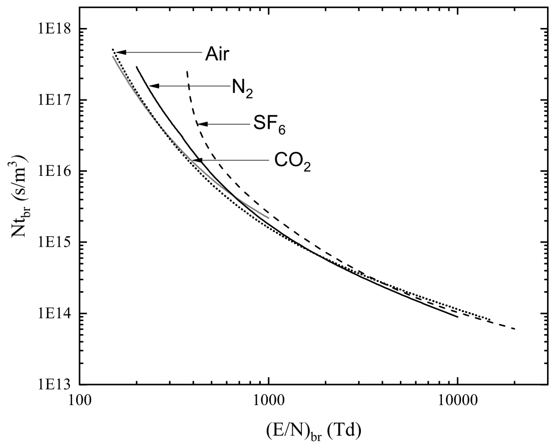


(d) $(Nt_{br})$ as function of $(E/N)_br$. Related experiment results are seperately shown in [29]

Figure 2.3: Field time characteristics comparison of $SF_6$, $CO_2$, $N_2$ and dry air[29].

Liu et al. [29] determined three key parameters; elective ionization ($\alpha_{eff}$), electron mobility($\mu_e$), and ionization front velocity($\bar{v}_{front}$), which are finally used to determine time to breakdown for a particular applied field. Definitions of $\alpha_{eff}$ and $\mu_e$ will be explained in detail in **Chapter 3**. Ionization front propagation velocity($\bar{v}_{front}$), is defined

[1] $E/N$ is the reduced electric field, where $E$ is the electric field and $N$ is the concentration of neutral particles. Its unit is $Townsend$ (symbol $Td$). The mean energy of electrons (and therefore many other properties of discharge) is typically a function of $E/N$ in gas discharge physics, where it is used as a scaling parameter. In ideal gases, the concentration $N$, which is simply related to pressure and temperature, determines the mean free path and collision frequency. Electric fields govern the amount of energy gained by successive collisions. In effect, the reduced electric field is a scaling factor so, for example, increasing the electric field intensity by some factor $q$ would be equivalent to reducing gas density by some factor $q$.

as the inter electrode gap divided by time to breakdown ($t_{br}$), which is the time necessary for the ionization front to form and cross the gap. In **Figure 2.3c**, $\bar{v}_{front}$ for $CO_2$ is similar to that for air for all values of $E/N$. In comparison with the average velocities obtained for other investigated gases at $360Td$, $SF_6$ has the lowest nominal average velocity, $0.3 \times 10^6 m/s$.

Ionization frequency ($v$) is = $\alpha_{eff}$*$v_{drift}$ where $v_{drift}$ is electron drift velocity. Also. $v_{drift}$ = $\mu_e$.E (product of electron mobility and the electric field). Thus, the relationship between time to breakdown, $t_{br}$, and reduced breakdown field, $E/N$, can be established as **Equation 2.1**

$$t_b r.N = \frac{18}{[\alpha_{eff}.\mu_e](E/N)} \tag{2.1}$$

where both, $\alpha_{eff}$ and $\mu_e$, are functions of $E/N$ as already obtained from fluid diffusion model(**Figure 2.3a** and **2.3b**). This kinetic relationship is used to obtain field-time breakdown characteristics for gases.

For all investigated gases, **Figure 2.3d** shows the reduced breakdown field values at different values of $N.t_{br}$. At longer breakdown times (i.e. higher values of $N.t_{br}$ at constant pressure), $SF_6$ exhibits a higher breakdown field than the other gases. The breakdown fields of all gases are similar at lower values of $N.t_{br}$. This model presented by Liu et al. [29] is helpful in further investigation of the transient breakdown processes in gases.

## 2.2. Discharge process in $CO_2$

Thanks to its lower environmental impact, reasonable dielectric strength and ability to quench an arc, $CO_2$ offers great potential for replacing $SF_6$ in high-voltage transmission and distribution networks. Seeger et al. [19] is providing more information about how the critical field, streamer inception, streamer stability field, streamer propagation, streamer-to-leader transition, statistical time lag, formative time lag in $CO_2$ gases play crucial roles in determining the breakdown process. Seeger et al. [19] investigated the streamer inception and propagation at ambient temperature in various pressure range of $CO_2$, for both polarities using stepped DC voltage. Experimental setups consisted of two types. Setup-1; a small protrusion in a uniform background and setup-2; a point-to-plane field. The pressure range used for experiments in setup-1 was $0.1 - 0.5MPa$ with two different gap distances; $30mm$ and $60mm$. The pressure range used for experiments in setup-2 was $0.1 - 0.5MPa$ with gap distances $40mm$ and $60mm$. Together, both experiments allow the comparison of streamer properties in uniform and non-uniform background fields. They used a photomultiplier (PMT) and an image intensified camera to investigate the discharge events optically. For both polarities, streamer stability fields, streamer radii, and streamer velocities are deduced.

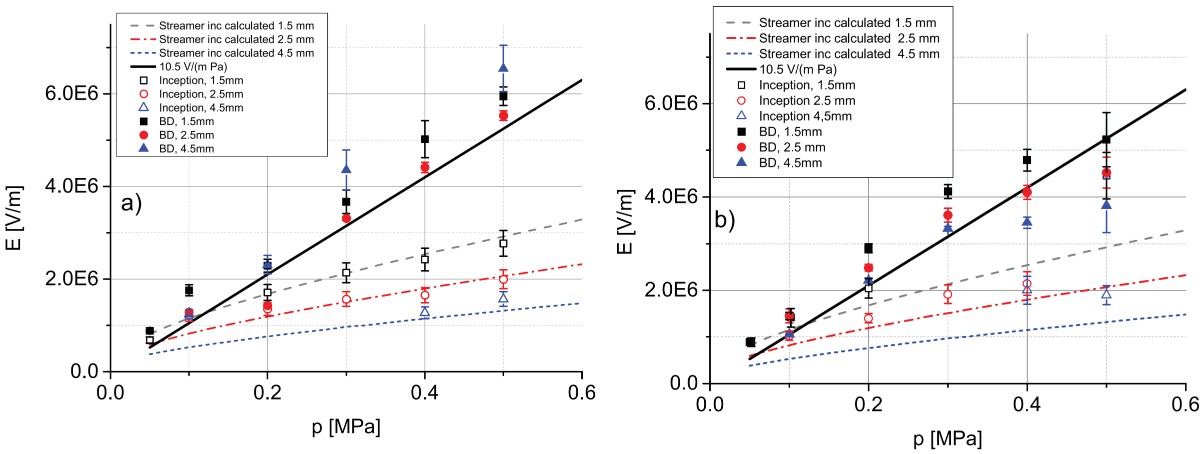


(a) for negative polarity (b) for positive polarity

Figure 2.4: Average inception and breakdown (BD) fields at (a) negative and (b) positive polarity in setup 1 (pin in a uniform field). The error bars represent the $1\sigma$ standard deviation of the experimental values. The calculated streamer inception fields (thin curves) also shown. A thick line with a pressure-reduced field of $10.5V/(m.Pa)$ is shown which corresponds to experimentally obtained breakdown field. Pictures are taken from [19].

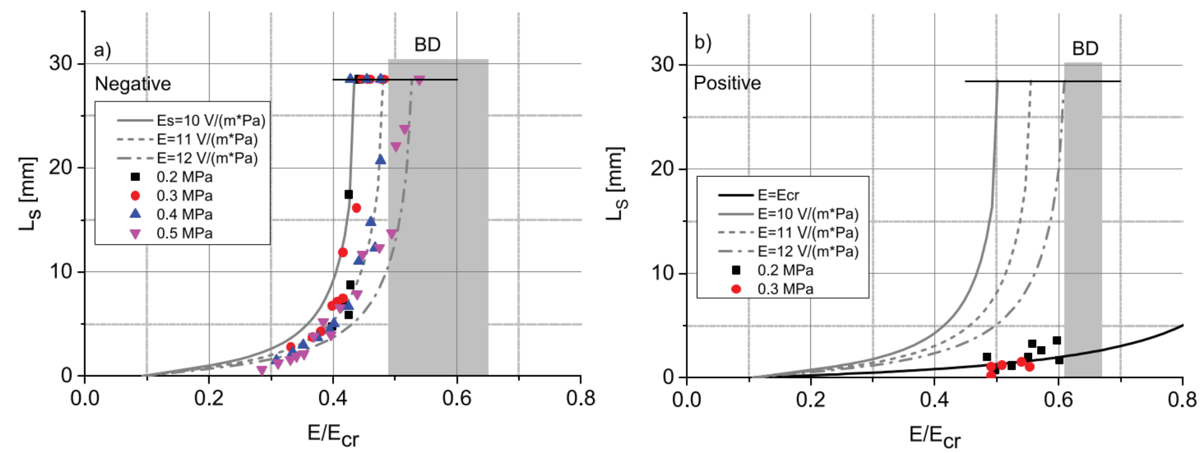


(a) for negative polarity (b) for positive polarity

Figure 2.5: Streamer lengths versus reduced background field $E/E_{cr}$ with 1.5mm needle at (a) negative and (b) positive polarities. Each symbol represents an individual voltage application. The critical field was $E_{cr}$=$E_{cr,0}$·p and $E_{cr,0}$=$21.5V/(m \cdot Pa)$. In the horizontal lines are the propagation lengths for gap crossing, corresponding to the gap length $D$ minus the needle length $Lp$. The picture is taken from [19].

As shown in the **Figure 2.4b**, because of the larger scatter at higher pressures, inception fields at positive polarity are higher than the streamer inception predictions. And needless to say, breakdown fields are gradually reduced for larger pins. Seeger et al. [19] also observed that for negative polarity, **Figure 2.5a**, the streamer stability field was roughly half the critical field (i.e. $10 - 12V/m.Pa$), while for the positive polarity, the streamer stability field coincided with a value around the critical field (i.e. $21.5V/m.Pa$) at pressure ranges above $2bar$. For negative polarity, the increased length of the discharges can be described by pressure reduced streamer stability fields(**Figure 2.5**). According to the **Figure 2.5a**, streamers cross gaps close to breakdown, so the breakdown field is approximately equal to the streamer crossing field. When the positive polarity is present, only short discharges can be seen in **Figure 2.5b**. The discharges are aligned with a streamer stability field close to the critical field. This clearly shows a difference in discharge behaviours for two different polarities[19].

Seeger et al. [19] used setup-2 (small sphere in the non-uniform field) to understand the behaviours in the non-uniform background field. The measured and calculated streamer inception fields show good agreement (**Figure2.6**). Because of the larger critical volumes, statistical time lags were shorter, allowing for more precise measurement of inception fields than setup 1. At negative polarity, breakdown fields increase linearly with pressure in a similar manner to setup 1, i.e., non-uniformity of the background field does not seem to be important, and only pressure and gap distance are decisive for the breakdown voltage. The results show that streamer propagation at a constant pressure-reduced streamer stability field is decisive for breakdown at negative polarity in the investigated pressure range up to $0.5 MPa$. The breakdown at positive polarity is on the same line as the pressure reduced field of $10.5 V/(m \cdot Pa)$ at pressures up to $0.1 MPa$. At pressures above $0.1 MPa$, the breakdown fields saturate and in the camera images, leaders are detected[19].

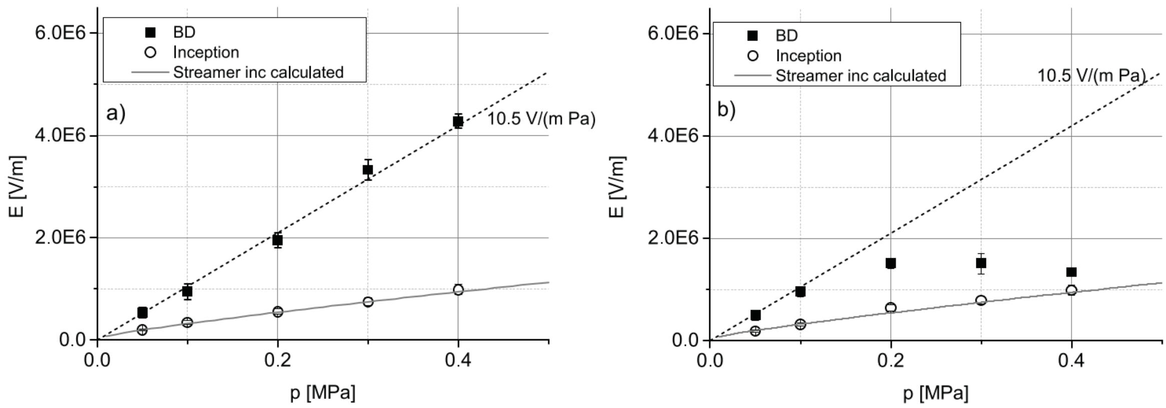


(a) negative (b) positive

Figure 2.6: The average inception and breakdown fields in set-up 2 (sphere in the non-uniform field) (a) with a negative polarity and (b) with a positive polarity. The error bars represent the 1σ standard deviation of the experimental values. Calculated average streamer inception fields are shown for comparison (solid curves). This dashed line with a pressure-reduced field of $10.5 V/(m.Pa)$ is provided for reference to aid understanding.[19].

In the same publication, Seeger et al. [19] reported that streamer stability is independent on the field homogeneity and it mainly depends on pressure, and polarity. They observed that, for the uniform and non-uniform field (setup-1&2), the measured negative streamer pressure-reduced stability field of about $11 \pm 2V/(m \cdot Pa)$ which is close to the value reported for negative streamers in air and remains constant in the whole range of pressures. Furthermore, the streamer stability field at positive polarity increases with the square-root of pressure and reach at about $0.2 MPa$ the pressure-reduced critical field. This behaviors is opposite to air (see **Figure 2.7**), and the values for positive streamers are remarkably higher than in air. Above $0.2 MPa$, the positive streamer stability field approaches the critical field, which was expected only for strongly electronegative gases like $SF_6$, due to the efficient electron attachment.

From the experimental results, they could also determine the streamer radius and streamer velocity. It is expected that the streamer radius scales inversely with the pressure and hence a proportionality constant exist ($C_s$) such that, $C_s$ = p ×$R_s$ [16]. $R_s$ is the radius of the streamer and $C_s$ is found out from experiments after a thorough inspection of the image intensified pictures and measurements. The measured values roughly agree with the scaling using average values $C_s$ = $13.4 \pm 3$ and $25 \pm 3 m.Pa$ for positive and negative respectively. Moreover, their experiment results showed that streamer velocities increased monotonically with background fields in both setups, and ranged between $1 \times 10^5$ to $0.6 \times 10^5$ m/s.

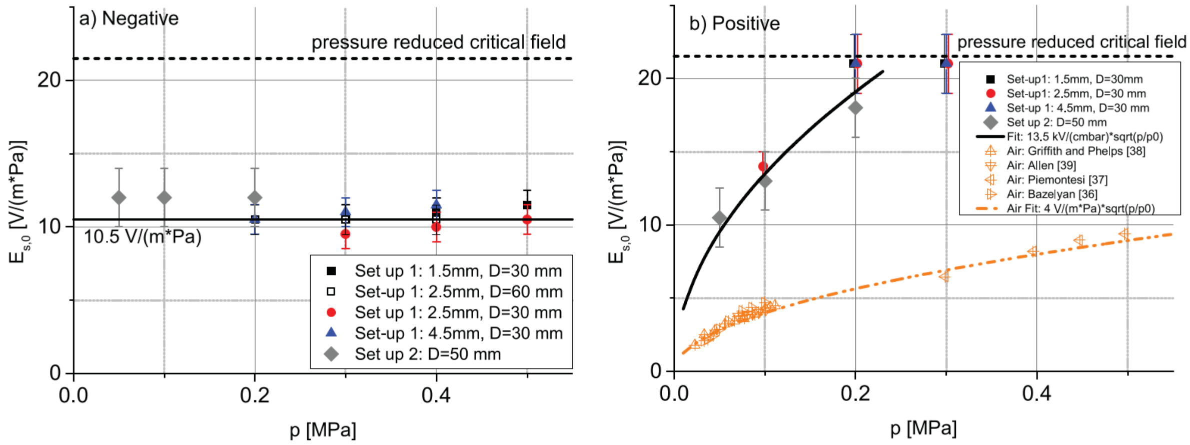


(a) negative (b) positive

Figure 2.7: The average pressure reduced streamer stability fields in setup 1 and setup 2 versus pressure for both polarities are shown in Figure 2.7. The error bars represent the uncertainty range of the evaluation. This line has a pressure reduced field of $10.5 V/(m.Pa)$. The dash-dotted line and the symbols along it show the pressure-dependence of dry air[19, 30].

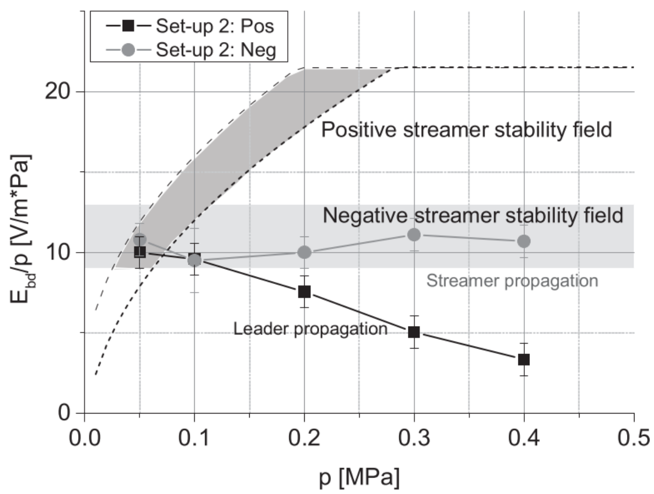


Figure 2.8: Diagram of pressure-reduced breakdowns in setup 2 (non-uniform field). By comparison, the shaded areas depict the measured ranges of reduced streamer stability fields for each polarity[19].

Seeger et al. [19] summarized their findings concerning $CO_2$ breakdown mechanisms and their dependencies as shown in **Figure 2.8**. For negative polarity, the breakdown fields are in good agreement with the measurement of $11 \pm 2V/(m \cdot Pa)$ for all investigated pressures. Therefore, a breakdown can be explained by streamer crossing, which is followed by streamer to spark transition after a sufficiently long voltage application time. Positive polarity breakdown fields are similar to negative breakdown fields at pressures below $0.1MPa$. As a result, the breakdown is still possible at low pressures due to streamer crossings. Streamer propagation cannot be decisive for breakdown above $0.1MPa$, as the breakdown fields are well below the streamer stability field. It was evident that leaders were appearing at these pressures. Therefore, positive polarity and pressures greater than $0.1MPa$ will result in a breakdown due to leader propagation.

Under conditions relevant to high voltage insulation systems, Seeger et al. [31] studied the breakdown field and the streamer inception field strengths of synthetic air, $CO_2$, a mixture of $CO_2$ and $O_2$, and $CF_4$. These tests were carried out on electrodes with nearly uniform fields and different technical surfaces. A positive polarity switching impulse (SI) voltage($130\mu s/2.1ms$) of peak value $300kV$ was applied. The results show a saturation of the breakdown electric field strength above $2MPa$. The streamer inception calculations were used to explain this effect. For different gases, the lowest saturation breakdown electric field strengths range from $200$ to $300kV/cm$. The breakdown electric field strength does not change if the gas becomes supercritical. Thus, it appears that the particle number density and the surface structure are the main controlling factors for the breakdown within the parameter range investigated. Investigation results pertaining to $CO_2$ and $CO_2/O_2$ mixture are given in **Figure 2.9**.

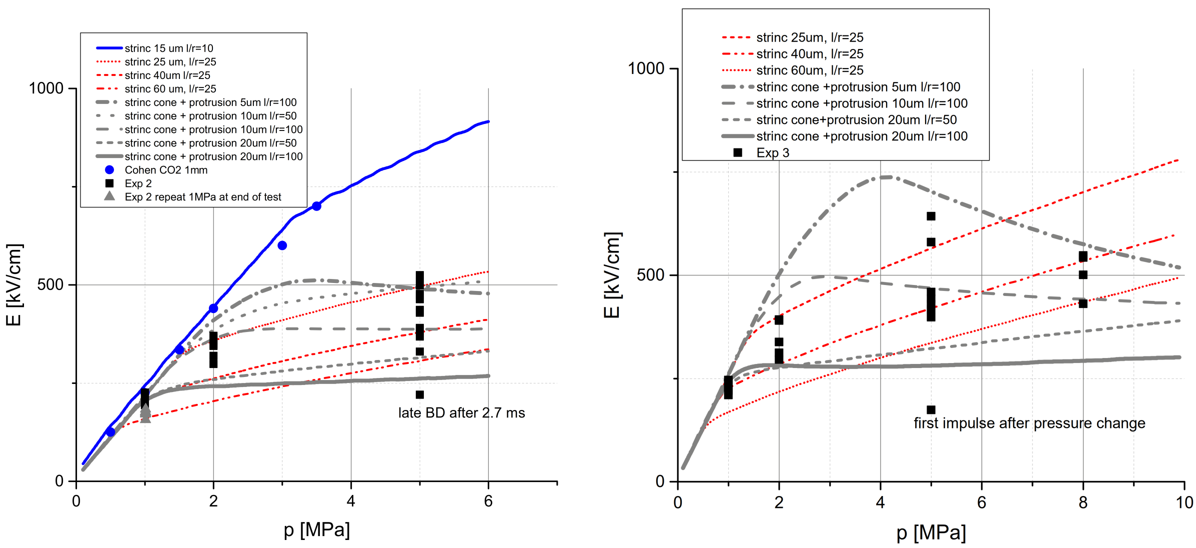


(a) Streamer inception in $CO_2$ at various pressure

(b) Streamer inception in $CO_2/O_2$ (80/20 mixture) at various pressure

Figure 2.9: Comparison of streamer inception field of $CO_2$ and $CO_2/O_2$ (80/20) in various pressure in nearly uniform fields. The field at which saturation occurs changes when the degree of surface roughness (dotted lines) varied[31].

Kumar et al. [32] evaluated the breakdown of $CO_2$, $CO_2/O_2$ mixtures in AC, DC and $2/160\mu s$ impulse powered weakly non-uniform field (rod-plane arrangement with $30mm$ gap). If AC and DC (positive and negative) waveforms are used, the breakdown field approximately equals $11kV/cm.bar$. For positive impulse, the breakdown voltage is higher and the time lag to breakdown is scattered, indicating a lack of starting electrons from $CO_2$ gas.

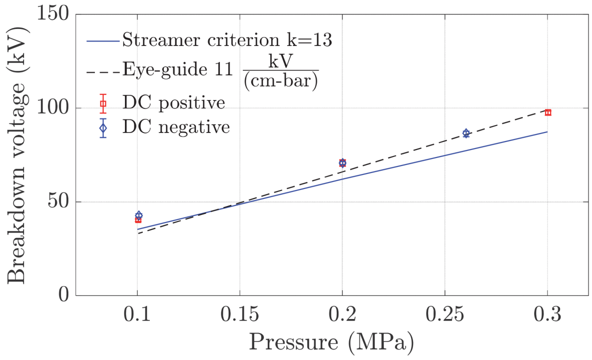


(a) $CO_2$ breakdown strength under DC positive and negative polarities compared with values predicted by streamer criterion. Positive and negative breakdown strength are equal[32]

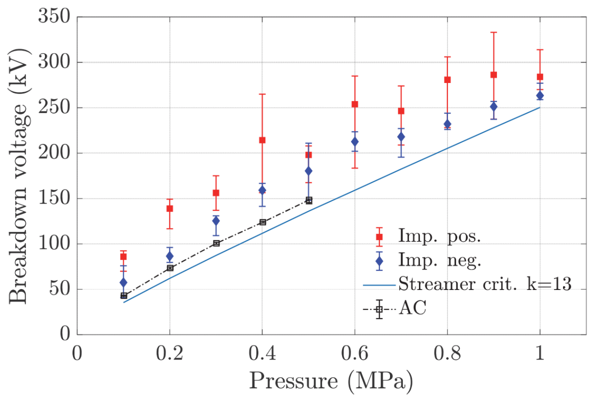


(b) Breakdown results for pure $CO_2$ gas for LI and AC waveforms are compared. The error bars for LI represents the maximum withstand and minimum breakdown voltages. U50 values for LI positive polarity are higher than negative breakdown voltage. Minimum breakdown strength of negative impulse is similar to that of AC[32].

Figure 2.10: Comparison of AC,DC and LI breakdown values of pure $CO_2$ in weakly non-uniform field (rod-plane with 30mm gap[32]).

$CO_2$'s DC breakdown strength was measured between $0.1$ and $0.3MPa$ for positive polarity and between $0.1$ and $0.27MPa$ for negative polarity. **Figure 2.10a** displays the results. It also displays a calculated value corresponds to $11kV/cm.bar$, which is approximately the streamer inception field and shows good agreement with the breakdown voltage. In both positive and negative DC fields, the breakdown strength is the same. They observed that, AC (**Figure 2.10b**) and DC (**Figure 2.10a**) breakdown voltages for both polarities of pure $CO_2$ are nearly equal. At $0.1MPa$, the minimum breakdown strength of negative polarity impulses approaches that of AC. Compared to negative polarity, positive polarity requires a higher breakdown voltage and also a wider error bar for determining breakdown strength.

In **Figure 2.11**, Kumar et al. [32] illustrates how most breakdowns occur around or before the peak of the pulse when applying a negative polarity impulse. As the peak voltage increases, the time lag diminishes. For positive polarity pulses, a higher voltage is needed for a breakdown; additionally, most breakdowns occur after the pulse peak (statistical time lag in the order of $10\mu s$). In contrast to negative polarity, there is more scatter in the time lag. Moreover, it does not display a decreasing time lag with increasing applied voltage and is random. They clearly pointed out the lack of the starting electrons is the likely the cause of the higher breakdown strength and longer time lag for positive impulses.

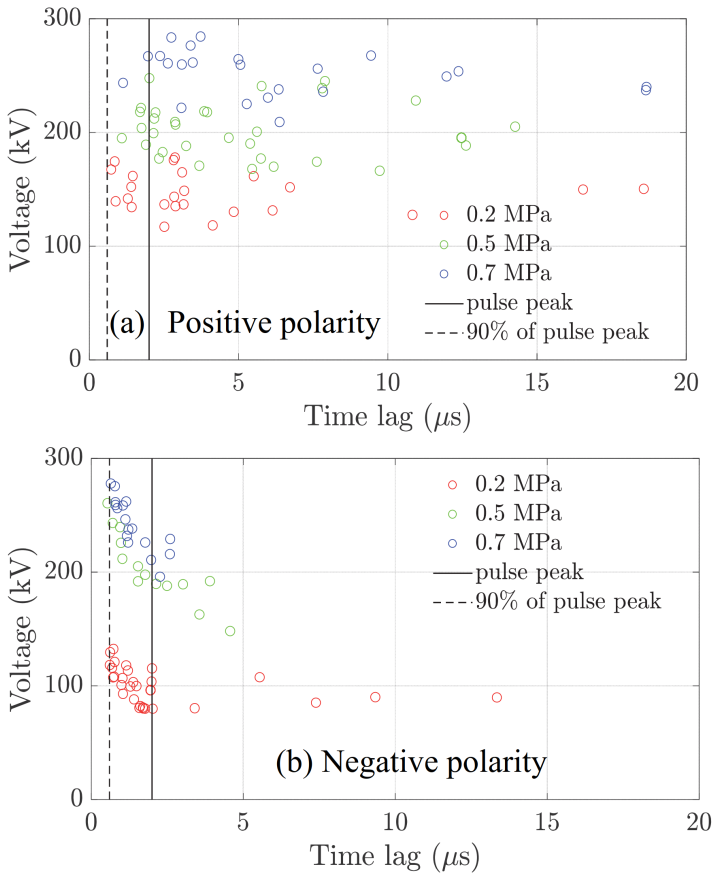


Figure 2.11: Time to breakdown for a rod-plane geometry (weakly non-uniform field) on applying (a) positive polarity and (b) negative polarity impulse. For positive impulse large scatter in time lag is observed[32].

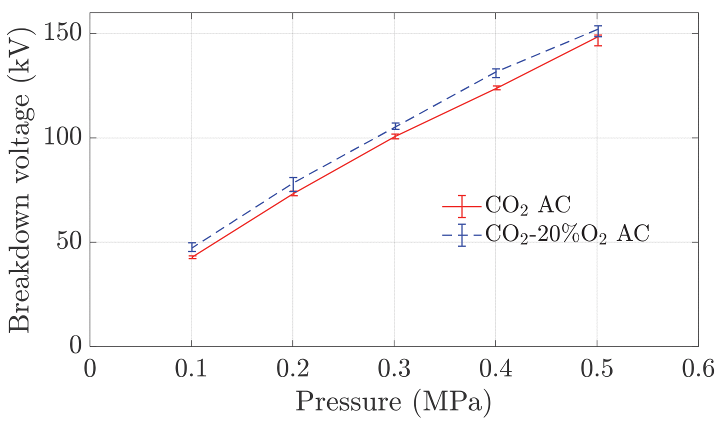


Figure 2.12: AC breakdown strength in $CO_2$ and $CO_2/O_2$for a rod-plane geometry (weakly non-uniform field). An ( 6%) increase in breakdown strength is observed under $CO_2/O_2$ (80–20%) mixture[32].

Kumar et al. [32] also studies the effect of mixing of $O_2$. According to **Figure 2.12**, by adding 20% oxygen to $CO_2$, the median AC breakdown strength increases by about $5kV$ for all the pressures. As compared to pure $CO_2$, breakdown strength increases by about $9\%$ at $0.1MPa$, $4.5–7\%$ at $0.2$ to $0.4MPa$, and $2.4\%$ at $0.5MPa$. Under non-uniform fields applied with AC waveforms, the breakdown strength increases by about $6\%$.

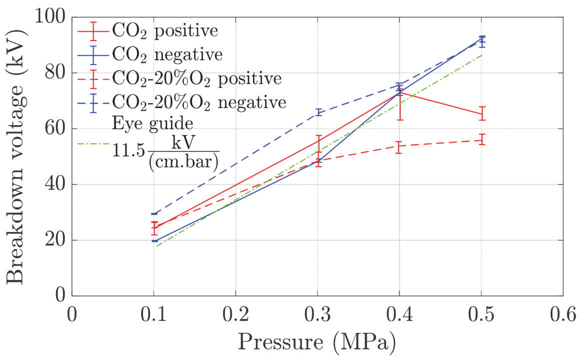


(a) When DC voltage applied.

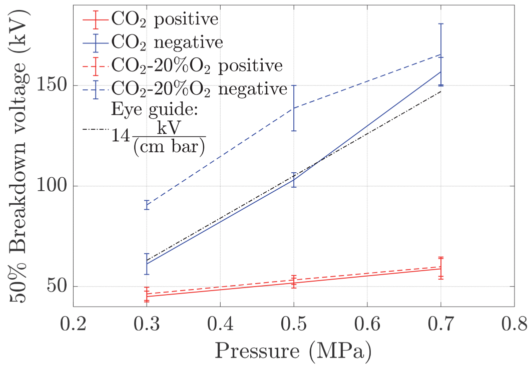


(b) When LI voltage applied.

Figure 2.13: Breakdown voltage of $CO_2$ and $CO_2/O_2$ $(80–20\%)$ in strongly non-homogeneous fields (point-plane electrode with $15mm$ gap)[32].

The breakdown strength of $CO_2/O_2$ mixtures $(10-30\%)$ when negative polarity impulse is applied is significantly higher than that of positive impulse when measured in pressure ranges of $0.3-0.7MPa$ in strongly non-uniform fields. In the case of strongly non-uniform field, **Figure 2.13a** shows that the breakdown strength of pure $CO_2$ under negative polarity DC field increases linearly from about $11.5kV/cm.bar$ to $0.5MPa$. In the case of positive polarity, however, the exact trend is not clear due to higher scatter at $0.4MPa$ (small sample size). $CO_2/O_2$ mixtures $(80–20\%)$ shown a marginally improved breakdown strength for the negative polarity DC field compared to pure $CO_2$. According to Kumar et al. [32], the saturation observed at positive polarity is due to the streamer to leader transition as explained in[19]. For impulse waveform (**Figure 2.13b**), the difference between positive and negative breakdown strength is much larger. The negative breakdown strength of $CO_2$ is significantly higher than the positive impulse. The addition of $20\%$ oxygen to $CO_2$ significantly increases negative breakdown voltage, whereas positive breakdown voltage is only marginally increased. Weakly non-homogeneous fields show the opposite polarity effect.

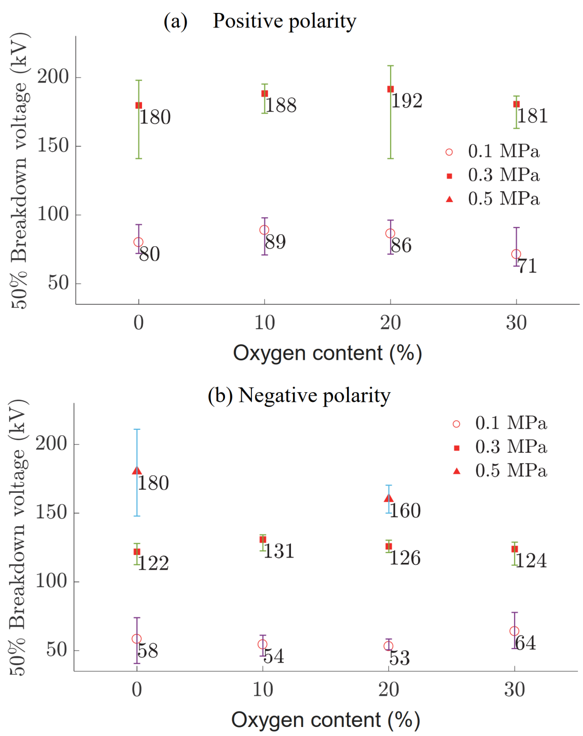


Figure 2.14: Comparison of breakdown level in $CO_2/O_2$ mixtures for impulses; (a) positive polarity, (b) negative polarity. The error bars represent the maximum withstand and minimum breakdown voltages[32].

**Figure 2.14** show the the trend of breakdown strength for positive and negative polarity impulses. For all measured pressures, the $50\%$ breakdown voltages are within the error bars and no clear trend with oxygen content can be observed.

In **Figure 2.15**, it can be seen that all breakdowns occur before the peak of the pulse for the positive polarity with no scattering, due to the strong field enhancement at the tip. However, the late and clustered breakdown in $CO_2$ with negative polarity impulse, a time period in the order of $20\mu s$ is needed for breakdown, close to the breakdown value.

In order to check weather the time lags were caused by the lack of starting electrons in $CO_2$, Kumar et al. [32] repeated experiments at $0.3MPa$ by artificially supplying free electrons with UV radiation. The time lag to breakdown for negative polarity impulse is shown in **Figure 2.16**. It is seen that the time lag to breakdown is still high even with UV-C irradiation. Therefore, as expected, the lack of starting electrons in the negative polarity impulse is not a cause for the high time lags observed (it could be also due to lack of sufficient UV). In order to understand this further, experiments on negative polarity were extended with a higher gap of 50mm. It indicates that increasing the gap distance leads to quicker breakdown. Kumar et al. [32] point out that the long time lag can be attributed to the time required for streamer propagation and spark transition or due to the corona stabilization effect and it is not related to the first electron. According to them, the exact discharge mechanism for this time lag in pure $CO_2$ is unclear and they recommend further research on this.

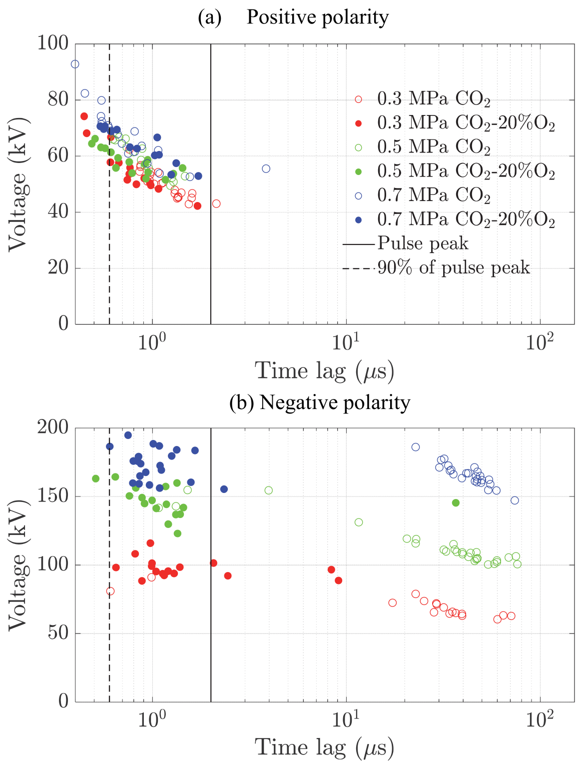


Figure 2.15: Time to breakdown observed in strongly non-uniform fields (point-plane) for (a) positive and (b) negative impulse. In pure $CO_2$ breakdown for positive polarity pulses is around the peak of the pulse, but for negative polarity late and clustered breakdown (>20 μs) is observed [32].

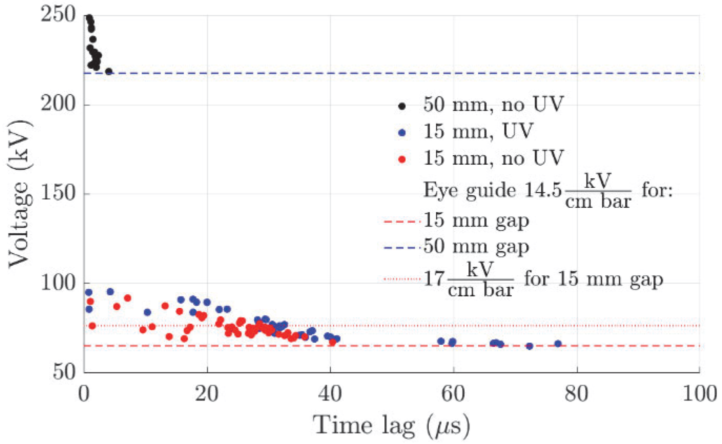


Figure 2.16: Comparison of total time lag to breakdown with and without UV irradiation in pure $CO_2$ gas (for gap = 15 mm and 50mm)[32].

## 2.3. Conclusion

There are two categories of research works on $CO_2$ presented in this review. In the first part, $CO_2$ is compared to SF6 and other gas candidates, mainly $N_2$. Our study indicates that $CO_2$ has great potential for replacing $SF_6$ in high-voltage transmission and distribution networks. Its lower environmental impact, reasonable dielectric strength, and ability to quench an arc are reasons for this. In the second part, we dig deeper into the electrical discharge process in $CO_2$ (and $CO_2/O_2$) under a wide range of operating conditions. There is clear information in the literature review about the steamer inception field, the leader inception field, the steamer stability field, the breakdown field, and the time to breakdown for both uniform and non-uniform fields. The key findings are summarized below.

⇒ Experiment results of Seeger et al. [19] in *uniform background field* shows that, the inception and breakdown fields increase with pressure for both polarities. For the positive polarity, however, the experiment results are higher than predicted. The lack of easy access to the first electron is the reason for this.

⇒ Experiment results of Seeger et al. [19] in *strongly non-uniform background field* shows that, the inception and breakdown fields increase with pressure for negative polarity. Accordingly, non-uniformity of the background field does not seem to matter, and only pressure and gap distance are relevant to the breakdown voltage. The positive polarity follows the same pattern at the beginning. At higher pressures, however, the breakdown field becomes saturated. If the field is sufficiently high, streamer to leader transition occurs, resulting in leader breakdown.

⇒ Investigations on the lengths of arrested streamers in *uniform field* performed by Seeger et al. [19] revealed that, for negative polarity, the streamer stability field was roughly half the critical field (i.e. $10 - 12V/m.Pa$) while for the positive polarity, the streamer stability field coincided with a value around the critical field (i.e. $21.5V/m.Pa$) at pressure ranges above $0.2MPa$. This clearly shows a difference in discharge behaviours for two different polarities. This also means that the length of negative polarity streamers is longer than positive polarity and it crosses the gap earlier. *Non-uniform field* cases exhibited the same behaviour. This shows that streamer stability is independent of the field homogeneity and is mainly determined by pressure and polarity.

⇒ Experiments by Seeger et al. [31] to examine the breakdown field and streamer inception field strengths of synthetic air, $CO_2$, a mixture of $CO_2$ and $O_2$, and $CF_4$ for pressure ranges up to $10MPa$ with *nearly uniform fields* using technical surfaces shows that, inception field increases linearly with pressure up to about $2MPa$ and saturates above $2MPa$ saturates.Variations in surface roughness change the field where saturation occurs. This means that the gas's breakdown field and inception field remain unchanged when it is operated at supercritical pressures.

⇒ Experiments performed by Kumar et al. [32] in $CO_2$ in *weakly non-uniform field* shows that, For AC and DC fields, the breakdown field is approximately $11kV/cm.bar$. The breakdown field of LI positive polarity is slightly elevated compared to negative polarity due to the lack of a start electron. Positive polarity produces a higher breakdown time and more scattered breakdowns.

⇒ Experiments performed by Kumar et al. [32] in $CO_2/O_2$ mixtures (10% to 30%) in *strongly non-uniform field* shows that, the breakdown strength when negative polarity impulse is applied is significantly higher than the breakdown strength of positive impulse when measured at pressure ranges of $0.3 - 0.7MPa$.

⇒ For *strongly non-uniform field*, Kumar et al. [32] showed that the negative polarity DC field marginally improved breakdown strength for $CO_2/O_2$ mixtures (80-20%) when compared to pure $CO_2$. As the negative polarity DC field is applied, the breakdown strength of pure $CO_2$ increases linearly from about $11.5kV/cm.bar$ to $0.5MPa$. However, in the case of positive polarity, the exact trend is not clear due to high scatter. Further research is needed to confirm the findings.

⇒ For *strongly non-uniform field*, Kumar et al. [32] showed that, with positive polarity due to strong field enhancement at the tip, the breakdown occurred before the peak of the impulse voltage in both $CO_2$ and $CO_2/O_2$ mixtures, indicating that the breakdowns were faster. Just as in the case of positive polarity, the $CO_2/O_2$ mixture also recorded breakdowns before the peak. In pure $CO_2$, a clustered and delayed breakdown was observed with a negative polarity impulse. It can be explained by *the corona stabilization effect*[2] and *streamer-to-leader transition*.

[2]When the needle is energized with the negative polarity field, a cloud of positive ions near the tip shields the discharge, hence requiring a high breakdown voltage. However, when positive polarity is applied, positive ions are pushed into the gap, enhancing the field in the gap and leading to a breakdown.

# 3
# Theory

This part describes the discharge mechanism in the gas, what are the key features of $SF_6$ and $CO_2$ and what are the main differences between them as insulation gases.

## 3.1. Gas discharge physics

Gases have proven their performance as an electrical insulator due to their low conductivity, low dielectric losses, independence from applied frequency, and low relative permittivity ($\epsilon \approx 1$). However, when the electric field stress becomes sufficiently high, the discharge processes takes place.

### 3.1.1. Townsend discharges

J. S Townsend explained the discharge mechanism in gases with at pressure or small electrode gap. Such discharges, later known as *Townsend Discharges*, happen due to electron-ion exchange and collision and explains the process of *electron avalanche*. When a free electron is present in the electric field, the electron tends to drift towards the anode, colliding with adjacent atoms and molecules. If the kinetic energy of the electron is high enough, the collision will become an *ionizing collision*, which causes excitation of molecules and release of another electron. These freed electrons then get accelerated in the electric field and collide with another molecule. This process will continue and cause an *electron avalanche*[5] as shown in **Figure 3.1**.

Townsend theorized the mechanism by introducing two ionization coefficients. The *first ionization coefficient* ($\alpha$) represents a number of free electrons produces through ionization collision of one single electron per unit length, and *second ionization coefficient*($\gamma$) represents the number of free electrons produced from the secondary collision of positive charges in the gas per unit length. Based on these two coefficients, *Townsend's Ignition Criteria*, **Equation 3.1**, shows that the breakdown process will follow if the left side of the equation equal to 1[5].

$$\gamma(e^{\alpha d} - 1) = 1 \tag{3.1}$$

Where $d$ is the short distance between the electrodes. The number of electrons *n* formed when the first electron travel *x* along the electric field is given by **Equation 3.2**[33].

$$n = e^{\alpha x} \tag{3.2}$$

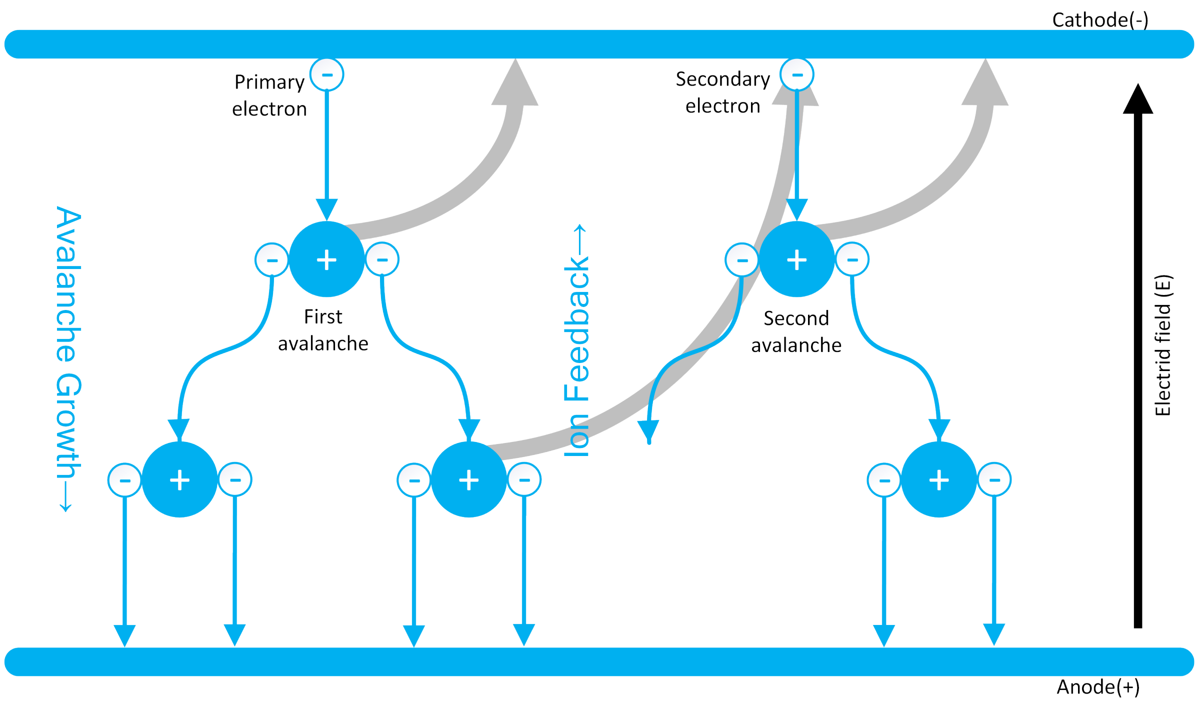


Figure 3.1: Simplified illustration of electron avalanche - picture adapted from[5].

Even though Townsend could explain the discharge process in low-pressure gas and across small gaps, he couldn't realize the effect of photo ionization and space charges. It was observed that the formative time lag of spark formation in pressurized gases and larger gaps were much shorter than what Townsend could explain.

### 3.1.2. Streamer discharges

Raether[34] and Meek[6] independently discovered the significance of *space charges* in the gas discharge process later known as *streamer mechanism*. When the number of electrons in an avalanche reaches the order of $10^6 - 10^8$, they significantly influence the electric field near the avalanche. Mobile electrons will form a spherically shaped *avalanche head* with a negative charge and increased in diameter by a diffusion process. Less mobile ions form the *avalanche tail* and create a positively charged region. Such a charge cloud is known as *space charge* and they significantly enhance the electric field at its spherical head[5] as illustrated in **Figure 3.2**.

Due to very high field enhancement at the head of the avalanche, the number of ionization collisions quickly increases. Photo-ionization causes photon emission generates many free electrons around the avalanche and thus generating many more such avalanches very quickly. The super-positioned structure of all such self-sustained avalanches is known as *streamer*. Since photo-ionization is a very quick process, the streamer crosses the electrode gap within the propagation time of a single avalanche. See **Figure 3.3**

In electron attaching gases such as $SF_6$, thus formed free electrons can get re-attached to the gas molecules when colliding with them. This process is known as *electron attachment* and accounts for the *electron attachment coefficient*($\eta$). In this case, the *effective ionization coefficient*($\alpha_{eff}$) is the difference between electrons generated and re-attached[5] as shown in **Equation 3.3**.

$$\alpha_{eff} = \alpha - \eta \tag{3.3}$$

In this case, the number of electrons *n* formed when the first electron travel distance *x* along the electric field is given by **Equation 3.4**, which completely describes the growth of an *avalanche*. Experiments and theory show that both $\alpha$ and $\eta$ are determined by the *electric field (E)* and *gas density ($\delta$)*. That means, they both depends on the ratio *E/$\delta$*[33].

$$n = e^{(\alpha-\eta)x} \tag{3.4}$$

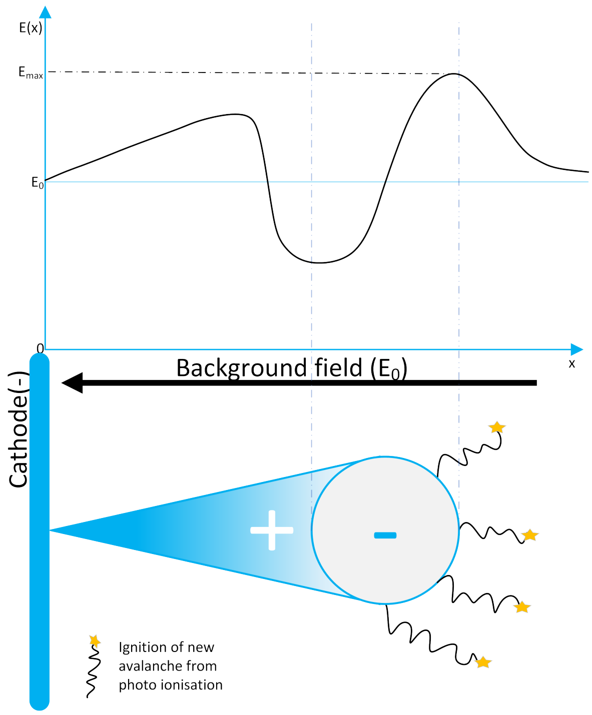


Figure 3.2: Simplified illustration of space charge. This picture is an adapted version of figure showed in [5].

If the background field is homogeneous or slowly decaying, the streamer will grow towards the opposite electrode, leading to a current peak if it reaches the electrode. The thermal ionization followed by the streamer can form a high conductive arc. Whereas, in the case of a strong in-homogeneous electric field, recombination will dominate at a certain point and streamer growth will be no longer possible. Such non-growing stable discharges are called *corona*.

The *electron detachment* is another process to create free electrons in insulating gases such as $SF_6$. Conductive surfaces with high electric field stress emit electrons through field emission if a negative electric potential is applied. However, in the case of the positive electric field, the free electrons mostly come from the gas itself.

As explained earlier, in order to have a breakdown, the number of electrons generated through ionization collision shall be higher than electron attachment. That means

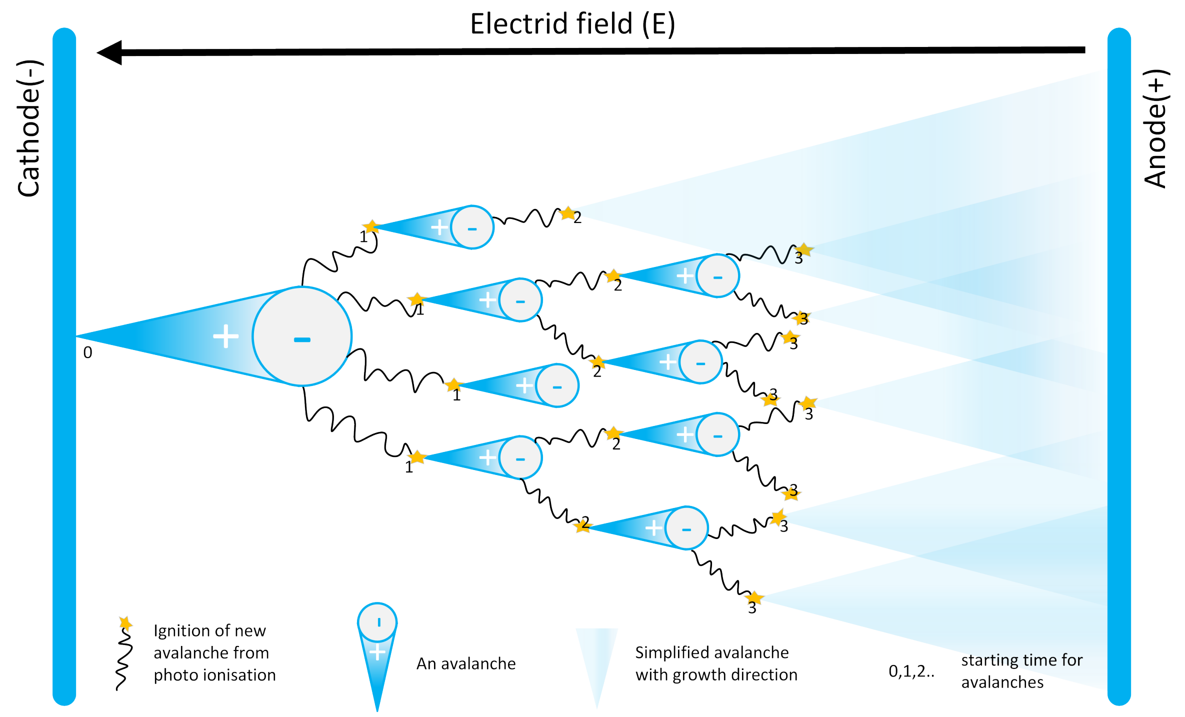


Figure 3.3: Simplified streamer model[5].

$\alpha_{eff}$ shall be greater than zero. The electric field at which this occurs is termed as *critical electric field* ($E_{crit}$). $E_{crit}$ is $89kV/cm.bar$ for $SF_6$ . Additionally, the number of electrons in the avalanche must reach to an order of $10^6 - 10^8$. This is known as the *critical number of electron* ($N_{crit}$). Raether's ignition criteria is given as **Equation 3.5**.

$$\int_0^d \alpha_{eff} dx \geq In(N_{crit}) = \kappa \tag{3.5}$$

The above equation is also known as the *streamer criteria* where $d$ is the electrode gap distance and $\kappa$ is a constant specific to the insulation gas. For $SF_6$, the values of $E_{crit}$ and $\kappa$ are $89kV/cm.bar$ and 10.5 respectively[17]. The similar values of $CO_2$ are $E_{crit}$ = $21.5kV/cm.bar$ and $\kappa$ = 13[19].

Depending upon how the streamers are formed and direction of propagation, they can be classified as *positive streamers*, *negative streamers* and *mid streamers*.

### 3.1.3. Positive streamers

If the electric field in front of the anode is high enough, the anode (point A - see **Figure 3.4**) initiates an avalanche that propagates toward the anode. When the avalanche reaches the anode, the electrons are absorbed into it, leaving behind the net positive space charge. If the number of positive ions in the avalanche head is larger than a critical value, secondary avalanches created by the photons are attracted toward the positive space charge. The positive space charge is neutralized by the electrons in the secondary avalanches, creating a weakly conducting channel. Consequently, a part of the anode potential is transferred to the channel, making it positively charged and increasing the electric field at the tip. The high electric field at the tip attracts more electron avalanches to it, and the channel grows as a consequence[33]. Such discharges travels away from anode and are called *positive streamer*.

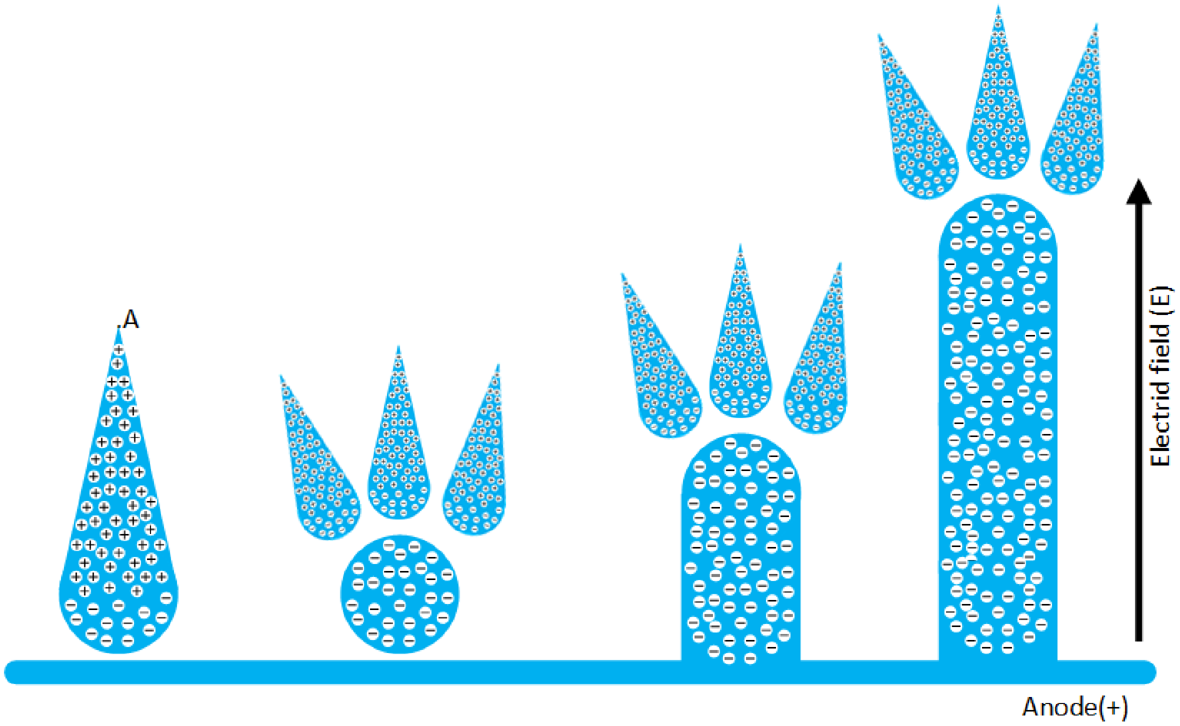


Figure 3.4: Illustration of positive streamer - Picture adapted from [33].

### 3.1.4. Negative streamers

*Negative streamers* are anode directed streamers. A photo-electron generated close to the cathode (point A - see **Figure 3.5**) generates an avalanche that moves away from the cathode, leaving behind a positive charge close to it. When the avalanche reaches a critical size, the positive charge of the avalanche starts attracting secondary avalanches to it. As in the case of positive streamers, the electrons in the secondary avalanches neutralize this positive charge, effectively moving it toward the cathode. When the positive charge reaches the cathode, the field enhancement associated with the proximity of positive space charge to the cathode leads to the emission of electrons from the latter. These electrons will neutralize the positive space charge, creating a weakly conducting channel that connects the negative head of the electron avalanche to the cathode. Part of the cathode potential will be transferred to the head of this weakly ionized channel, increasing the electric field at its head. This streamer head now acts as a virtual cathode, and the process is repeated. Repetition of this process leads to the propagation of the negative streamer away from the cathode [33].

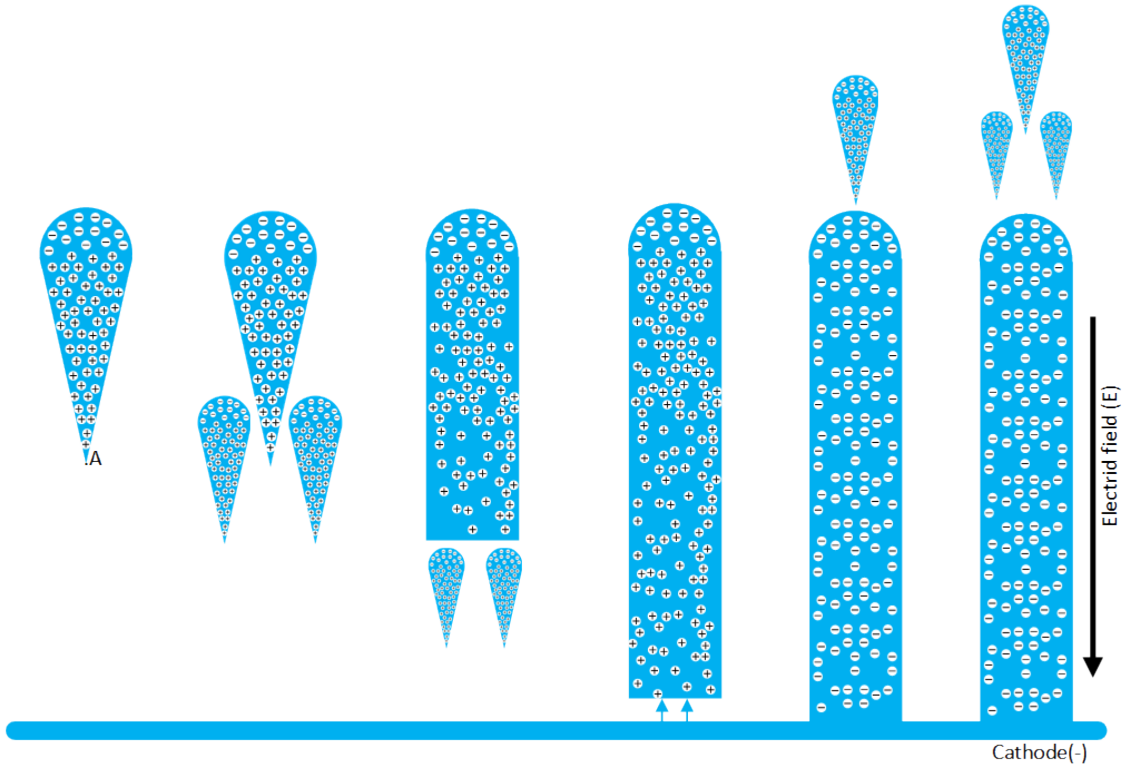


Figure 3.5: Illustration of negative streamer - Picture adapted from [33].

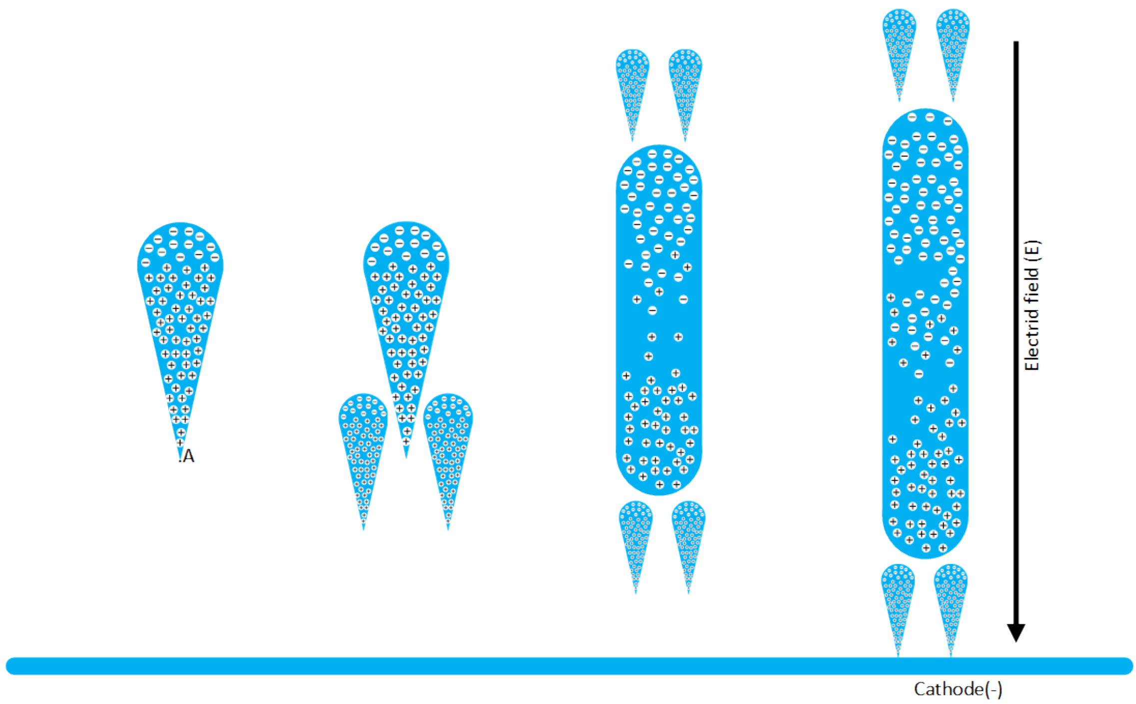


Figure 3.6: Illustration of mid streamer - Picture adapted from [33].

### 3.1.5. Mid streamers

A mid-gap streamer is bidirectional discharge who two ends travel towards the cathode and the anode. If the electric field is very high, then the positive space charge of the primary avalanche can reach the critical size necessary to form a streamer before it reached the anode. This may lead to the formation of a bidirectional discharge as depicted in **Figure 3.6** [33].

### 3.1.6. Streamer breakdown

A steamer or a gap-crossing streamer may not necessarily results in the breakdown of the insulation. This is because the conductivity of the streamer channel is rather small and the temperature of the streamer is only ambient. However, a propagating streamer will create an ionized track if the background electric field is higher than the so-called *streamer stability field* ($E_{st}$). When the ionized track crosses the gap, it will create a cathode fall region near the cathode, which is basically is a sharp drop of voltage at the ionized track near the cathode. Now the streamer discharge starts developing a potential wave and after several tens of nanoseconds, the axial distribution of the electric field in the channel will become nearly uniform. If the background electric field is higher than the critical field, the conductivity of the channel increases further, and therefore current in the channel also increases over time. If the background field is less than the critical field, the conductivity shall be decreasing due to net negative ionization. However, there are many processes in plasma physics, that slow down the decay of the net ionization and finally change it to positive. Therefore, increased conductivity and current can lead to a breakdown in this case as well. This process is also called *streamer to spark transition*[35].

### 3.1.7. Leader breakdown

The *streamer-to-leader transition* is the transformation of a low conductive streamer volume into a high conductive plasma channel with low voltage drop, known as a *leader*[13]. Such a transition of streamer channel to leader channel is caused by ohmic heating of streamer channel when a charge $Q$ pulse passes though it. This charge deposits energy $Q.E$, resulting in a temperature of the channel. This causes an initial over-pressure in the channel and thereby the channel to expand [18]. After the inception of a leader discharge, very long distances will be bridged if the voltage is slightly increased. Therefore, leader inception voltages are only slightly below

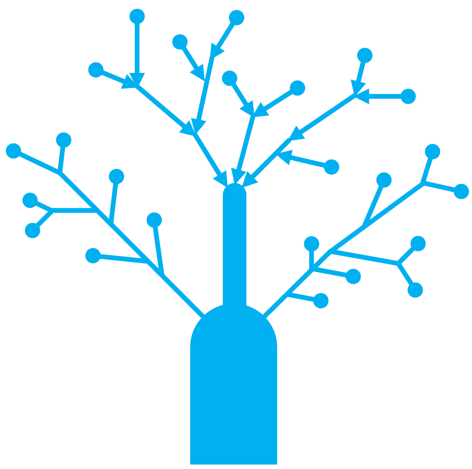

Figure 3.7: Simplified illustration of stem formation; arrow indicated movement of charges in the streamer to form *stem*. This picture is an adapted version of figure showed in [15].

breakdown voltages[5].

There are different types of leader inception mechanisms identified, which mainly depends on the nature of nature of the gas and electrical field. In insulation gases, two main mechanisms have been identified. They are the *precursor* mechanism[13, 15, 18] and *stem* mechanism[14, 15, 18]. The *stem* formation occurs due to the channel expansion in a branched *streamer corona*. If sufficient number of streamers feed their current in to a common channel (*stem*), the thermal expansion of that channel occurs which results in reduction of gas density in the stem (see **Figure 3.7**). This causes a reduction of the critical field in the stem to go below the applied field. The ionisation then restarts creating a highly conductive leader channel[15].

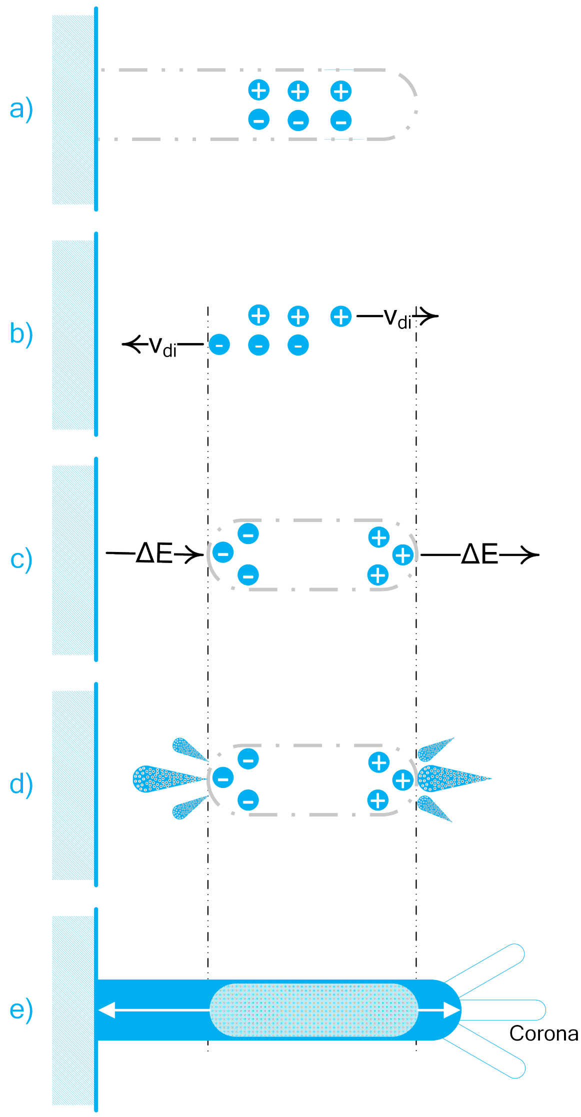


Figure 3.8: a) Ions remains from the previous streamer. b) Charge separation by ion drift. c) Field enhancement due to ionic space charge. d) Restarting of ionisation at the ends of space charge filaments. e) *Precursor* formation towards electrode. This picture is an adapted version of figure showed in [15]

The *precursor* is formed due to ion drift and is only observed in electronegative gases like $SF_6$. During streamer propagation, ions of different polarity drift apart and create space charges. These space charges locally enhance the field such that the ionization is restarted. The current associated with these events will distort the field around it and produces a conducting filament that propagates towards the electrode as a leader channel[15](see **Figure 3.8**).

Now we know how leader inception happens by formation of the *stem* and the *precursor*. If the electric field is sufficiently high, leader inception can lead to a complete breakdown across the gap through a process called *stepped leader propagation*. Schematic representation of *leader breakdown* is shown in **Figure 3.9**.

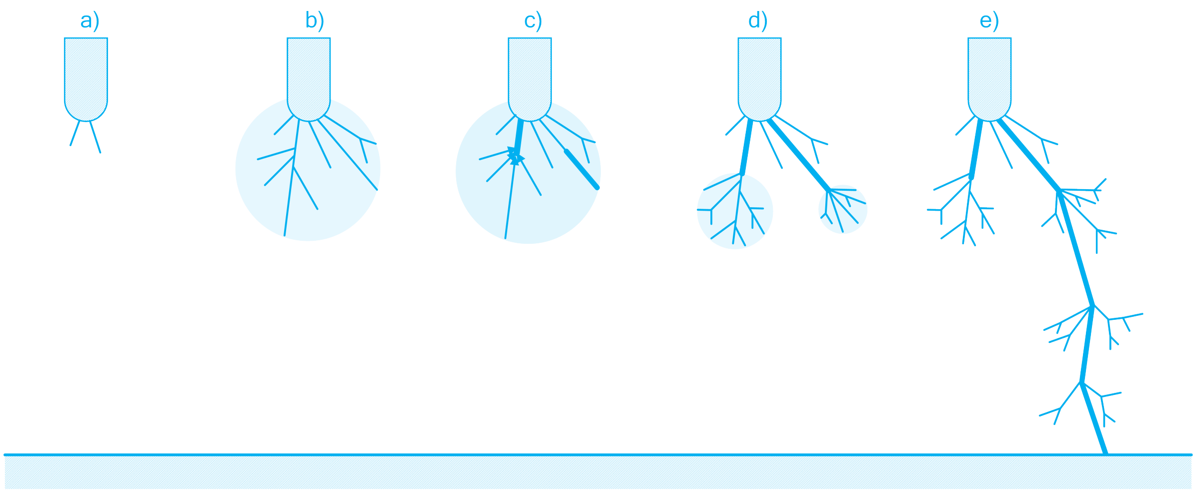


Figure 3.9: a) First streamer inception (streamer inception criterion). b) first corona growth completed. c) formation of *stem* and *precursor* from streamers. d) leader inception from *stem* and *precursor*. e) Stepped leader propagation leading to breakdown across the gap - Picture adapted from [15]

## 3.1.8. Temporal development of gas breakdown

The temporal development of a breakdown sequence is shown in the **Figure 3.10a**. The figure corresponds to an impulse voltage and the voltage application time starts from $t = 0$. At $t = t_0$, the voltage reached $V_0$ which produces an electric field exceeding $E_{crit}$. Since the availability of the first electron is statistical in nature, the initiation of discharge will start after a time lag, called the *statistical time lag*($t_s$). In the case of negative polarity, *statistical time lag* is determined by electron production rate from the electrode surface due to field emission. In the case of positive polarity, *statistical time lag* is determined by electron detachment rate in the gas, and it can be evaluated by the *volume-time law*. It describes the probability to encounter a free electron, able to initiate an avalanche of sufficient size within a certain volume and time.

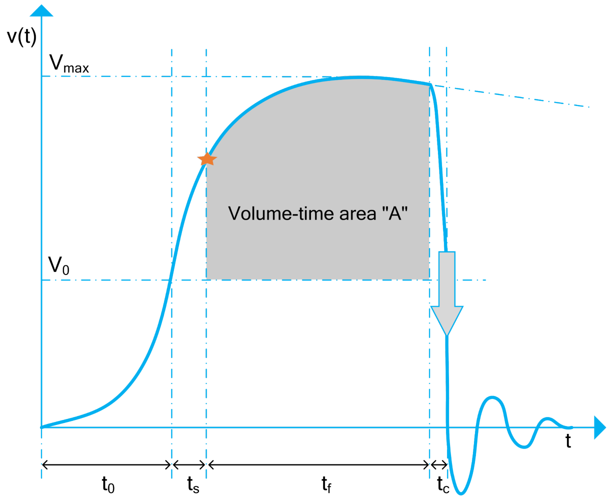


(a) Time characteristics of breakdown when impulse voltage is applied [5].

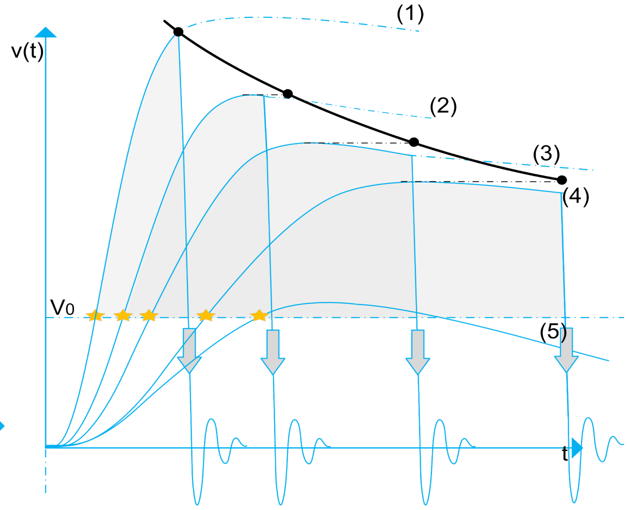


(b) Voltage and time dependency of breakdown when impulse voltage is applied. The statistical time lag is assumed as zero[5].

Figure 3.10: Time dependency of gas breakdown.

Following the *statistical time lag*($t_s$), the time taken for the discharge to bridge the electrode distance is known as the *formative time lag*($t_f$). It represents the time necessary to build up a streamer that spans both electrodes and/or the time frame for repeated streamer-leader transition until the electrodes are bridged and formation of high current discharge follows leading to final voltage collapse. the time taken for voltage collapse ($t_c$) is comparatively very short and it is determined by spark resistance laws and properties of discharge circuit. Total *time to breakdown*($t_{BD}$) is given by Equation. 3.6.

$$t_{BD} = t_0 + t_s + t_f + t_c \tag{3.6}$$

In **Figure 3.10a**, the grey highlighted area is know as the *volume-time area* and this area posses certain characteristics of the electrode arrangement and insulation gas. The *volume-time area* $A$ is always a constant for a given electrode arrangement and it can be mathematically represented as Equation. 3.7 (*Kind's voltage-time law or equal area criterion*)[5]. The practical implication of the *volume-time area* for a particular electrode arrangement and gas, is explained in **Figure 3.10b** for standard LI waveform (1.2/50$\mu$s) .If the we neglect statistical time lag, after the *volume-time area* $A$ is reached, voltage collapses and accordingly a distribution of the *formative time lag*($t_f$), which is also equal to the time to breakdown in this case, is obtained (see curves no. 1 to 4). If the necessary the voltage-time area is not reached although $V_0$ is exceeded, streamer growth stops before a conductive channel between the electrodes develops and the breakdown no longer occurs, (see curve no. 5).

$$\int_{t_0+t_s}^{t_0+t_s+t_f} [v(t) - V_0]dt = A = Constant. \tag{3.7}$$

## 3.2. $CO_2$ as gas insulation

$CO_2$ is a colourless gas. Gases such as carbon dioxide are odourless at low concentrations but have an acidic odour at sufficiently high concentrations. At standard temperatures and pressure, carbon dioxide has a density around 1.98 kg/m3, about 53% higher than that of dry air. A carbon dioxide molecule consists of a carbon atom covalently bonded to two oxygen atoms[1] (see **Figure 3.11**). It is naturally present as a trace gas in Earth's atmosphere (0.04%).

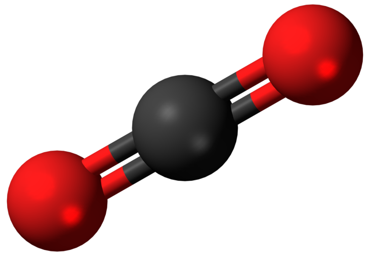

Figure 3.11: Molecular geometry of $CO_2$

Beginning in the early 1970's, researchers began to investigate the physical properties of $CO_2$. As the search for an alternative to $SF_6$ has intensified since it was classified as a climate gas, this process has been accelerated. The use of $CO_2$ as an insulation medium has shown promise over $SF_6$.

$CO_2$ is non-flammable and electron-attaching[36]. As a result, it can be used as the main insulation medium in gas-insulated lines (GIL) as well as breaking the current in circuit breakers[37]. $CO_2$ has a boiling point of $-78.5^oC$ at atmospheric pressure, which is lower than even $SF_6$, allowing it to be used at lower temperatures as well. However, the dielectric strength of $CO_2$ is only $32-37\%$ of that of $SF_6$. Hence, $CO_2$ should be used at higher pressures in order to have the same insulation strength as $SF_6$. $SF_6$ has a critical electric field of approximately $21.5kV(cm.bar)$ at room temperature[38].

## 3.3. $SF_6$ as gas insulation

$SF_6$ (*sulfur hexafluoride*) is an electrical insulation gas and arc suppressant. It is an inorganic substance, which is colourless, odourless, non-flammable, and non-toxic. The *octahedral* geometry of $SF_6$[2] is formed by six fluorine atoms attached to a central sulfur atom (see **Figure 3.12**). In other words, it is *hypervalent*.

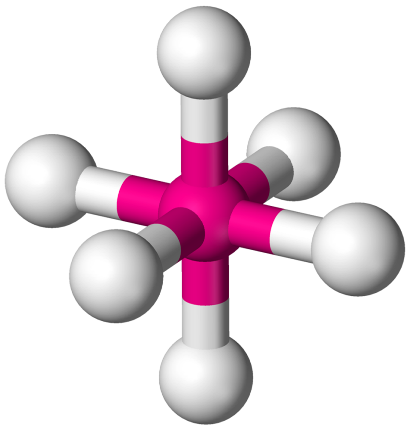

Figure 3.12: Molecular geometry of $SF_6$

Since $SF_6$ is a nonpolar gas, it is poorly soluble in water, but can be dissolved in nonpolar organic solutions. At sea level, it has a density of $6.12g/L$, which is considerably higher than the air's density ($1.225g/L$). Generally, it is transported as a liquefied compressed gas.

In the electrical industry, circuit breakers, switchgear, and other equipment usually use sul-

[1] https://en.wikipedia.org/wiki/Carbon_dioxide
[2] https://en.wikipedia.org/wiki/Sulfur_hexafluoride

fur hexafluoride $SF_6$ as a dielectric medium. Due
to its much higher dielectric strength than air or dry nitrogen, $SF_6$ gas under pressure is used as an insulator in gas-insulated switchgear (GIS). Because of the gas's *electronegativity* and density, the dielectric strength is high. Because of this property, electrical assets are able to be reduced significantly in size. $SF_6$ is chemically broken down by an arc, but most of the decomposition products tend to re-form $SF_6$, a process referred to as "*self-healing*".

$SF_6$ at high pressures has been increasingly used as an insulation medium in high voltage applications since the 1950s. The rigid *octahedral* molecular structure of $SF_6$ is held together by small binding distances and high bond energies. Due to this, the $SF_6$ molecule is very stable at atmospheric conditions[5, 39]. $SF_6$ has a very low condensation temperature of $-63^oC$ at $1bar$. As a result, it can be used at low ambient pressure. Condensation temperatures increase with higher pressure. As an example, the condensation temperature of $SF_6$ at $5bar$ is $-30^oC$. $SF_6$ can, in such a case, be mixed with other gases, such as N2, to lower the condensation temperature. Decomposition products of $SF_6$ are very reactive, so they immediately recombine to form $SF_6$[5, 39].

The intrinsic field strength of $SF_6$ (also know as critical field) is $E/p = 89kv/(cm.bar)$[39]. $SF_6$ gas has a high affinity for electrons. Thus, free electrons get easily re-attached to molecules. The equation represents the effective ionization coefficient ($\alpha_{eff}$) of $SF_6$[5].

$$\frac{\alpha_{eff}}{p} = k_i\left(\left(\frac{E}{p}\right) - \left(\frac{E}{p}\right)_0\right) \tag{3.8}$$

Where $k_i = 27.7/kV$ and $(E/p)_0 = 89kv/(cm.bar)$ at temperature $293K$[5].

$SF_6$ is a very large gas molecule and hence its *mean-free-path*($\lambda$) is very small. Due to this short distance between the electron and the gas molecules, the electrons can't gain enough momentum to cause an ionization collision, so they attach to the molecules. The small mean free path combined with a high electron affinity, making it an extremely effective dielectric gas. $SF_6$ is highly susceptible to strong non-uniform fields because of its small *mean-free-path*. As a result, if the local field is sufficiently high, the electrons will travel the short distance to ionize a new $SF_6$ molecule and create an electrons avalanche very rapidly. This is why $SF_6$ is so sensitive to rough surfaces and protrusions[5, 39].

# 4

# Method

This section describes the experimental setup and the procedure used in this project which includes field calculation using FEM tool for each test object, numerical estimation of breakdown and inception voltages, and the overall procedure adopted when running each experiment. A separate section describes the procedure used for running breakdown tests and statistical analysis of breakdown data to determine breakdown voltages for each setup.

## 4.1. Experiment setup

All the experiments presented in this thesis are performed at the Van de Graaph Laboratory (VdG Lab) in *Hitachi ABB Power Grid Research Center*, located in Baden-Dättwil, Switzerland. Details of the setup along with measurement and optical diagnostic techniques used, are described below.

### 4.1.1. High voltage generation

The Van de Graaph Laboratory (VdG Lab) consists of a gas insulated setup, as shown in **Figure 4.1b**, with a *Van de Graaph Generator* as its high voltage source. The *Van de Graaph Generator* in the setup work on the same principle of operation as originally presented by the inventor Robert J. Van de Graaff in 1930's[40] with some necessary modifications.

The original design is as shown in [41]. When the motor of the *VdG* is turned on, the lower roller begins turning the belt. Since the belt is made of rubber, the lower roller begins to build a negative charge and by induction, the belt builds a positive charge on the outside surface. This charge imbalance occurs due to the lower roller capturing electrons from the belt as it passes over the roller. A conducting brush at the top of the belt is connected to the "collector". This comb transfers the positive charge off the belt to the collector as the rubber belt moves past it. At the base roller another comb drains the negative charges on the outside of the belt to the ground. At any instant, the terminal potential is $V = Q/C$, where $Q$ is the stored charge and $C$ the capacitance of the terminal to ground[41]. A simple schematic of the VdG generator used in the lab is as shown in **Figure 4.1a**. This is an upside-down version of the original shown in [41] with knives used instead of brushes. The upper knife is put under high voltage of either positive or negative polarity ($\pm 20kV$) so that charges can be sprayed onto the belt in this manner. The charge is then transported down on the belt, where it is scraped off the belt due to charge imbalance and transported to the exterior of the terminal. There, it is connected to a capacitor.

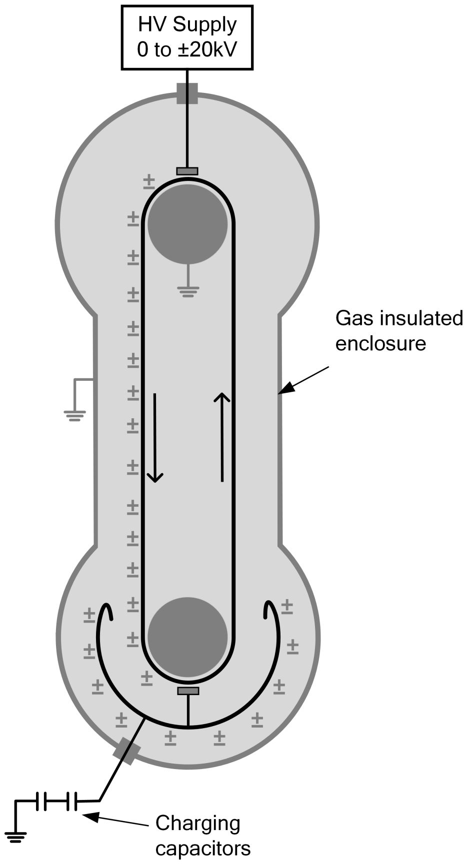


(a) Illustration of operation principle of Van de Graaf generator used in the lab setup

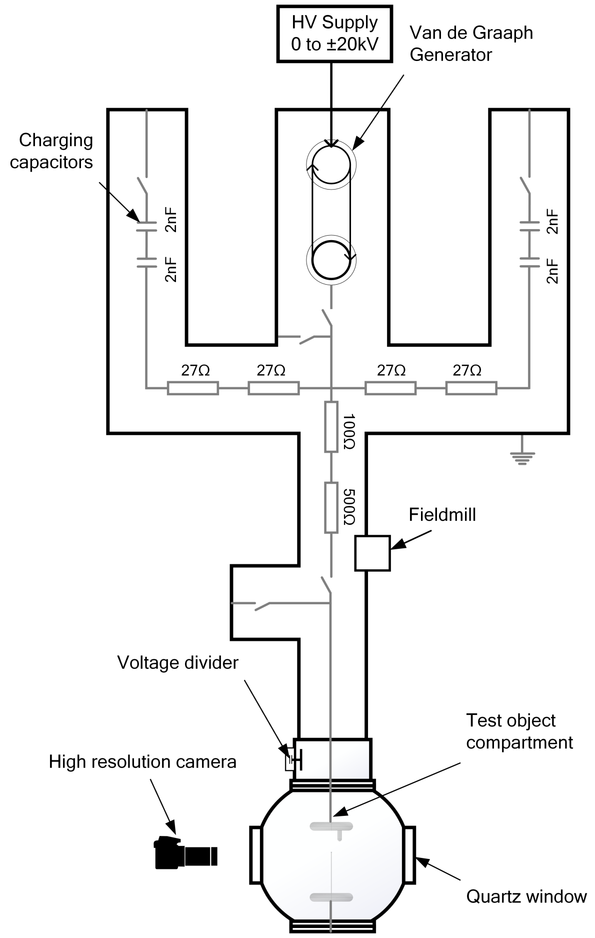


(b) Schematic of Van de Graaf generator based high voltage test setup used for experiments.

Figure 4.1: VdG Laboratory high voltage setup used in the experiments

A fully GIS enclosed setup is illustrated in **Figure 4.1b**. The various GIS compartments are filled with $SF_6$ at rated pressure. The two arms of stacked capacitors are charged via charging resistors using a VdG connected to it. Once the desired voltage is reached, the disconnector switch is closed and the capacitor voltage is applied to the test object via the damping resistor. The charging voltage is measured by a *fieldmill* and the voltage applied onto the test object is measured by a *capacitive voltage sensor*. This makes it space-efficient, safe to handle and less susceptible to electromagnetic interference. The setup allows dielectric testing up to 400 kV.

### 4.1.2. Measurement setup

The measurement of the applied voltage is done using a capacitive voltage divider attached in the GIS compartment and a high-speed oscilloscope. Two oscilloscopes were interchangeably used; a *LeCroy LT374* (with 500MHz bandwidth and upto 4GS/s sampling rate) and a high definition *LeCroy HDO6104a* (with upto 1GHz bandwidth and upto 10GS/s sampling rate). The voltage measuring arrangement along with optical diagnostics setup (explained in **Section.4.1.3**) is schematically illustrated in **Figure 4.4**.

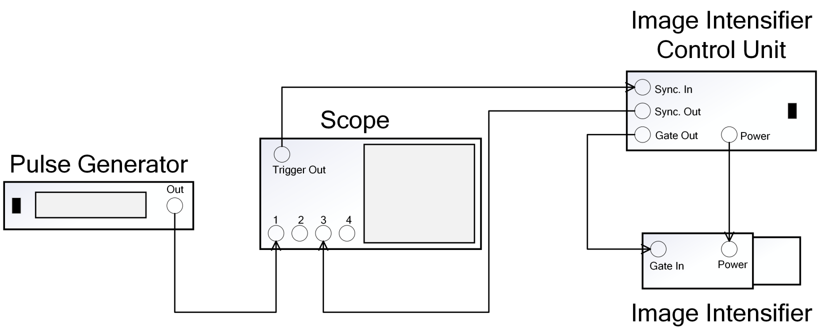


Figure 4.2: Measurement setup for scope intrinsic time delay measurement.

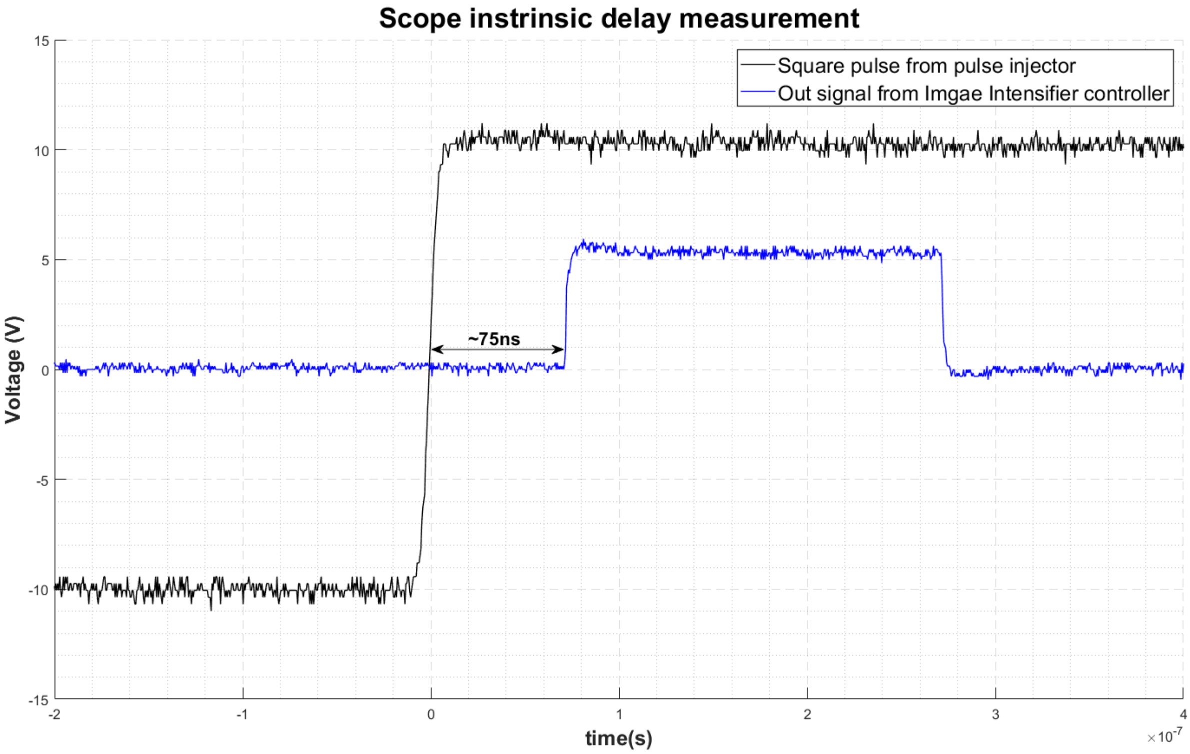


Figure 4.3: Intrinsic time delay measurement of the scope LeCroy LT374 trigger out chain.

During the experiments, it is often necessary to take the scope trigger signal from the Photomultiplier (*PMT*) and in such cases, the intrinsic time delay of the scope can be a limiting factor. The intrinsic time delay of the measurement scope setup has been measured using the setup shown in **Figure 4.2** and is determined as ≈*75ns* for LT374 and ≈*110ns* for HDO6104a (as shown in **Figure 4.3**).Therefore, the LT374 is preferred over the other due to its a lower measurement delay. The HDO6104a is used for determining inception voltages and measuring time delays, thanks to its higher resolution.

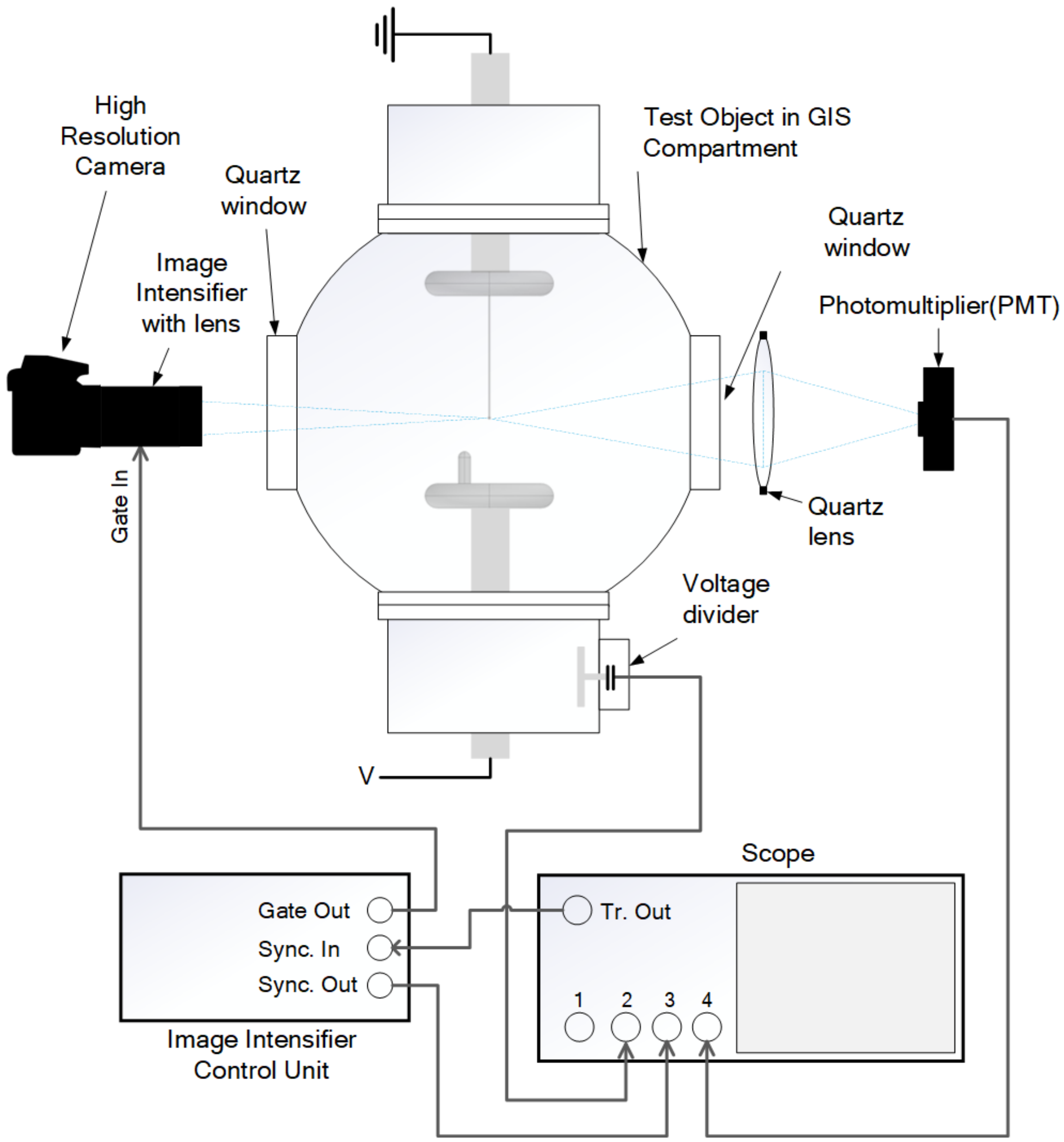


Figure 4.4: Voltage measurement and optical diagnostic setup used in the experiments. HV supply (negative polarity) is applied at the electrode marked as 'V'.

The voltage rise time (90% of peak) was $150ns$. Damped capacitive voltage dividers were used to measure the voltage rise, while a field mill was used to measure

DC voltage (*HAUG Statometer III*[1]). It was located in a metal enclosure with gas-insulated switchgear that also housed the test set-ups. This prevented electromagnetic interference from disrupting diagnostic measurements, thereby eliminating the need for shielding.

### 4.1.3. Optical diagnostic setup

A photomultiplier (*PMT*) is a vacuum tube consists of an input window, a photocathode, a focusing electrode, an electron multiplier and an anode usually sealed into an evacuated glass cylinder(tube). A schematic representation of *PMT* is shown **Figure 4.5**. They are widely used in laboratories to detect extremely low light levels, *e.g.* light emitted during streamer inception. In this work, H9307 type photomultiplier(voltage output type) tube with E717-500 type connector (both from HAMAMATSU) is used.

When the light passes through the input window, it excites the electrons in the photocathode so that the photoelectrons are emitted into the vacuum due to the photoelectric effect. These photoelectrons are accelerated by the electric field and focused by the focusing electrode onto the first dynode where they are multiplied by means of secondary electron emission. This secondary emission is repeated at each of the successive dynodes[42]. This enable *PMT*'s to measure weak light levels down to single photons.

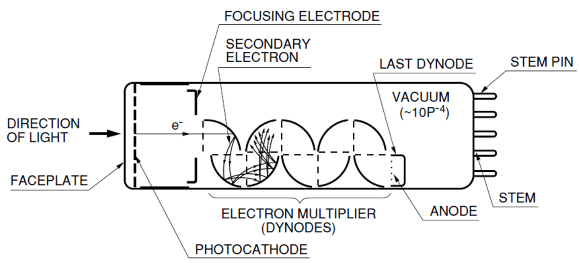


Figure 4.5: Illustration describing operation principle of a PMT - Figure taken from [42].

In order to make *PMT* detect weak light during discharge inception from the test object, an external quartz lens (refractive index = 150) is utilized. The positioning of the lens and *PMT* can be estimated using text book formula given below (**Equation.4.1** and as illustrated in **Figure 4.6**), where $d_i$ is the distance to the image (*i.e.* *PMT*) and $d_o$ is distance to the test object ( =525mm). The same was verified using an LED light source placed right behind expected discharge inception point during the test and reproducing the image of the light source on a white screen placed in the position as the *PMT*. This LED focusing technique was repeated every time time changes made to the test object or in test compartment.

$$\frac{1}{f} = \frac{1}{d_i} + \frac{1}{d_o} \tag{4.1}$$

An *Image Intensifier* along with a *High Definition Camera* is used to make images of the discharges during its propagation across the gap. The purpose of an image intensifier is twofold. One obvious purpose is, as the name suggests, it intensifies the image and and thereby enables capturing maximum spatial information of the

[1]Check http://www.haug-static.com/static-measuring-statometer_III.htm for details

discharge. An image intensifier boosts the intensity of the weak light emitted from the streamers or leaders. It converts incoming photons to electrons and then back to photons significantly increasing the light intensity. Another feature is that, since the photo-cathode can be switched between on and off in a matter of nanoseconds, the image intensifier can act as an ultra-fast shutter for the camera to which it is connected, thus enabling capture of still images of the discharges.

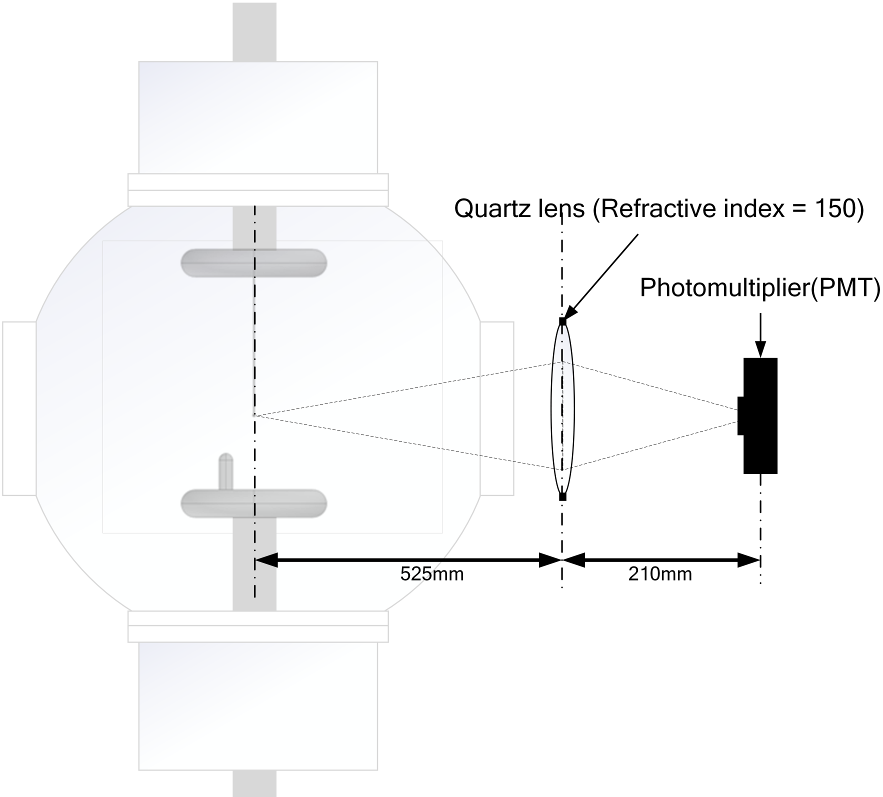


Figure 4.6: Optical calculation and placement of PMT to detect weak light from the test object

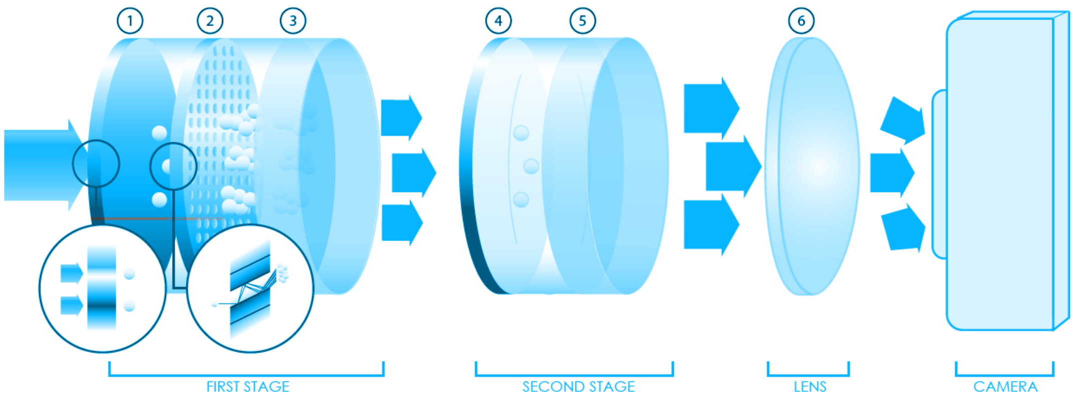


Figure 4.7: Schematics to explain working principle of Image Intensifier(picture from Lambert's website; see footnote)

As depicted in **Figure 4.7**, at stage-1, the photo-cathode in the image intensifier converts incoming photons to electrons. The electrons coming from the photo-cathode is then accelerated towards the micro-channel plates where they are multiplied. The electron gain can be controlled by adjusting the voltage of micro-channel plates. This cloud of electrons gets accelerated towards the anode screen, where the electrons are converted back into photons by the phosphor layer. In the stage-2, photons are again converted to electrons by the photo-cathode and accelerated to the anode screen where the image appears. The relay lens transfers the image from the back of the intensifier onto the mounted camera.

*HiCATT* system from Lambert Instruments. B.V.[2] is used as image intensifier with gate time varied from several *nano* seconds to *micro* seconds. The DSLR camera *NIKON D7000* is used for capturing the images with ISO setting varied from 2500 to 3200.

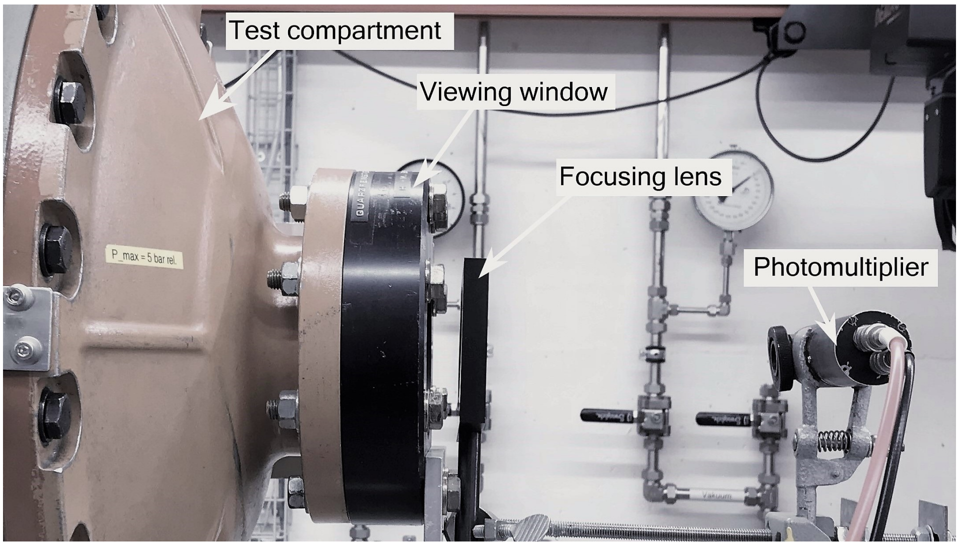


(a) Photograph that shows position of PMT and focusing lens

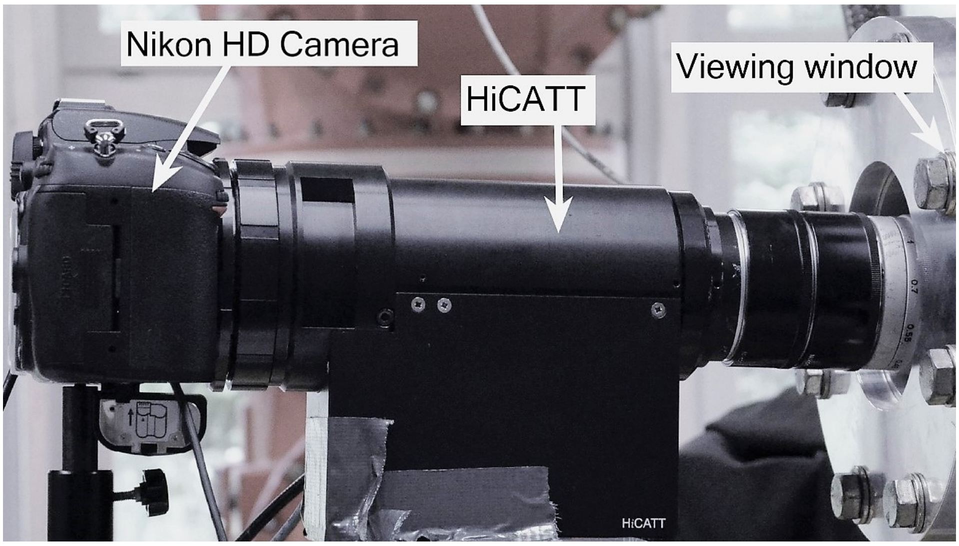


(b) HiCATT (Image intensifier) and Nikon D7000 (DSLR camera)

Figure 4.8: Optical diagnostic setup used in the experiment

[2]Details can be accessed on https://www.lambertinstruments.com/image-intensifiers

### 4.1.4. Test objects

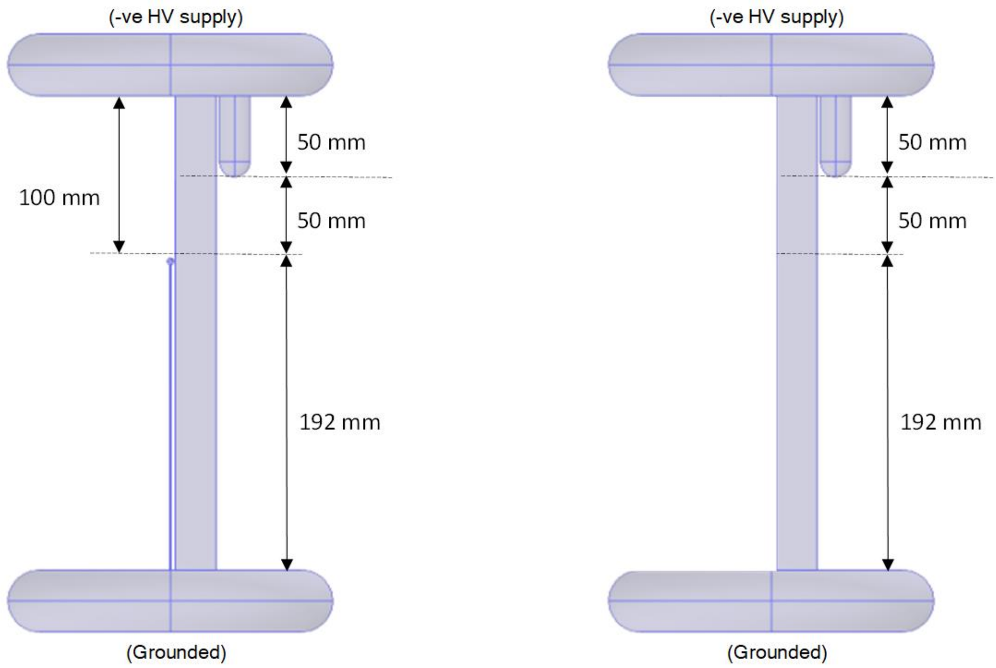


(a) Test object-1 used for breakdown tests, inception measurements and optical investigation.

(b) Test object-2 used for optical investigation of secondary discharge from plug.

Figure 4.9: The two main test objects used in the experiments. In both test objects, top plate where plug is located, is supplied with negative polarity high voltage. The Opposite side was grounded.

Two test objects were used for the experiments. Test object-1 consists of a steel rod with a sphere on one end as shown in **Figure 4.9a**. The radius of the spherical tip of the rod is $2mm$, and the total height is $192mm$. A $100mm$ radius circular plate (with thickness=$38mm$ and edge curvature radius =$19mm$) is provided on the side opposite it, with a 100mm gap between them. This gap distance is typical for high voltage applications. As a result of the rod, a strongly non-uniform background field can be generated. A steel plug (height = $50mm$, radius = $9.5mm$, and tip radius = $9.5mm$) is connected to a steel plate that is vertically separated from the rod by a $30mm$ gap. As a high field region, the plug is placed mainly to act as a potential source for the secondary discharge under investigation. The dimensions of the plug are similar to the parts used in many high-voltage applications. The plug was separated from the rod using a PTFE plate of $25mm$ thickness. Thus, breakdown across the rod and plug will be avoided, and optical diagnostics will become easier.

Test object-1 is mainly used for three purposes;-

1. Run breakdown tests on $SF_6$ and $CO_2$ at different pressure ranges and determine the breakdown voltages.
2. Run a set of breakdown tests and determine inception voltage, statistical time lag and formative time lag of the main discharging produced in the rod (which is going to cause breakdown).

3. Run another set of tests with optical diagnostics and investigate the occurrence of inception at the plug (secondary discharge).

Test object-2 is basically the same as test object-1, except the main breakdown source (the rod with the spherical tip) is absent (see **Figure 4.9b**). The purpose of this test object is to investigate the inception and statistical time lag of a discharge event when a propagating discharge is absent near its vicinity. the maximum field on the surface of the plug is approximately the same in both test object-1 and test object-2 and hence comparison of discharge inception in both test objects will give us a meaningful result. We perform an optical investigation on test item-2 both for $CO_2$ and for $SF_6$ at various pressure ranges.

### 4.1.5. Experimental limitation

It is important to point out some of the limitations of the *Van de Graaf* based test system used in this study. Below are the details.

1. When there is inception/partial discharge but no breakdown in the test object, there is a decaying voltage due to the lack of a constant energy source. As a result, the voltage applied cannot be considered as DC anymore.

2. Although the maximum voltage limit of the test system is $400kV$, the maximum voltage achieved in practice was only $340kV$. There was apparently a problem with a solid insulation component and fixing it was not a viable solution at the time.

3. As the maximum achievable voltage without decay was around $300kV$, it was difficult to obtain sufficient data about the statistical time lag and inception voltage when testing with $SF_6$.

Another limitation is related to the oscilloscope. In order to measure voltage and set up the image intensifier trigger, two different scopes were used. Details are presented in **Section 4.1.2** and **Figure 4.2** and **4.3**. In **Figure 4.2**, it was explained that the lowest intrinsic delay was obtained when LT374 is used, which was $75ns$. When using $0.6MPa$ $CO_2$, $0.4MPa$ $SF_6$ and $0.6MPa$ $SF_6$, discharge propagation was fast and formative time lag was less than $100ns$. There was no way to set the intensifier gate trigger effectively in such cases. This occurs because the gate of the image intensifier is delayed by intrinsic time and will only open after this time, so the discharge will already have bridged the gap.

One important point to note is that the VdG test setup used at that time was only capable of supplying negative polarity voltages. Previous studies (Seeger et al. [19] using DC in the pressure range $0.1MPa$ to $0.4MPa$ and Kumar et al. [32] using LI in the pressure range $0.2MPa$ to $0.7MPa$) shows that the breakdown fields increase linearly with pressure for negative polarity in non-uniform fields. That means, non-uniformity of the background field does not matter; only pressure and gap distance matter[19]. As such, by applying negative polarity, we can ensure that the only factors affecting inception at the plug (secondary discharge) are the background field and pressure. Also, inception detection at negative polarity exhibits fewer scatters than a positive polarity. It has been decided to apply negative polarity at the plug area to look for secondary discharges since it is the main area for observation for secondary discharges. The rod is grounded, which means that the rod was at positive E-field.

## 4.2. Procedure

From the flow chart below (see **Figure 4.10**) shows the systematic approach that has followed throughout this project.

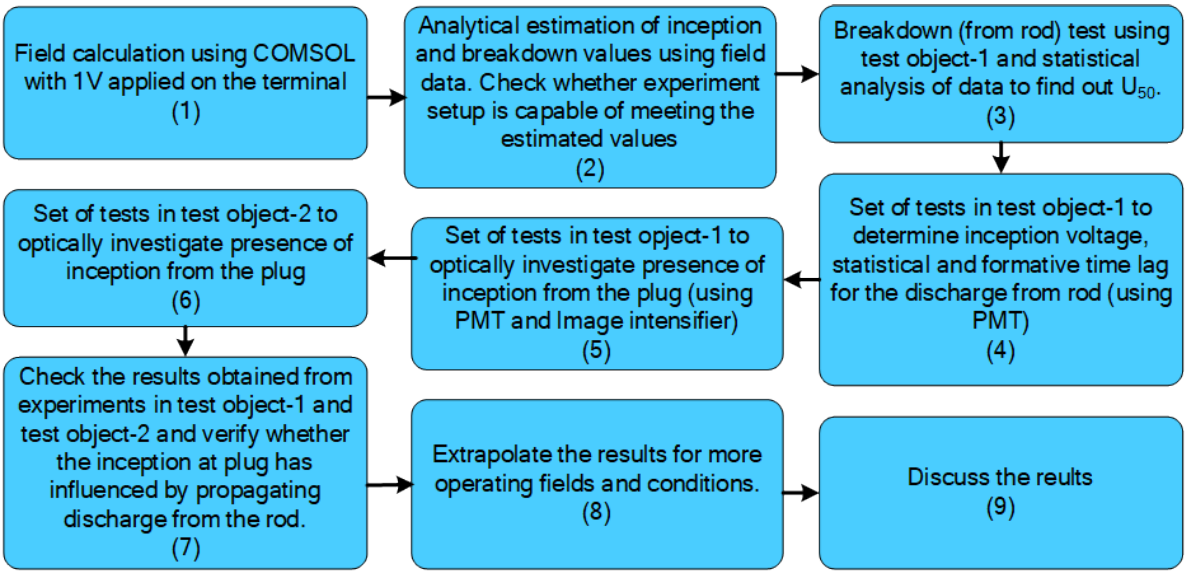


Figure 4.10: Systematic procedure followed in this project

Further details are given in the upcoming subsections.

### 4.2.1. Field calculation

COMSOL Multiphysics AD/DC electrostatics module is used for all electrical field calculations. Simulations are carried out using rods having an applied voltage of -1V (or, in the case of test object-2, the plate that is normally connected to the rod). The field calculations have three main objectives:-

⇒ To determine the magnitude of the E-fields at the tip of the rod and surface of the plug during and before discharge propagation.

⇒ To prepare input field values for the MATLAB script-based tool. the Hitachi ABB PG CB research group developed this tool that allows us to calculate the background field, streamer inception, leader inception, and breakdown voltage for different pressures and temperatures. For each of the test objects, inception and breakdown values are calculated. Details are discussed in **Chapter 6**.

### 4.2.2. Calculation of inception and breakdown voltage

As stated in the previous section, the inception and breakdown calculation is performed using an in-house tool developed by the *Hitachi ABB PG* CB research group. The tool needs E-field values along the axisymmetric line (line along which breakdown is expected) as the main input along with pressure and temperature.

Details about how this tool works have been discussed in [19] and [17]. As given by **Equation.4.2**, the streamer inception is based on the integral in the axial direction z (input from the field simulation in COMSOL) over the effective ionization coefficient ($\alpha_{eff}$), which is controlled by the electric field, temperature, and pressure.

$$\kappa = \int_0^{l_{cr}} \alpha_{eff}.dz, \tag{4.2}$$

with $\kappa$ = $10.5$[43] for $SF_6$ and $13$ for $CO_2$ [19].

A critical length $I_{cr}$ is the distance at which the electric field falls to the critical field $E_{cr}$ = $E_{cr,0}$×$p$, where $E_{cr,0}$ = $89V/(m.Pa)$ for $SF_6$ and $21.5V/(m.Pa)$ for $CO_2$. Streamer $L$ is the length of the channel following the requirement that the potential at the open end of the channel equals that of the background field. When the **Equation.4.3** conditions are met, this is the case.

$$\int_0^{l_{cr}} (E(z) - E_{cr}).dz = \int_{l_{cr}}^{L} (E_{cr} - E(z)).dz, \tag{4.3}$$

As shown in [44] the maximum streamer length $L_{max}$ is given by **Equation.4.4**.

$$L_{max} = \frac{U}{E_{cr}} \tag{4.4}$$

As outlined in [18], to achieve breakdown the transition from streamer to the leader as well as leader propagation is necessary. One can take it as given that the streamer channel field is at the critical field [44]. Here, the same approach given in [45] to the leader breakdown criterion is used. The streamer channel tip needs to be enhanced above the critical field level in order to initiate the leader. If the streamer corona current heats the channel sufficiently, the field at the tip is sufficiently enhanced to ensure that the voltage drop (**Equation.4.5**) along the channel after the heating is less than the voltage drop of the background field.

$$\Delta U_c = \int_0^{L} E_{cr,f}.dz = \int_0^{L} E_0.dz, \tag{4.5}$$

Following channel heating and expansion, the channel field $E_{ch}$ was assumed to be at the critical field $E_{cr,f}$ corresponding to a higher temperature $Tf$ and a higher atmospheric pressure $P$. [18, 45]. It is approximately sufficient that the channel voltage drop $Uc$ along the leader channel is equal to the background field voltage drop $U0$ in uniform background fields $E0$, as discussed in [18]. Using a non-uniform background field, such as that described in [45], it is necessary to reduce the channel voltage drop significantly to counterbalance the background field decay (**Equation.4.6**).

$$\frac{\Delta U_c}{U_0} \leqslant \kappa \tag{4.6}$$

with $\kappa$ < 1.

The leader breakdown criteria is defined in terms of leader length and this is done for simplicity. When the leader length reaches 90% of the total gap length, that has been considered as a breakdown.

A detailed explanation of leader inception and breakdown is given in [18], which also mentions the numerical tool used for this purpose. Several simplifications have been made to the tool in order to reduce complexity and they are as follows:-

⇒ It ignores the spatial randomness of the leader propagation direction by assuming that it propagates along the axis of symmetry of the protrusion(rod or plug) parallel to the background field $E0$.

⇒ Leader branching is not taken into account.

⇒ It assumes that the electric field distribution is *Laplacian* and neglects the effects of space charges.

### 4.2.3. Experiment procedure

Experiments were conducted on two test objects, test object-1 (**Figure 4.9a**) and test object-2(**Figure 4.9b**), as explained earlier in **Section.4.1.4**. They can be categorized into three types depending on the objective.

1. Experiments to determine the $50\%$ breakdown voltage ($U_{BD50}$) of test object-1.
2. Tests to determine inception voltage, statistical time lag, and formative time lag (using the PMT in both test objects 1 and 2).
3. Investigating secondary discharges from the plug of test object-1 (using the Image Intensifier and PMT).

Detailed descriptions are provided in the upcoming sections.

### 4.2.4. Breakdown test procedure

Up and Down testing is the most famous method for estimating the required breakdown probability voltage. It is intended to estimate voltage levels for a given breakdown probability. Any quantile can be evaluated using the Up and Down procedure, for example. The $U2\%$ or the $U10\%$. It is usually determined by evaluating the $50\%$ quantile. One of the main advantages of this method lies in the relatively low experimental effort to estimate specific quantiles. Nonetheless, this method does not always provide full breakdown probability information. Furthermore, this method can only be used for applications that involve impulse voltages or step-DC.

For our purpose, we are going to use a step DC voltage source (see **Section.4.1.1**) to deduce a lightning impulse equivalent $50\%$ breakdown voltage. It has been shown that breakdown tests with a time to breakdown($t_{bd}$) below or equal to $10\mu s$ with applied DC are comparable to the $LI$ level, based on Hitachi ABB Power Grids CB research team's previous research. Therefore, since we wanted breakdown statistics that occurred within a short time frame of $10\mu s$, the Up and Down method was not the best. It is not practical to set the *time to withstand* to microseconds when using the Up and Down method; instead, it is normally set to some tens of seconds. There is no practical way to get enough statistics so that we can classify them as breakdowns in such a case. Therefore, a random voltage procedure was used.

A random-voltage procedure is a non-standard experiment (only used at Hitachi ABB PG Research Centre) that tries to minimize the disadvantages of the Up and Down method. The random voltage procedure is designed to generate a useful data set for estimating the breakdown probability distribution while minimizing statistical dependencies in the experiment. By using this method, we obtain the maximum amount of information with the least number of shots and random voltage applications, which results in a random breakdown and distribution. As a result, systematic conditioning is reduced.

The procedure is as follows:-

1. Considering that the breakdown probability curve follows a normal distribution, one needs a rough estimate of the $50\%$ breakdown voltage and the standard deviation. An educated guess (based on analytically calculated results) or a short and rough Up and Down procedure can be used to achieve this.

2. A voltage window is then selected based on U50 ±3×$\sigma$ and a certain number of voltage applications are selected (typically 100-200), evenly and randomly distributed in the window.

3. A random voltage vector and an associated breakdown/hold vector are the outcomes of the experiment. Using a generalized linear model, the data - i.e. continuous voltage input versus binary result outcome (breakdown or withstand) - can be fitted to a probability distribution function.

The post-processing is further described in **Section.4.3**.

### 4.2.5. Tests to determine inception and time lags

In this test, a PMT measurement setup is used (as shown **Figure 4.4**). With a camera and photomultiplier, discharge inception is detected across a wide range of voltages ($50kV$ to $300kV$). At this stage, an image intensifier is not being used as it was not necessary. As the HD camera shutter was open for 30 seconds, it was able to capture an integrated image of all the lights emitted within the compartment. Inception should appear in both camera and PMT signals if it has been detected. With the oscilloscope, the statistical lag of inception can be determined by examining the PMT signal. The LeCroy HDO6104a oscilloscope (with a bandwidth of up to $1GHz$ and a sampling rate of up to $10GS/s$) was used for this purpose. The high sampling rate makes it a good fit. In order to detect time lag for late inceptions, the scope was set in 2 sequences (sequence mode) with $50\mu s/div$ horizontal scale in each sequence. The voltage measurement channel was always set as the trigger. In order to avoid over exposure of the image, HD camera ISO was set to a minimum ($ISO100$).

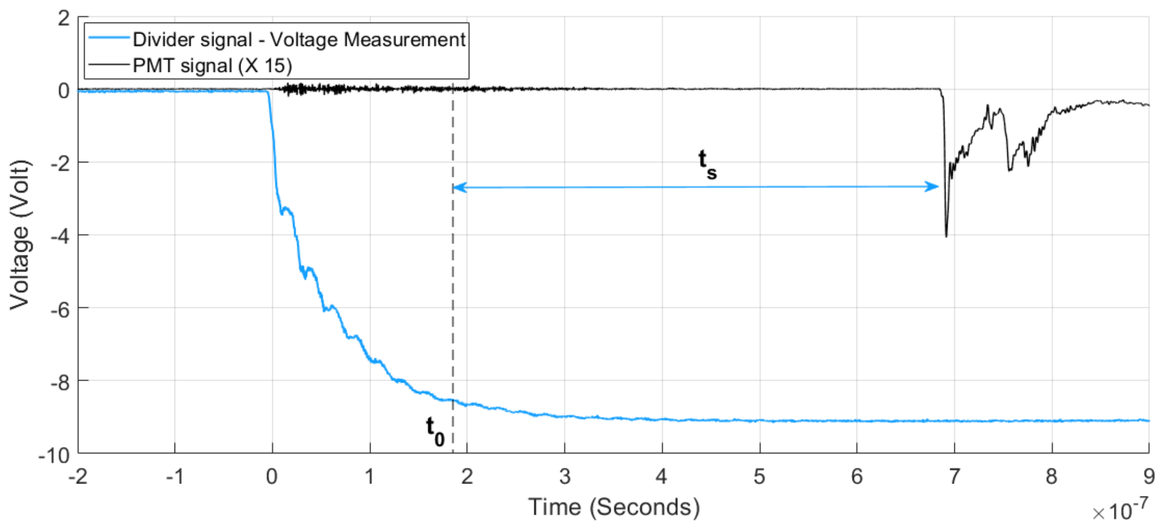


Figure 4.11: PMT signal from an arrested leader event highlighting statistical ($t_s$)

**Figure 4.11** shows a typical PMT signal recorded in scope. Statistical time lags can be assessed from such recordings. The first electron event always creates the largest peak in the PMT signal, followed by the first corona[19]. Statistics time lag ($t_s$)[5] describes the time it takes for the voltage to reach a steady level and to detect the first corona.

In addition to the statistical time lag, the formative time lag can also be recorded when the applied voltage reaches the breakdown region. **Figure 4.12** illustrates formative time lags and statistical time lags from PMT signals. Formative time lag($t_f$) is how long it takes a discharge to pass the gap. Time can be measured from the time of the first corona (streamer) event to the time when there is a voltage collapse[5].

## 4.2.6. Tests to detect secondary discharge

Optical diagnostic arrangement as shown in the **Figure 4.4** was used for this set of tests. The formative time lag and breakdown voltage range for each applied voltage must be known in advance when performing these tests. To capture an image of the propagating discharges, the trigger to the image intensifier shall be set on the first corona detection from the PMT and the gate shall be open only for a few $\mu s - 100ns$ during the formative time lag. The much larger light emitted from the breakdown event can overexpose the image intensifier and the camera if the gate and trigger are not properly set. The phosphorus coating of the image intensifier can be damaged by such frequent overexposure.

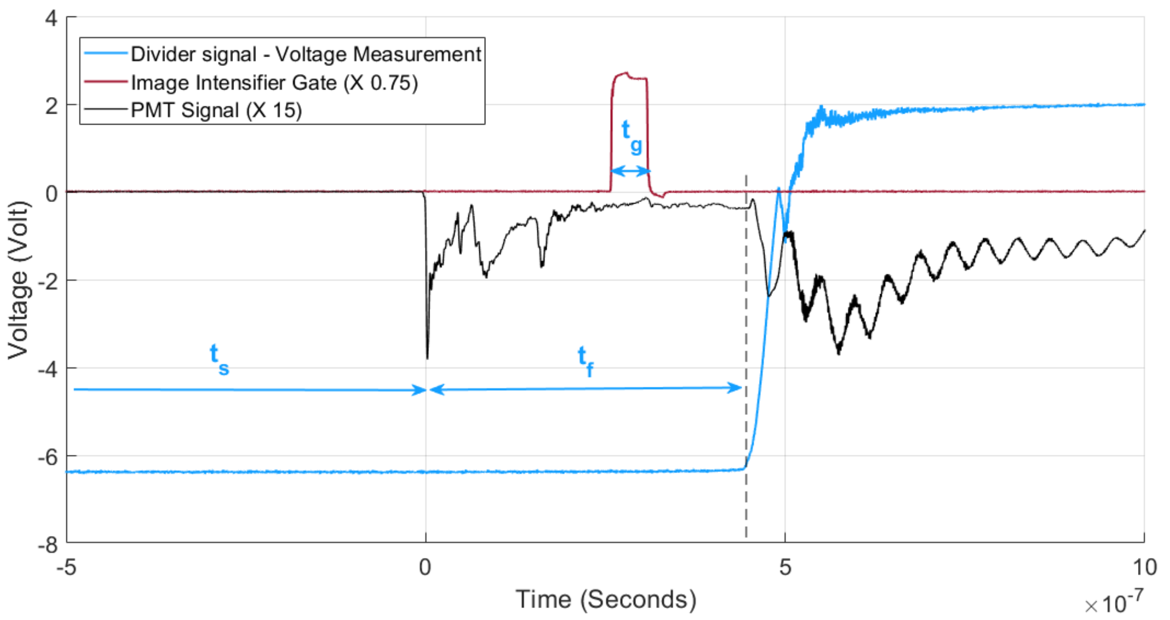


Figure 4.12: PMT signal from a breakdown event highlighting statistical($ts$)and formative($t_f$) time lag

The intrinsic delay of the scope will largely limit positioning of the image intensifier gate time in the formative window in this case. Because there is only a $75n$s internal delay in this scope, we are using the LeCroy LT374 for these tests.

**Figure 4.12** illustrates this. In this example, the trigger source was set to the PMT signal channel, and the trigger out of the scope was connected to the image intensifier trigger-in. The gate opens for a pre-determined gate time as soon as PMT detects a first corona event, triggering the image intensifier. instead, the gate opened after a $75ns$ delay (LeCroy LT374). The problem of time delay largely restricted the optical investigation at high pressures. It makes sense since breakdown voltage was higher at higher pressures, and formative time lag was smaller at higher voltages. In short, the scope delay makes optical diagnostics impossible due to the smaller values of formative time lag approaching some $100ns$.

Consider, for instance, a predetermined formative time lag of $300ns$ and an already known scope delay of $75ns$. A good image of propagating discharge must be obtained if we set the scope trigger on the PMT signal and gate time at around $50 - 100ns$.

## 4.3. Statistical analysis of experiment data

A non-parametric empirical cumulative distribution based on *Turnbull's algorithm* is used to build the statistical model of a breakdown experiment, followed by fitting a *three-parameter Weibull Distribution* to extract its parameters. The upcoming section explains how it is done. By this means, the $50\%$ breakdown voltage and the standard deviation can be easily be determined.

### 4.3.1. ECDF based on Turnbull's algorithm

An *Empirical Cumulative Distribution Function (ECDF)* is calculated so that a distribution function can be fitted to the experimental results. Iterative estimation of the survival function, $S(X)$, was used for doubly censored data. Using the survival function, the failure function $F(X)$ was calculated as $F(x)$ = 1 - $S(x)$. Bruce W. Turnbull proposed this non-parametric estimator in 1974[46].

Initially, the algorithm was supposed to determine the distribution of the time for an event to occur when censored data was provided. Suely R. Giolo has implemented and illustrated this algorithm[47]. Based on limited information about the exact time of death, Giolo used the algorithm to estimate patients' lives. The breakdown tests in this project was performed using random voltage application and the breakdown voltage level obtained in this way can be considered as a doubly censored data. Rather than using time, a voltage increase was used in the current project, using MATLAB scripts created by the *Hitachi ABB PG* CB Research team.

Taking each experiment as an independent event, it is unknown at any moment exactly what voltage should be applied to cause a breakdown. Suppose a voltage was applied and it resulted in a hold, then the exact breakdown voltage, the voltage that would have caused a breakdown at that moment, was higher than the applied voltage. In the event of a breakdown caused by the applied voltage, the breakdown voltage was equal to or lower than the applied voltage. Thus, voltages that resulted in a hold, not a breakdown, could be considered right-censored data. Voltages that resulted in breakdowns were then considered left-censored data, while the exact voltage that would have caused a breakdown remained unknown. The following steps explain the method and algorithm based on Giolo's version.

#### Determining intervals and creating coefficient matrix $\alpha$

Assuming $0$ = $x_0$ <$x_1$ < $x_2$ < $x_i$ < ... < $x_m$, represents a sorted grid of all unique voltages that includes all $X_i$ records for $i$ = $1$,...$n$, where $n$ is the number of all recorded voltages and $m$ is the number of unique voltages recorded. For the $i$th observation define a weight $\alpha_{ij}$ to be $1$ if the voltage interval $(L_a, U_i]$ contains the voltage $X_i$ where $L_i$ is the lower limit of the interval and $U_i$ is the upper limit of the interval. $\alpha$ is a matrix with the dimension $[nxm]$. The weighted alpha indicates that the exact breakdown voltage at the applied voltage $X_i$ could have been at the voltages $x_j$ where $\alpha_{ij}$ = $1$ [47].

#### Determining the Weight $\alpha_{ij}$ for censored data

Since the exact breakdown voltage was unknown, all data from the random test method was censored. Based on the assumption that no breakdowns would occur at zero voltage, the lower limit $L_i$ for left-censored (breakdowns) data was set to zero. The upper limit was set at the recorded voltage. This indicates that the actual breakdown voltage at the voltage $X_i$ was in the interval $(0, X_i]$. Thus, all $\alpha_{ij}$ coefficients associated with this were set to $1$. The breakdown voltage for right-censored values (holds) should be higher than the recorded voltage $X_i$. It should be in the interval $(X_i, \infty)$, in which all corresponding $\alpha_{ij}$ were set to $1$[47].

### Turnbull's algorithm

The algorithm proposed by Turnbul in [46] which later adapted by Giolo[47] involves the following steps.

1. Make and initial guess for $S(x_j)$ from either the Kaplan-Meier estimator (also given in Step.5) or simply taking $\frac{1}{n+1}$.
2. Compute the probability $p_j$ of the event happening at the voltage $x_j$ using
$$p_j = S(x_{j-1}) - S(x_j) \quad j = 1, ...m \tag{4.7}$$
3. Estimate the number of $d_j$ that occured at $x_j$ using
$$d_j = \sum_{i=1}^{n} \frac{\alpha_{ij} p_j}{\sum_{k=1}^{m} \alpha_{ij} p_k} \quad j = 1, ...m \tag{4.8}$$
4. Compute estimated number at risk at $x_j$, $Y_j$ using
$$Y_j = \sum_{k=j}^{m} d_k \quad j = 1, ...m \tag{4.9}$$
5. Using the product-limit estimator (the Kaplan-Meier estimate), obtain the new estimate for $S(x_j)$ based on the values of steps 3 and 4.
$$S(x_j) = \prod_{i=1}^{m} (1 - \frac{d_i}{Y_i}) \quad j = 1, ...m \tag{4.10}$$
6. When the algorithm reaches a self-consistency, the updated version of S is close to the previous version at a predefined limit. Otherwise repeat step 2 to 5 with new estimation for $S_{new}$ as new guesses estimate.
$$max|S(x_j)_{old} - S(x_j)_{new}| < 1.10^{-5} \tag{4.11}$$

At a given voltage, the survival function indicates the probability of a hold. As holds and breakdowns can be viewed as complementary events, the empirical cumulative distribution function can be calculated by $F = 1 - S$. A MATLAB script based on the above steps has been used to create ECDF of the breakdown data.

### 4.3.2. Fitting to Weibull distribution

*3-parameter Weibull* distributions are extreme value distributions. It is particularly appropriate for the description of breakdown processes, because it is normally assumed that there is a minimum breakdown voltage, i.e. a location parameter $U0$. We assume $U0$ to be the streamer inception voltage ($U_{streamer,Inc.}$).

As a result of all the extreme values for all possible events, the cumulative distribution function shows an analytical expression in the **Equation 4.12**. This holds for all values U that is higher than the initial value $U0$.

$$F(U) = 1 - exp^{-\left\{\frac{U-U0}{U63-U0}\right\}^{\delta}} \tag{4.12}$$

The *Weibull* distribution can be described by three parameters; $U0$ (location parameter, Initial value, lower extreme value), $U63$ ($63\%quantile$), and $\delta$ (shape parameter or slope). In general, the *3-parameter Weibull* distribution gives a good estimate of the cumulative frequency polygon for a series of measurements when you combine the parameters of location, shape, and scale[5].

Previous literature, such as [48] and [49] have emphasized the suitability of the *Weibull* distribution for such applications. The experimental results indicate that the pulsed breakdown voltage in pressurized $CO_2$ follows the *Weibull* distribution[48]. Odd et al[50] used $Turnbull$ estimator in combination with a *Weibul fit* to estimate breakdown voltage for protrusions under similar conditions.

The non-parametric *Turnbull* algorithm is fitted to the *3-parameter Weibull* distribution using a MATLAB script. The *fit* function in MATLAB is mainly used for fitting to **Equation 4.12** with the *Nonlinear-Least-Square-Error (NLSE)* method. In [51], the advantages of the least square method for such purposes are outlined.

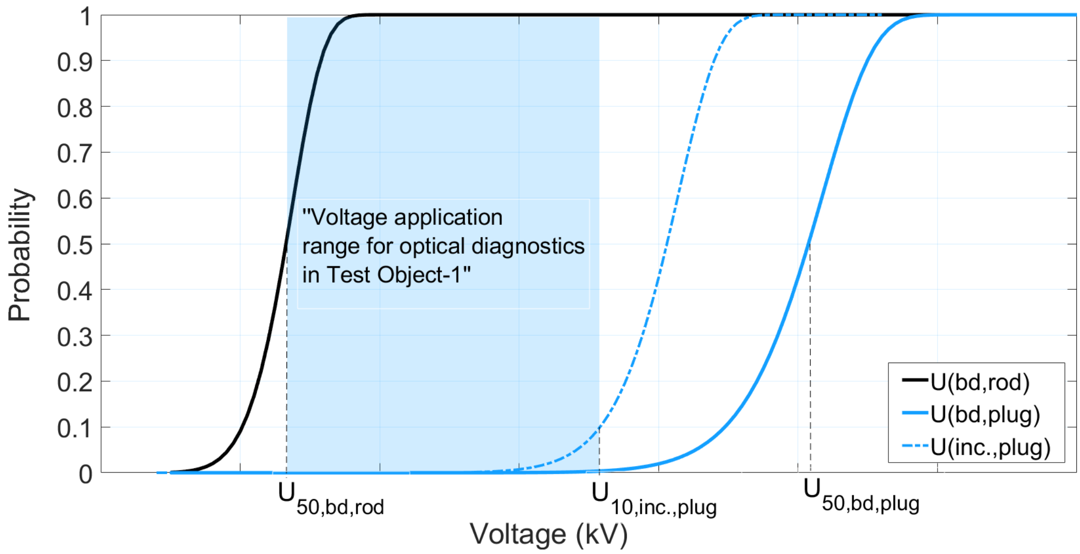


Figure 4.13: The Figure shows ideal voltage range for optical diagnostic tests in Test object-1. Inception and breakdown distribution of plug (*blue line* and *blue dotted line* are shows only for understanding.

The $50\%$ breakdown voltage ($U50$) obtained from the distribution is generally accepted as the standard breakdown voltage. Therefore, $U50$ is calculated from *Weibull* distribution using a simple graphical method. Under various conditions, this breakdown voltage value is used to understand suitable voltage applications in **Test object-1**. Ideally, the voltage applied shall be $\geqslant U50_{rod}$ ($50\%$ breakdown voltage of the plug) and $< U10_{plug,inc}$ ($10\%$ streamer inception voltage of the plug) and this is graphically represented in **Figure 4.13**.

## 4.4. Additional information

As far as this experiment is concerned, it is important to notice the following.

1. The experiment uses a $CO_2/O_2$ $(90 : 10)$ mix as the insulation medium instead of pure $CO_2$. Accordingly, if the filling pressure is $0.6MPa$, first pure $O_2$ is pumped until $0.06MPa$, then pure $CO_2$ (which constitutes $0.56MPa$) is pumped until total pressure reaches $0.6MPa$. Previous publications [31, 32, 37] have shown that the breakdown strength of the $CO_2/O_2$ mixture is comparable to pure $CO_2$. Because of the electron attaching the property of $O_2$ and its ability to prevent the formation of carbon soot during arcing, $CO_2/O_2$ is an interesting mixture. In this experiment, the $CO_2/O_2$ mix is selected based on its actual use in some products.

2. A VdG-based test voltage injection setup is used in this experiment. The test injection setup was set up so that it provided stepped DC voltage up to approximately $330kV$ with negative polarity. Test objects are placed in the compartment so that, when the voltage is turned on, a negative polarity field appears on the plug surface, and with respect to that, a positive polarity field appears on the rod. Thus, the primary discharge from the rod occurs when it is stressed with a positive field and it ultimately leads to a breakdown. Similarly, the plug from which we expect secondary inception to occur is stressed with negative polarity. The following understandings guided polarity selection. According to [19, 32, 50], the breakdown field of negative polarity (for LI waveform) is comparatively lower than that of positive polarity and so we would expect to see a secondary discharge at a comparatively lower applied field if such a phenomenon occurs. Furthermore, negative polarity's statistical time is less scattered when compared to positive polarity. Keeping the negative polarity field at the plug as our focus will allow us to study it more thoroughly using analytical parameterization.

3. In order to reduce the effect of surface roughness, the plug surface is sandblasted to get an even surface roughness of size $50\mu m$

# 5

# Results

Calculations and tests are performed in accordance with the procedures described in the previous chapter, and results are presented in their respective sections.

## 5.1. Field calculations

The simulations are run using COMSOL Multiphysics. A 3D geometry was created using the Design Module, while the DC/AC module was used to calculate electric field values. It is necessary to provide the E-field value along the breakdown path (the decay of electric field strength) so that the inception and breakdown values can be calculated using MATLAB scrips developed by Hitachi ABB PG Team. A similar approach can also be seen in [19, 50].

### 5.1.1. Field calculation for Test object-1

The geometry for test object-1 (**Figure 5.1a**) was created in accordance with dimensions shown in **Figure 4.9a**. A relative permittivity of $2.1$ is selected for the $PTFE$ material. A $-1V$ voltage is applied to the plate where the plug is located, and the rod is grounded. According to the field calculation result (**Figure 5.1b**), the maximum field is $212V/m$ at the rod surface and $70V/m$ at the plug surface. For both the plug and the rod (**Figure 5.2**), the decaying electric field strength along the vertical path is extracted and prepared as the input parameters for the MATLAB-based tool (refer to **Section 4.2.2**). Similarly, **Figure 5.2** shows field along a vertical path from plug when there is a propagating discharge from rod. These field values are used to calculate inception and breakdown voltages from the plug in such conditions.

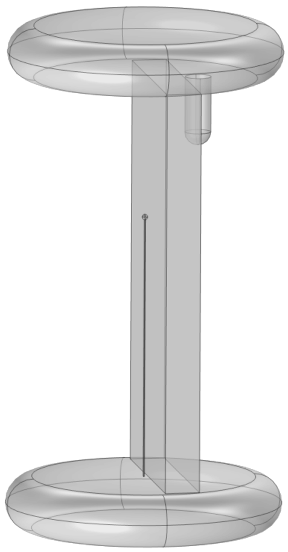

(a) Geometry of Test object-1; all dimensions are as per Figure 4.9a

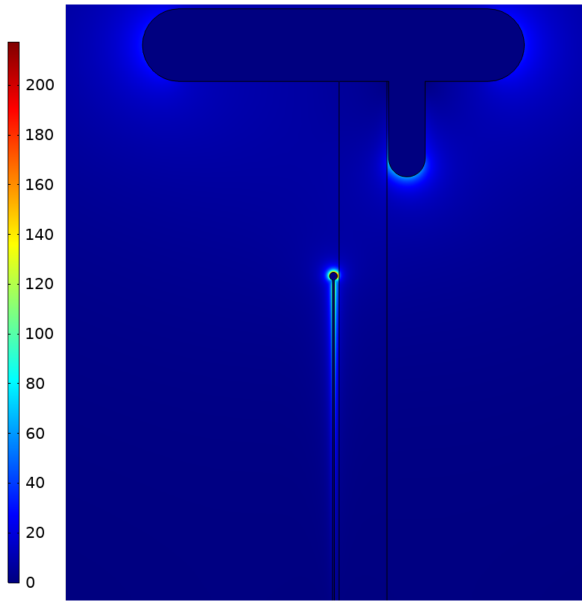


(b) Field distribution when -1V applied to the electrode where the plug is connected and the rod is grounded

Figure 5.1: Field distribution when -1V applied to the electrode where the plug is connected and the rod is grounded

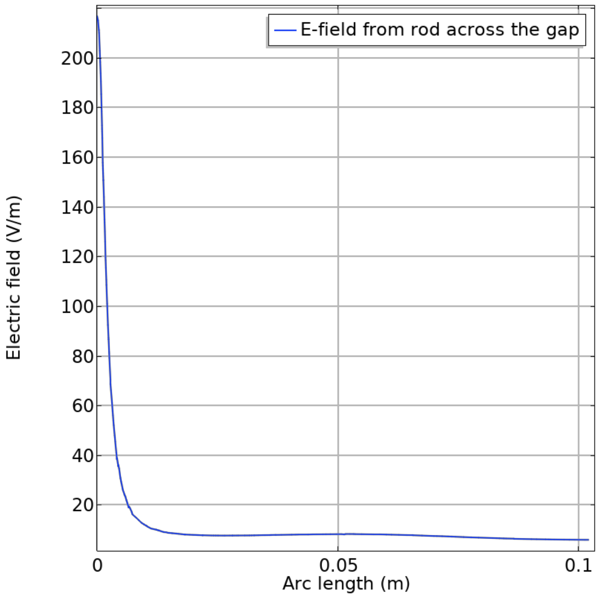


(a) Test object-1; E-field along the vertical line from the rod surface to opposite electrode

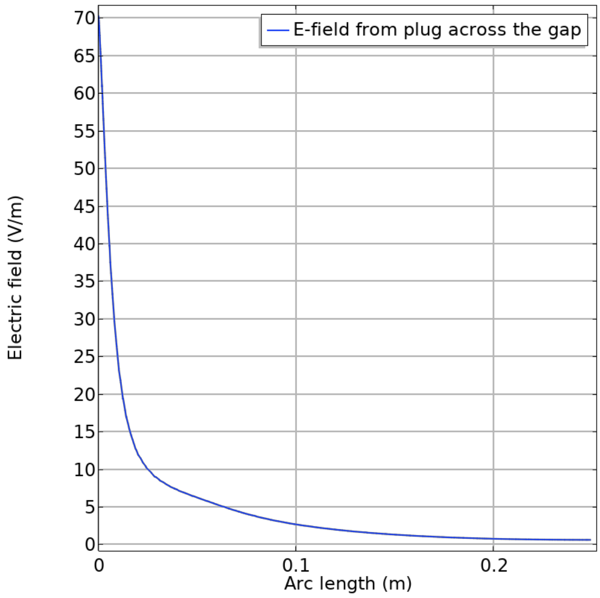


(b) Test object-1; E-field along the vertical line from the point on plug surface (where field is maximum) to opposite electrode

Figure 5.2: Input values used for analytical calculations of inception and breakdown (as explained in Section.4.2.2)

.

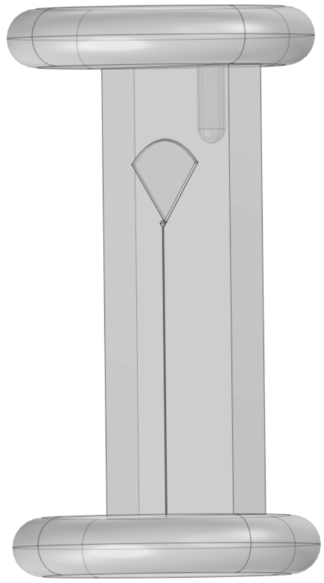

(a) Test object-1; geometry which also demonstrate propagating discharge from the rod

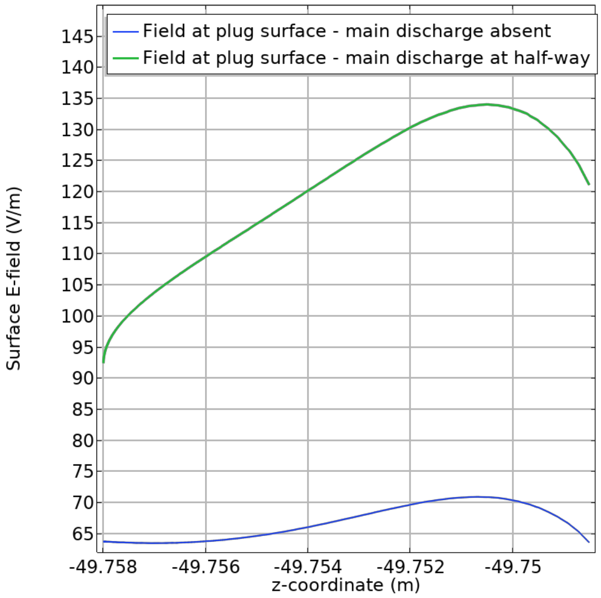


(b) Test object-1; Comparison of E-field along the surface of the plug (from top to the corner towards PTFE) with and without discharge propagation from the rod

Figure 5.3: Simulation of field enhancement at the plug surface in presence of a propagating discharge from the rod.

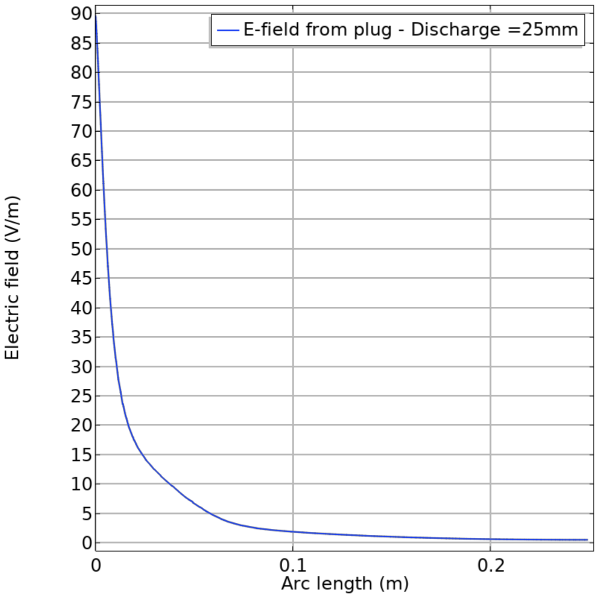


(a) Test object-1; E-field along the vertical line from the plug surface to opposite electrode when the primary discharge reaches 25mm (a quarter of the gap distance

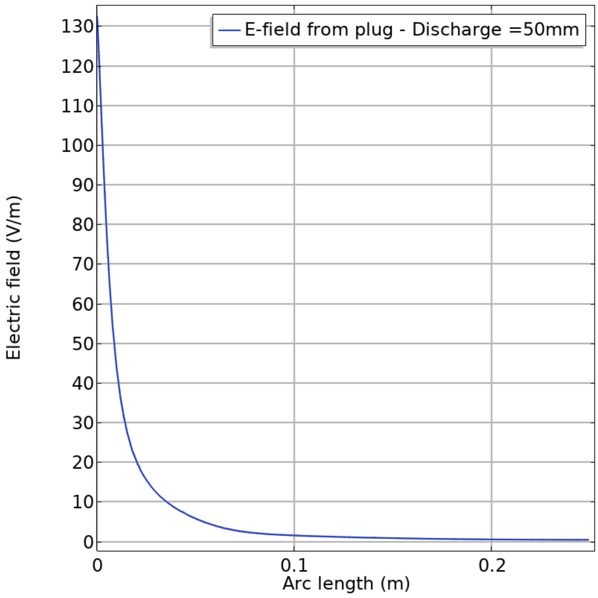


(b) Test object-1; E-field along the vertical line from the plug surface to opposite electrode when the primary discharge reaches 50mm (half of the gap distance

Figure 5.4: Simulation of field enhancement at the plug surface in presence of a propagating discharge from the rod (Input date of analytical estimation of breakdown values.)

An additional set of simulations is performed to understand the magnitude of field enhancement at the plug surface during discharge propagation from the rod. To accomplish this, a thin layer material with a high permittivity value $(e.g.10000)$ is created over the rod. According to the article[19], the discharge can be assumed as same size as the streamer radius, i.e., about some $100\mu m$ in thickness. To keep things simple, a thickness of $1mm$ is used in the simulation. The length of the discharge is varied. **Figure 5.3** compares simulation results for $25mm$ and $50mm$ lengths. In addition, these inputs are used in the calculation tool to learn how the inception and breakdown voltages changed in the presence of another propagating discharge. **Figure 5.3b** shows that the field at the surface of the plug almost doubled (to $135V/m$ from $70V/m$) when the propagating discharge reached halfway across the gap.

### 5.1.2. Field calculation for Test object-2

The purpose of test object-2 is to understand the inception field on the surface of the plug when the rod from test object-1 is absent. **Figure 5.5a** shows its geometry, and all its dimensions are the same as those of test object-1. **Figure 5.5b** compares the field values for plug in test object-1 and plug in test object-2. In both test objects, the plug is almost equally stressed if there are no any discharges from the rod.

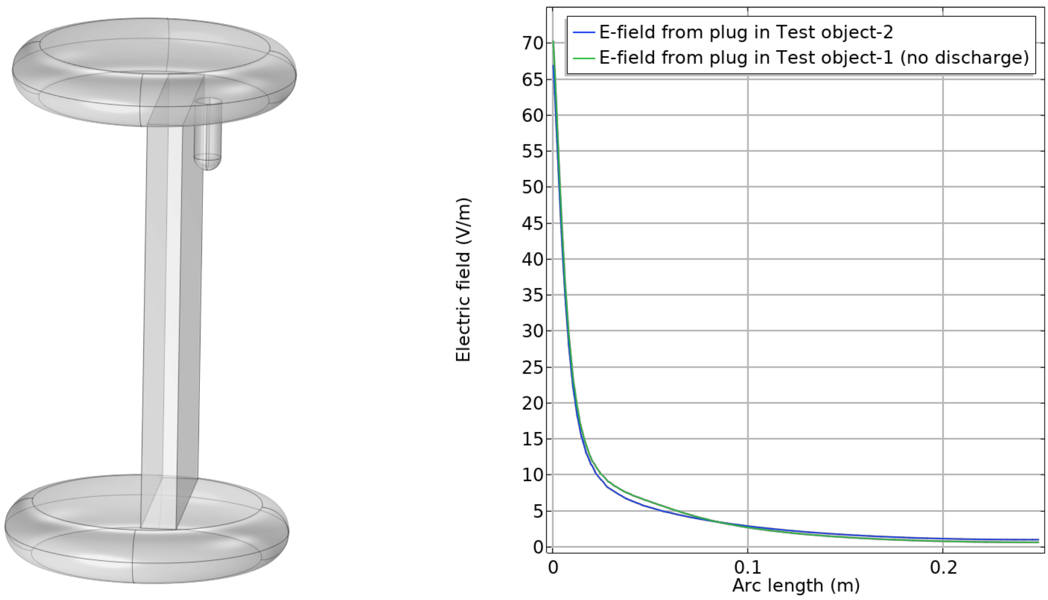


(a) Geometry of Test object-2; all dimensions are as per Figure 4.9b

(b) Comparison of E-field along the vertical line from the plug surface in Test object-1 and 2.

Figure 5.5: Comparison of E-field on the plug surface in Test object-1 when no discharge present and Test object-2 shows that their are exposed to very similiar field stress.

## 5.2. Analytical calculation result

The $VdG$ voltage injection setup is capable of producing $330-350kV$. A key element of the optical diagnostics experiment is to create a breakdown at the rod (higher stressed area) and examine the effect of propagating discharge on a plug discharge. In order to do this, we must first ensure that the test conditions are suitable to make a breakdown from the rod but not from the plug. Furthermore, the rod's breakdown voltage is within the limits of the $VdG$ test set. In order to check this, the breakdown and inception voltages are calculated analytically and the checked against the capacity of the test device.

For $300K$ temperature and $0.2 ... 0.6MPa$ pressures, breakdown and inception voltages have been calculated analytically and the results are listed in **Table 5.1-5.6**. $U_{str,inc.}$, $U_{lead,inc.}$ and $U_{bd}$ stands for streamer inception voltage, leader inception voltage and breakdown voltage respectively. The calculations were made with the help of a MATLAB-based tool developed by the Hitachi ABB PG Research team. Its working principle is explained in **Section 4.2.2**.

Streamer inception voltage $U_{str,inc.}$ is the voltage at which a streamer begins to appear. It occurs when a free electron is present and it begins an avalanche in a critically stressed electrode gap. Leader inception voltage $U_{lead,inc.}$ refers to the voltage at which the streamer transform to a leader due to *ohmic* heating when charges passes through it.

Furthermore, it is noteworthy that the streamer inception voltage is used as a threshold parameter (location parameter) in the $Weibull$ fit function, by which we are able to obtain $U63$ and $U50$ from the breakdown distributions (described in the **Sections 5.3** and **4.3.2**). This is because no breakdown occurs when the applied voltage is less than the streamer inception voltage.

The first column of **Table 5.1-5.6** indicates the location and polarity of the discharge inception. The second column indicates whether or not primary discharge from the rod was present when inception occurred, and if yes, the length of the primary discharge from the rod. The total gap distance is 100mm, so the 50mm long primary discharge has already reached halfway across the gap. For the conditions outlined in the first two columns, the remaining three columns represent streamer inception, leader inception, and breakdown voltage. The tool calculates breakdown voltages under the approximations given in **Section 4.2.2** and neglecting the availability of a *start electron*. We have seen that for the large gaps used in the present work a correction factor for LI voltage levels is needed, which was empirically determined to $1.6$.

The results of the analytical calculations can be interpreted as below;-

1. As indicated in **Table 5.1** - **5.2**, for $CO_2$/$O_2$ at $0.2MPa$ & $0.4MPa$, $U_{bd}$ for the $rod$ is less than that of the $plug$ and also comes within the voltage application range of the test injection set. Hence, these two cases can be taken for testing using the prepared test setup.

2. As indicated in **Table 5.4**, for $SF_6$ at $0.2MPa$, $U_{bd}$ for the $rod$ is less than that of the $plug$ and also comes within the voltage application range of the test injection set. Hence, this case can be taken for testing using the prepared test setup. The remaining two $SF_6$ cases goes beyond the voltage limit of the test kit and hence can't be considered for diagnostic testing(refer **Table 5.5** & **5.6**).

3. The inception voltages shown in the Tables are equivalent to DC levels as the MATLAB tool doesn't consider *first electron* criteria. In this investigation, the propagating discharge from the rod will be present only for a short duration of time (in $\mu s$). Hence, discharge inception voltage level of the plug with shorter duration will be more helpful.

| Location | Rod discharge present? | $U_{str,inc.}(kV)$ | $U_{lead,inc.}(kV)$ | $U_{bd}(kV)$ | |
|---|---|---|---|---|---|
| | | DC | DC | DC | LI |
| Rod (+ve) | - | 34 | 61 | 141 | $\boxed{225}$ |
| Plug (-ve) | No | 91 | 101 | 289 | $\boxed{462}$ |
| Plug (-ve) | Yes;25mm long | 71 | 78 | 133 | 212 |
| Plug (-ve) | Yes;50mm long | 51 | 54 | 189 | 302 |

Table 5.1: Calculated results for breakdown/inception from rod and plug in test object-1 with $CO_2$ at 0.2MPa. Temperature assumed is 300K.

| Location | Rod discharge present? | $U_{str,inc.}(kV)$ | $U_{lead,inc.}(kV)$ | $U_{bd}(kV)$ | |
|---|---|---|---|---|---|
| | | DC | DC | DC | LI |
| Rod (+ve) | - | 69 | 87 | 192 | $\boxed{308}$ |
| Plug (-ve) | No | 194 | 200 | 395 | $\boxed{632}$ |
| Plug (-ve) | Yes;25mm long | 152 | 160 | 318 | 508 |
| Plug (-ve) | Yes;50mm long | 104 | 107 | 256 | 409 |

Table 5.2: Calculated results for breakdown/inception from rod and plug in test object-1 with $CO_2$ at 0.4MPa. Temperature assumed is 300K.

| Location | Rod discharge present? | $U_{str,inc.}(kV)$ | $U_{lead,inc.}(kV)$ | $U_{bd}(kV)$ | |
|---|---|---|---|---|---|
| | | DC | DC | DC | LI |
| Rod (+ve) | - | 93 | 104 | 237 | $\boxed{380}$ |
| Plug (-ve) | No | 280 | 285 | 567 | $\boxed{907}$ |
| Plug (-ve) | Yes;25mm long | 218 | 221 | 363 | 582 |
| Plug (-ve) | Yes;50mm long | 150 | 152 | 451 | 722 |

Table 5.3: Calculated results for breakdown/inception from rod and plug in test object-1 with $CO_2$ at 0.6MPa. Temperature assumed is 300K.

| Location | Rod discharge present? | $U_{str,inc.}(kV)$ | $U_{lead,inc.}(kV)$ | $U_{bd}(kV)$ | |
|---|---|---|---|---|---|
| | | DC | DC | DC | LI |
| Rod (+ve) | - | 87 | 97 | 200 | $\boxed{322}$ |
| Plug (-ve) | No | 269 | 271 | 355 | $\boxed{567}$ |
| Plug (-ve) | Yes;25mm long | 210 | 212 | 278 | 445 |
| Plug (-ve) | Yes;50mm long | 142 | 144 | 215 | 344 |

Table 5.4: Calculated results for breakdown/inception from rod and plug in test object-1 with $SF_6$ at 0.2MPa. Temperature assumed is 300K.

| Location | Rod discharge present? | $U_{str,inc.}(kV)$ | $U_{lead,inc.}(kV)$ | $U_{bd}(kV)$ | |
|---|---|---|---|---|---|
| | | DC | DC | DC | LI |
| Rod (+ve) | - | 173 | 177 | 355 | $\boxed{568}$ |
| Plug (-ve) | No | 528 | 528 | 666 | $\boxed{1066}$ |
| Plug (-ve) | Yes;25mm long | 414 | 414 | 523 | 837 |
| Plug (-ve) | Yes;50mm long | 280 | 280 | 426 | 682 |

Table 5.5: Calculated results for breakdown/inception from rod and plug in test object-1 with $SF_6$ at 0.4MPa. Temperature assumed is 300K.

| Location | Rod discharge present? | $U_{str,inc.}(kV)$ | $U_{lead,inc.}(kV)$ | $U_{bd}(kV)$ | |
|---|---|---|---|---|---|
| | | DC | DC | DC | LI |
| Rod (+ve) | - | 257 | 262 | 532 | $\boxed{851}$ |
| Plug (-ve) | No | 787 | 787 | 995 | $\boxed{1592}$ |
| Plug (-ve) | Yes;25mm long | 617 | 617 | 780 | 1248 |
| Plug (-ve) | Yes;50mm long | 418 | 418 | 637 | 1020 |

Table 5.6: Calculated results for breakdown/inception from rod and plug in test object-1 with $SF_6$ at 0.6MPa. Temperature assumed is 300K.

The experiment results of three conditions ($0.2MPa$ $CO_2$, $0.4MPa$ $CO_2$ and $0.2MPa$ $SF_6$) will be discussed in the following sections.

## 5.3. Breakdown voltages

Breakdown tests are conducted for the following reasons.

⇒ Finding the LI equivalent breakdown voltage (50% quantile, U50) of test object-1 under all three test conditions (i.e. $CO_2/O_2$ at $0.2MPa$, $CO_2/O_2$ at $0.4MPa$, and $SF_6$ at $0.2MPa$).

⇒ The range of voltage application for the optical investigation test must be understood. In an ideal situation, the applied voltage would be sufficient to induce a propagating discharge (resulting in a breakdown) from the rod. Nevertheless, this voltage level shall not exceed the inception voltage of the plug. **Section 4.2.6** explains the objective and procedure of the optical investigation test. In this case, since the breakdown voltage of the plug is higher than the voltage limit of the VdG injection set, the upper limit of the voltage application couldn't be determined. This is further explained in **Section 5.4**.

**Figure 5.6**, **5.7** & **5.8** shows the breakdown distribution obtained from breakdown tests performed on Test object-1 in all three identified conditions (i.e. $CO_2/O_2$ at $0.2MPa$, $CO_2/O_2$ at $0.4MPa$, and $SF_6$ at $0.2MPa$).

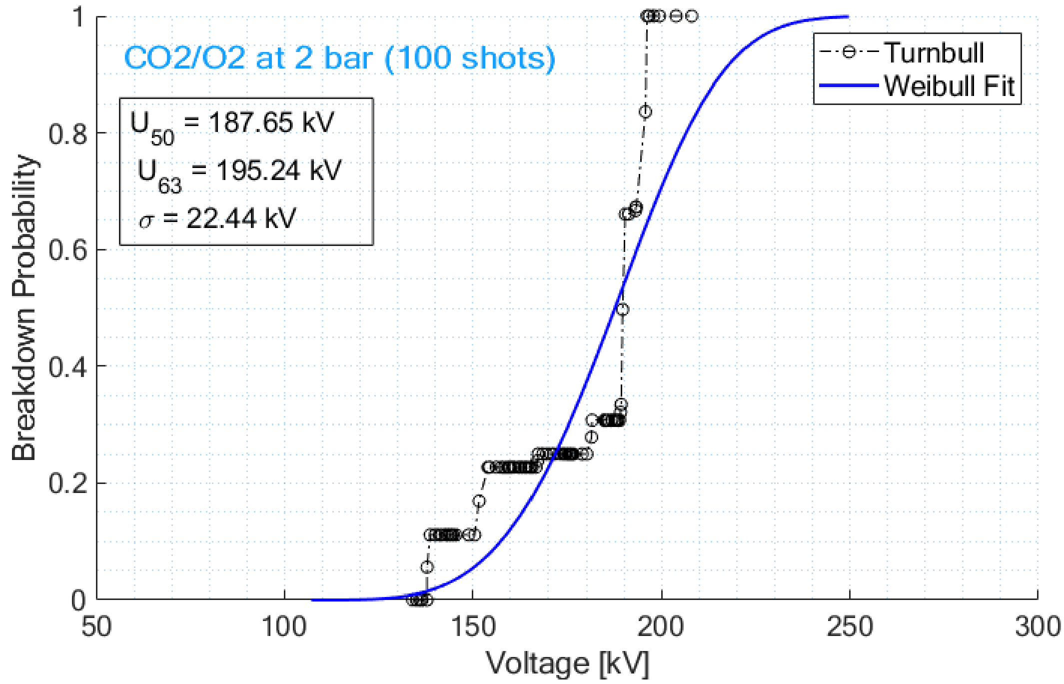


Figure 5.6: Graph showing breakdown data from 100 shots carried out at $0.2MPa$ pressure with $CO_2/O_2$ in Test object-1. For parameter extraction, a $3-parameter\ Weibull$ function is fitted to an empirical distribution created via a $Turnbull$ estimator.

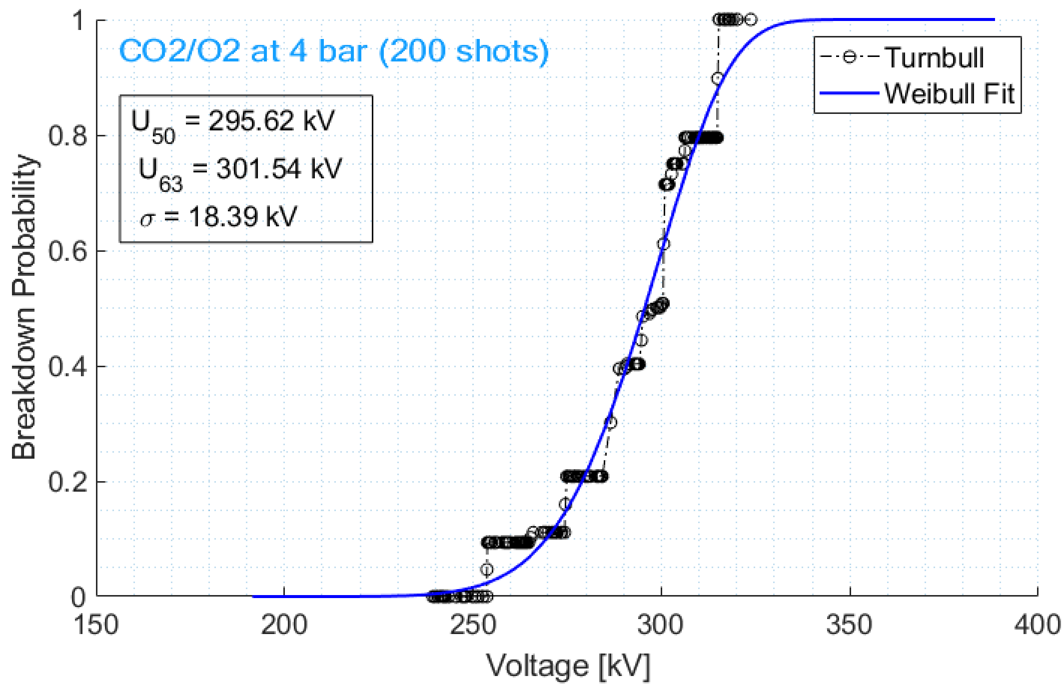


Figure 5.7: Graph showing breakdown data from 200 shots carried out at $0.4MPa$ pressure with $CO_2/O_2$ in Test object-1. For parameter extraction, a $3-parameter\ Weibull$ function is fitted to an empirical distribution created via a $Turnbull$ estimator.

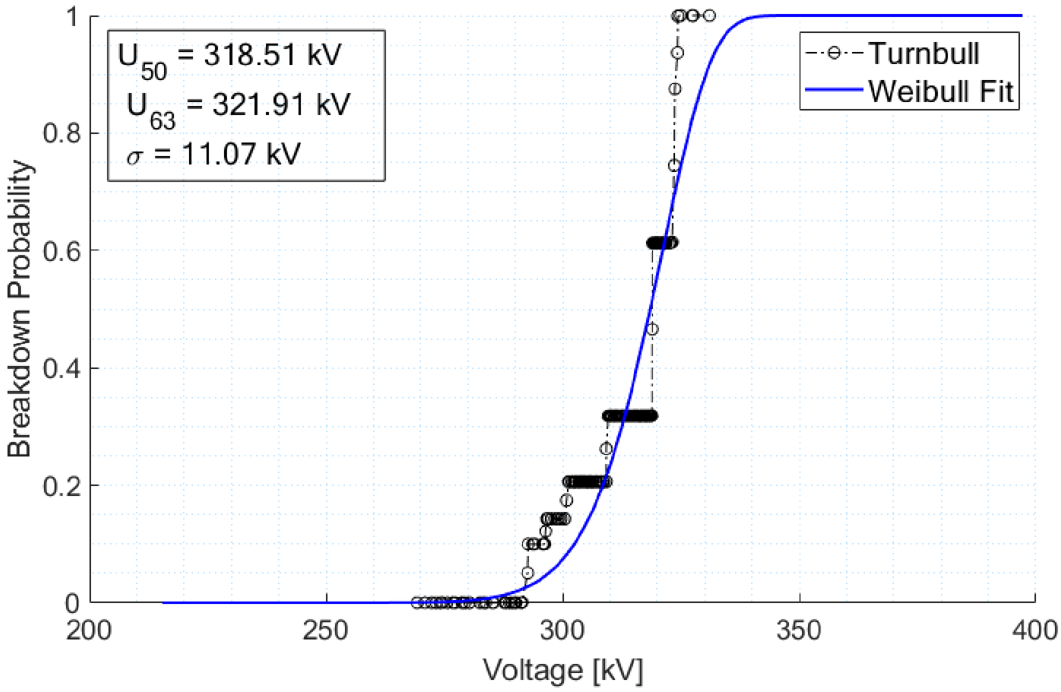


Figure 5.8: Graph showing breakdown data from $199$ shots carried out at $0.2MPa$ pressure with $SF_6$ in Test object-1. For parameter extraction, a $3-parameter\ Weibull$ function is fitted to an empirical distribution created via a $Turnbull$ estimator.

All breakdowns occurred from the rod as expected and **Table 5.7** summarizes the obtained results. The breakdown voltages given are LI equivalent values which are obtained by setting a threshold of $10\mu s$ in the breakdown time (explained in **Section 4.2.4**. The streamer inception voltage is used as *location parameter* of the *Weibull distribution* and the same is obtained from analytical calculation. In order to observe what happens to the plug when propagating discharge enlarges the field there at the plug, it is important that during the optical investigation the applied voltage is in the range listed.

| **Test condition** | **U50(kV)** | $\sigma$**(kV)** | $U_0$**(kV)** | $U_{bd,LI}$**(kV)** |
|---|---|---|---|---|
| $CO_2/O_2$ 0.2MPa | 187.65 | 22.44 | 34 | 225 |
| $CO_2/O_2$ 0.4MPa | 295.62 | 18.39 | 69 | 308 |
| $SF_6$ 0.2MPa | 318.51 | 11.07 | 87 | 322 |

Table 5.7: The table illustrates the breakdown test result for Test object-1 under all three plausible test conditions. $U_0$ is the calculated streamer inception voltage and is used as location parameter for Weibull distribution. Test results are comparable to those obtained from analytical calculations.

## 5.4. Time delay measurement of Test object-1

For this study, it is important to understand the statistical time lag and formative time lag of the main discharge (discharge from the rod in Test object-1, which may cause field enhancement at the plug as well as breakdown). Due to this, only the discharge

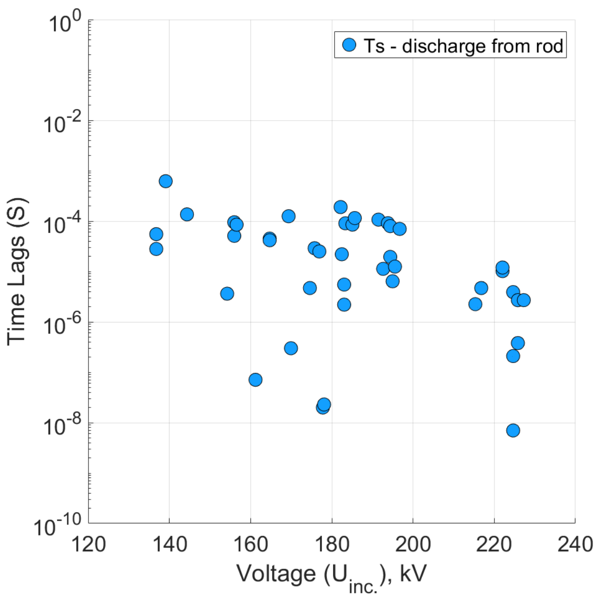


(a) Statistical time lag($t_s$) for different voltage ranges from inception to the maximum voltage.

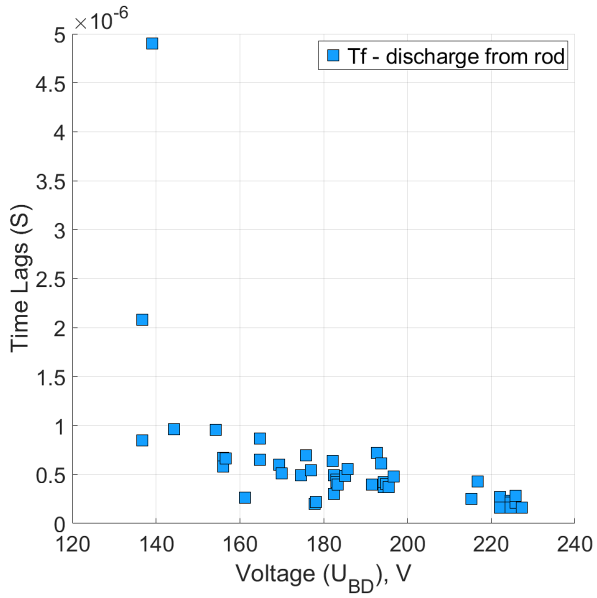


(b) Formative time lag($t_f$) for different voltage ranges from late breakdown to the maximum voltage.

Figure 5.9: Statistical time lag ($t_s$) and formative time lag($t_f$) measured for discharge from rod in test object-1 with 0.2MPa $CO_2$

from the rod is focused during these tests.

In **Section 4.2.5**, the procedure is outlined. Time lag information is analyzed together with possible secondary discharge initiations from the plug which will be detected in subsequent optical diagnostic tests. During the formative time, the discharge crosses the gap, eventually resulting in voltage collapse. Due to the fact that the discharge propagates across the gap over this interval, it is possible to set up the gate time in such a way that the image intensifier (HiCATT) activates for a shorter period of time than the formative time lag.

Because values varied significantly over the range of voltage, the plot of the statistical time lag ($t_s$) is always created on a semi-log scale. For the formative time lag ($t_f$), voltage has a linear relation with it. The reason for this is that formative time can be read along with the propagation velocity, which is directly proportional to the background field applied[19].

The statistical time lag($t_s$) is caused by the absence of the *first electron*, so that polarity of the field (or voltage) affects it. The polarity of the electric field at the rod is positive. In the case of positive polarity, the *first electron* is obtained from a critically stressed gas volume (*volume-time-criteria* [12, 52] - i.e. the volume where the critical field is exceeded and streamer inception can occur). Thus, the statistical time lags appear to be more scattered for lower gas densities (lower pressures) and less scattered for higher pressures. In higher gas pressures, there is a greater possibility of encountering a free electron in the critical volume.

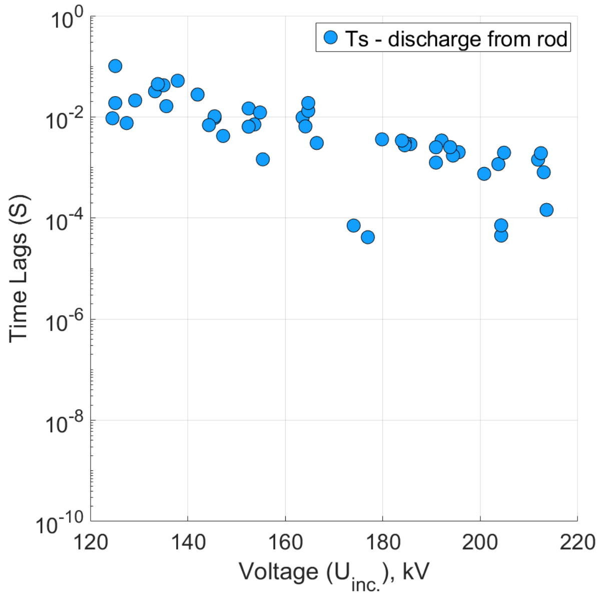


(a) Statistical time lag($t_s$) for different voltage ranges from inception to the maximum voltage.

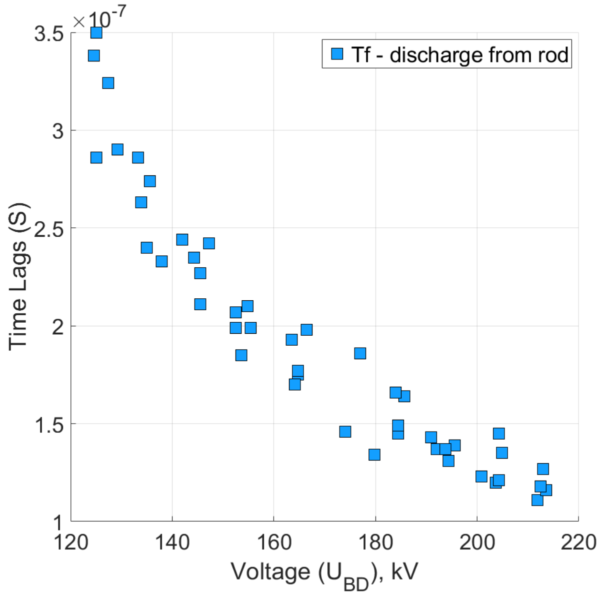


(b) Formative time lag($t_f$) for different voltage ranges from late breakdown to the maximum voltage.

Figure 5.10: Statistical time lag ($t_s$) and formative time lag($t_f$) measured for discharge from rod in test object-1 with 0.4MPa $CO_2$

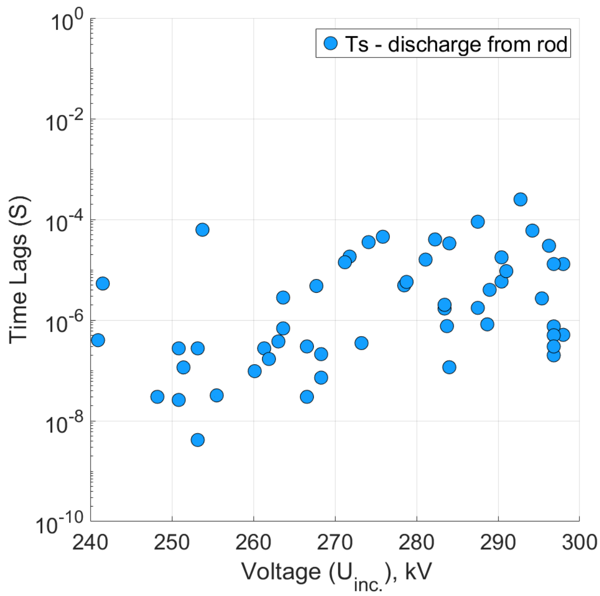


(a) Statistical time lag($t_s$) for different voltage ranges from inception to the maximum voltage.

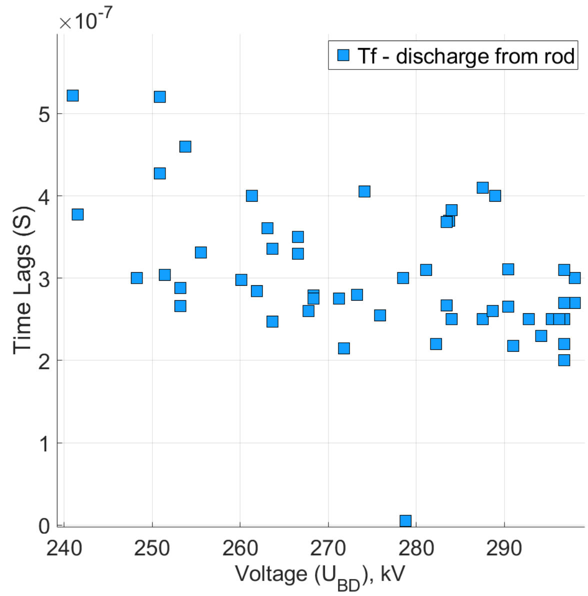


(b) Formative time lag($t_f$) for different voltage ranges from late breakdown to the maximum voltage.

Figure 5.11: Statistical time lag ($t_s$) and formative time lag($t_f$) measured for discharge from rod in test object-1 with 0.2MPa $SF_6$

**Figure 5.9a, 5.10a & 5.11a** show the distribution of the statistical time lag for $CO_2/O_2$ at $0.2MPa$, $CO_2/O_2$ at $0.4MPa$, and $SF_6$ at $0.2MPa$, respectively. With increasing voltage, $t_s$ decreases, as expected (as seen in [19, 32]). Because of the reason outlined earlier, $0.2MPa$ $CO_2$ and $0.2MPa$ $SF_6$ are more scattered, and a similar observation can also be seen in [19] & [32]. Since $SF_6$ at $0.2MPa$ was tested with a wide range of voltages, the statistical time lag distribution of this is more scattered (**Figure 5.11a**). The reason for this is that this setup had an inception voltage of $240kV$ and we were limited to testing that voltage only up to $300kV$ due to the limit of the VdG as previously mentioned. In order to understand the real trend of statistical time lag with increasing voltages, a much wider voltage range would be desirable.

**Figure 5.9b, 5.10 & 5.11b** show the distribution of the formative time lag for $CO_2/O_2$ at $0.2MPa$, $CO_2/O_2$ at $0.4MPa$, and $SF_6$ at $0.2MPa$, respectively. This information is used to set the gate time of the image intensifier. With $CO_2/O_2$ at $0.2MPa$ and $SF_6$ at $0.2MPa$, $t_f$ ranges from $10s$ of $\mu s$ to a few 100 $ns$ at higher voltages. As long as this range is acceptable, optical diagnostics can be configured easily. Nevertheless, when $CO_2/O_2$ is used at $0.4MPa$ (**Figure 5.10**), the formative time lag is in the range of $250ns$ to $100ns$ at higher voltages. With the oscilloscope and measurement chain having a significant intrinsic time delay ($75ns$) this is not well suited for obtaining an useful image with the optical diagnostic setup. Detailed explanation with procedure is given in **Section 4.2.6**.

## 5.5. Optical diagnostic results

In this set of experiments, optical diagnostics are used to analyze Test object-1 (**Figure 4.6**). **Section 4.2.6** explains the procedure. Basically, the goal is to find any indication of the inception at the plug. The breakdown in Test object-1 is clearly due to streamer propagation or primarily leader propagation from the rod across the gap. Between the rod and the plug, the $PTFE$ plate serves the following functions:

⇒ It prevents the breakdown across the gap between the plug and rod.

⇒ Breakdowns caused by branched streamers or stepped leaders follow a random path through the gap before they finally result in breakdowns. Streamers or leaders propagating from the rod tend to stick to the $PTFE$ surface as they travel through its path. Since the primary discharge is nearby, this provides the maximum opportunity for field enhancement at the plug. If a secondary discharge exists, the chances of finding it will be higher.

⇒ Any inception from the plug is associated with its own statistical time lag. Since the $photoemission$ from the primary discharge (from the rod) can easily provide the first electron required by the plug (at least over short distances, since the UV light will be absorbed over a short length), it is easy to influence the secondary discharge. Since we have $PTFE$ between the rod and the plug, this possibility is minimal in our case.

From the breakdown tests, we have information about the voltage at which a breakdown is initiated from the rod in all three test conditions identified. We also have the formative time lag information of these breakdowns which is obtained from a separate set of tests. In the optical diagnostic tests, the Test object-1 is prepared in the set up as described in **Section 4.2.6**. A number of test voltages are applied, which typically ranges from the late breakdown range to the voltages in the LI ranges obtained breakdown tests given in **Table 5.7**.

The photomultiplier (PMT) is optically focused on the tip of the rod from where the primary discharge is expected to incept and was used as the trigger source for the oscilloscope (LeCroy LT374). The trigger level is typically set to $80mV$ (however it was varied from $60mV$ to sometimes even $40mV$). The trigger-out signal of the scope is connected to the synch-in port of the HiCATT (Image intensifier). Hence, when a signal from PMT has triggered in the scope, the image intensifier is also triggered after the aforementioned intrinsic time delay of $75ns$ (explained in **Section 4.2.6**).

If we want to get an image of propagating discharge across the gap and what exactly happens at the plug while this discharge is propagating, the HiCATT gate time ($tg$) must be properly set. By setting the gate time (typically from few $\mu s$ to some tens of $ns$'s), we determine for how long the optical device shall be kept open. The image obtained from the $NIKON$ camera connected to it records only what happened during that very short period of time interval.

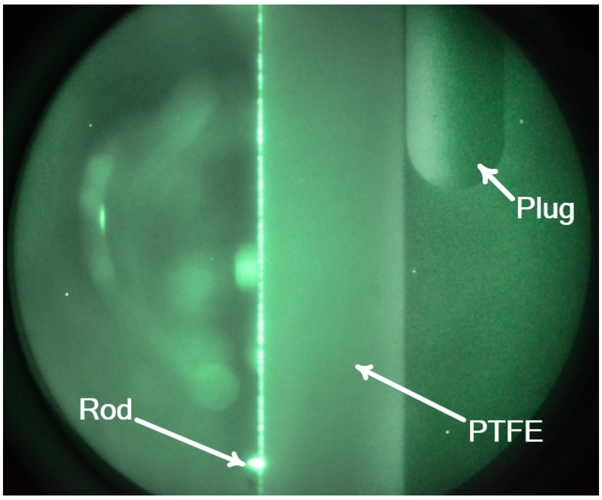

Figure 5.12: Photo capctured using HiCATT and NIKON camera to show the positions of the electrodes. All captured images of the discharge will be showing in the same frame.

In this experiment, determining the gate time for the image intensifier is difficult. As an example from the $0.2MPa$ $CO_2/O_2$ case, with $224kV$ applied, we saw a breakdown of the rod. This breakdown had a formative time lag of $210ns$. It means that the leader discharge which caused the breakdown was only present for a short period of time. To get a still image of what is happening during propagation, the image intensifier gate should be set between $5ns$ and $120ns$ (as close as possible). When the gate time is set higher than $120ns$, the HiCATT will be overexposed due to the strong light from the breakdown occurring after the formative time lag. Overexposing an image intensifier too frequently can damage its sensitive photo elements. As a precautionary measure, a value of $30-50ns$ will be selected in this case. Note that, as mentioned before already, we do not have the option of choosing gate time values up to the entire $210ns$. This is due to the internal scope time delay delaying the trigger of HiCATT by approximately $75ns$.

The next part of this section entails images that detected the potential secondary discharge from the plug. Since the light was very weak, the images do not clearly show the electrode positions, so they should be read with **Figure 5.12**. The respective recording from the oscilloscope is provided along with each image. The channel that was connected to the PMT signal was used to trigger the scope.

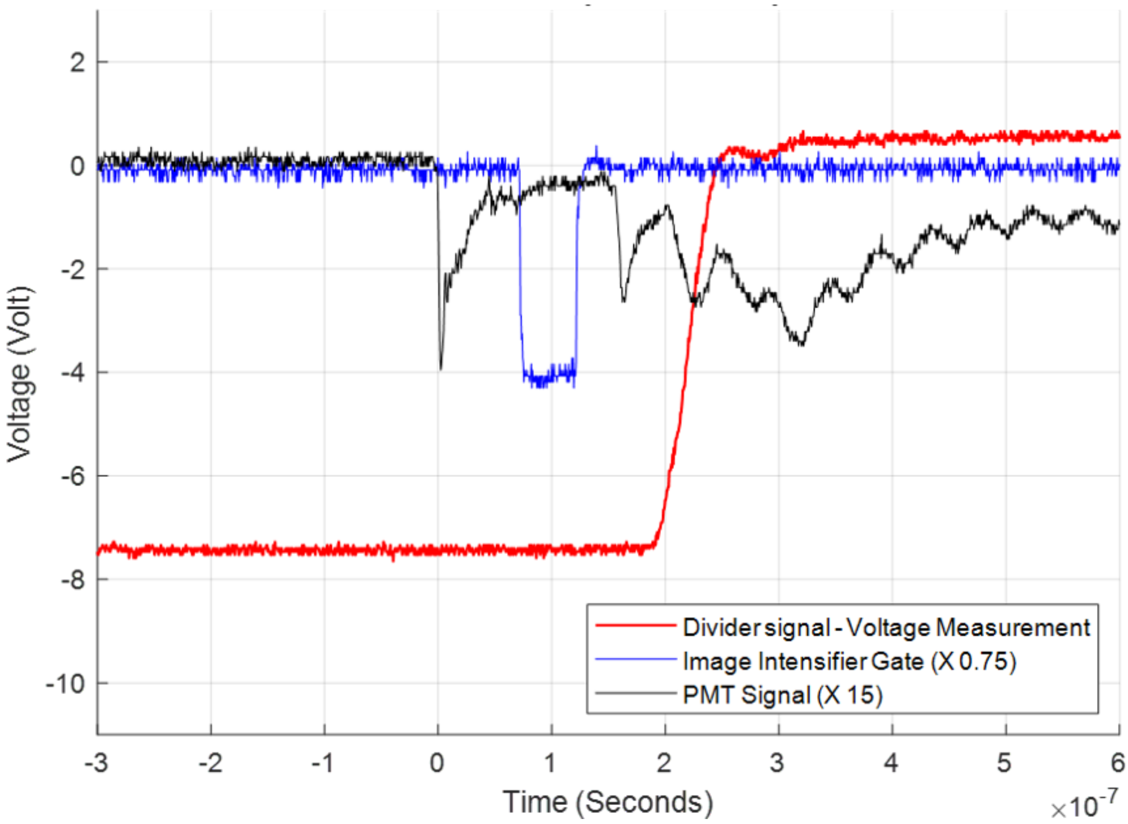


(a) Data recorded by LeCroy scope with signals obtained from PMT, Image-intensifier gate and voltage divider.

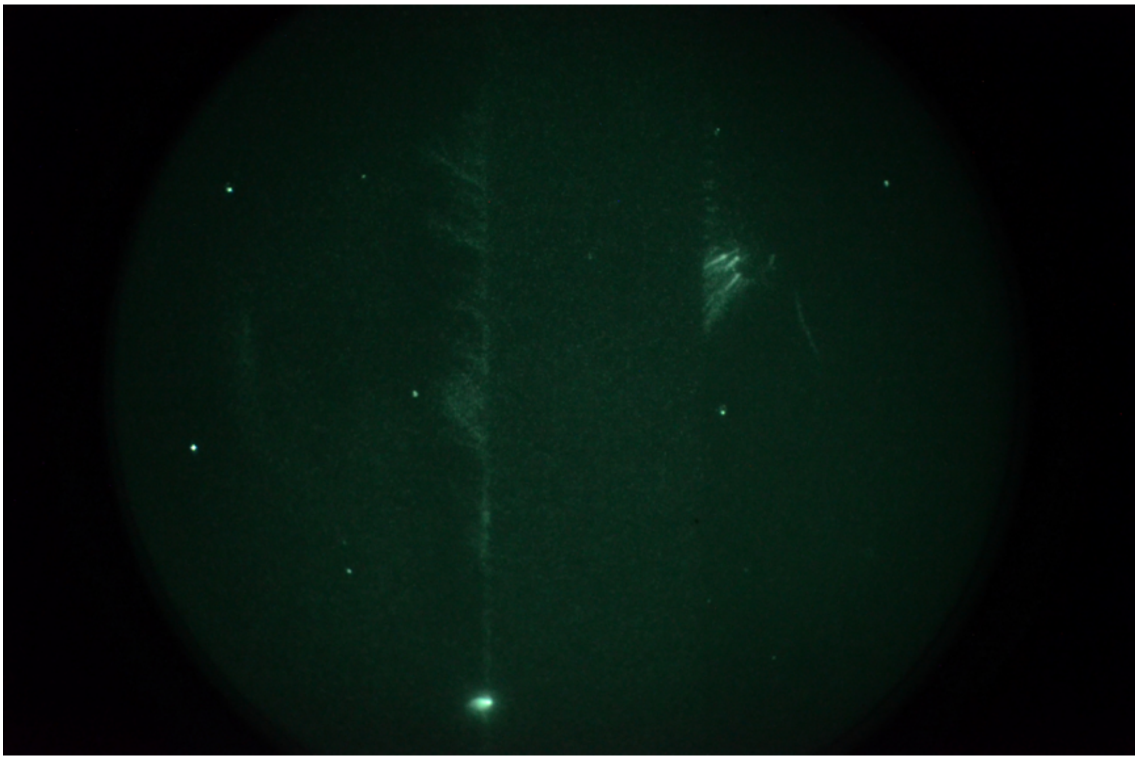

(b) Intensified image captured when gate time = 50ns

Figure 5.13: Optical diagnostic results obtained from experiment in Test object-1 with when $CO_2/O_2$ was filled at $0.2MPa$. Test voltage applied was $222kV$. Time lag readings of the primary discharge was $t_s = 42\mu s$ and $t_f = 180ns$. The captured image shows secondary discharge inception from the plug.

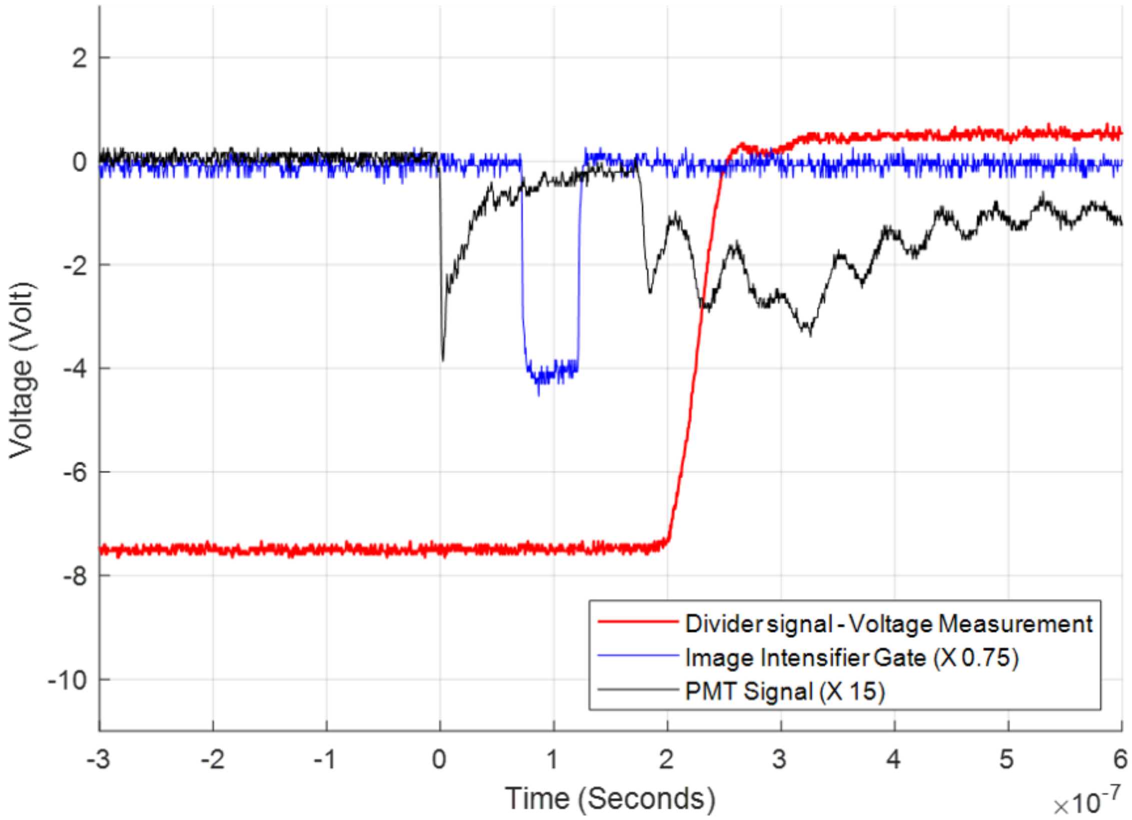


(a) Data recorded by LeCroy scope with signals obtained from PMT, Image-intensifier gate and voltage divider.

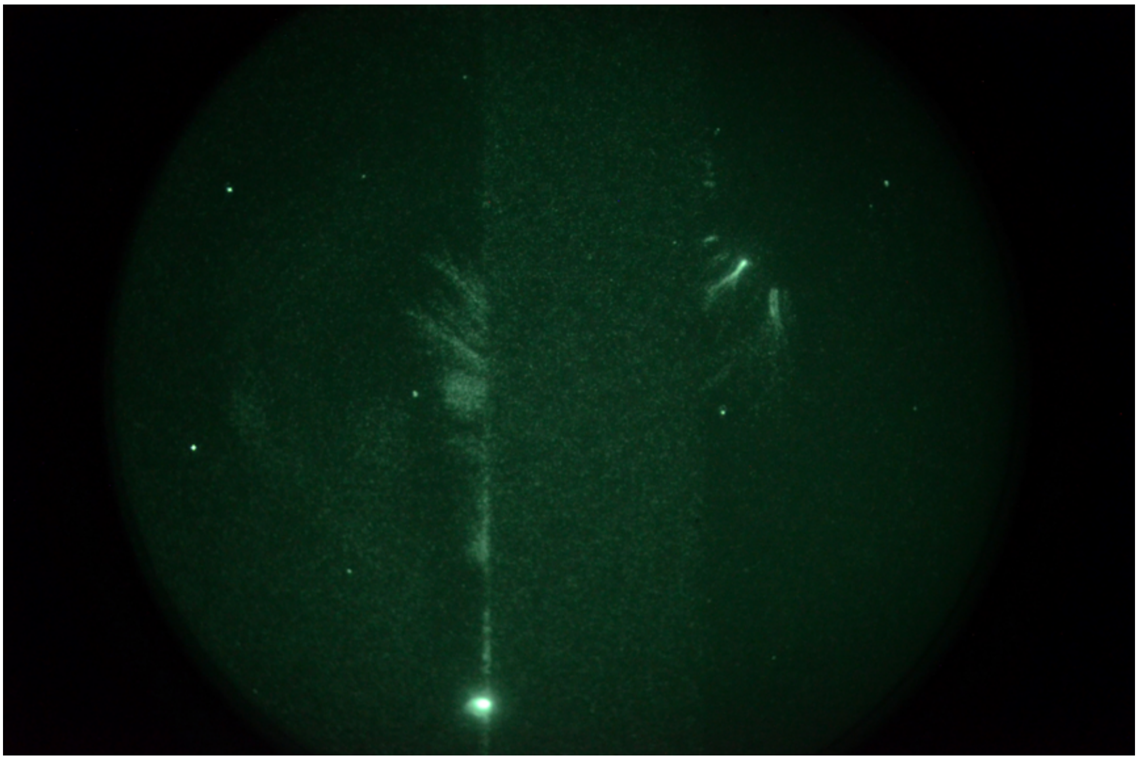

(b) Intensified image captured when gate time = 50ns

Figure 5.14: Optical diagnostic results obtained from experiment in Test object-1 with when $CO_2/O_2$ was filled at $0.2MPa$. Test voltage applied was $222kV$. Time lag readings of the primary discharge was $t_s = 28\mu s$ and $t_f = 200ns$. The captured image shows secondary discharge inception from the plug.

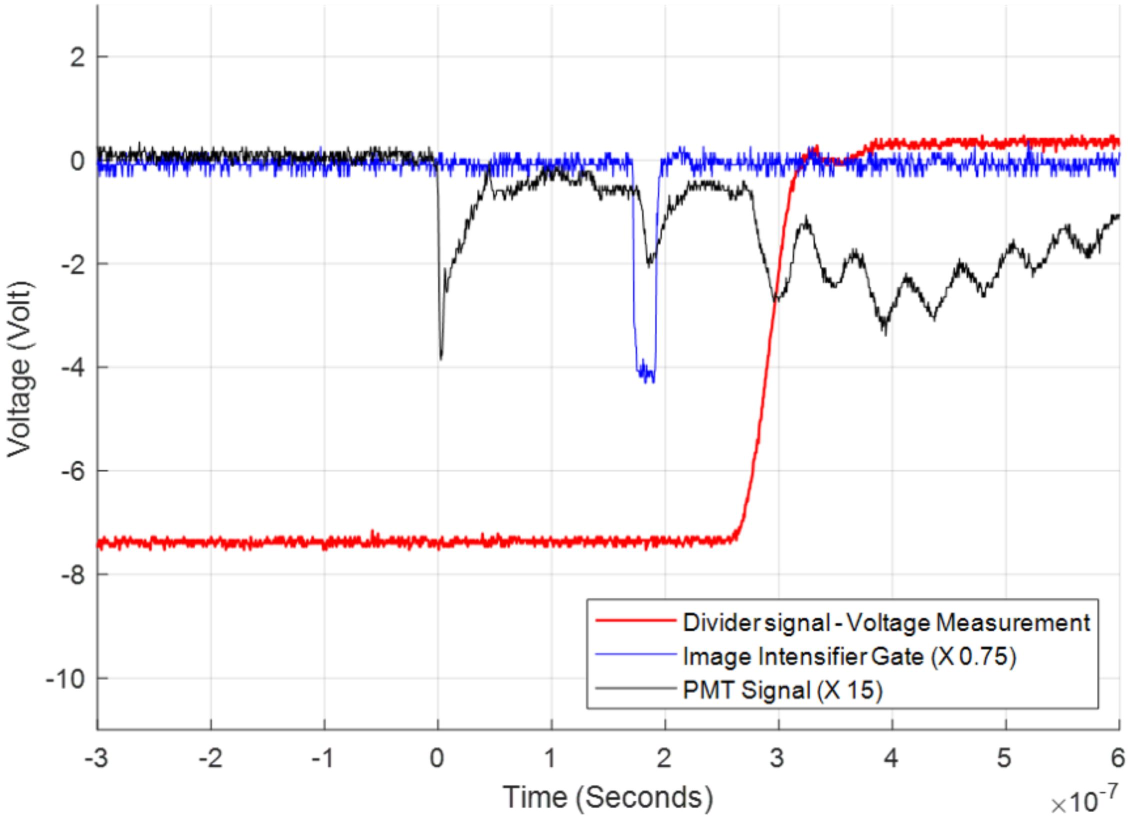


(a) Data recorded by LeCroy scope with signals obtained from PMT, Image-intensifier gate and voltage divider.

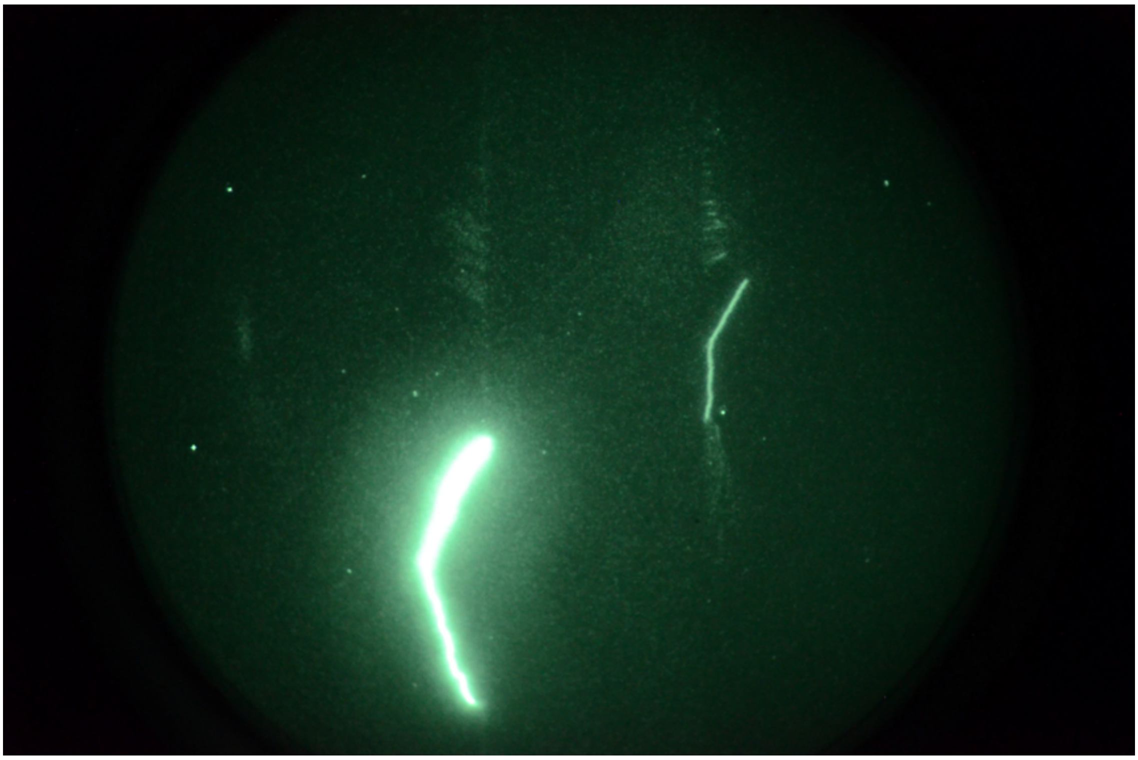

(b) Intensified image captured when gate time = 20ns

Figure 5.15: Optical diagnostic results obtained from experiment in Test object-1 with when $CO_2/O_2$ was filled at $0.2MPa$. Test voltage applied was $215kV$. Time lag readings of the primary discharge was $t_s = 2.2\mu s$ and $t_f = 250ns$. The captured image shows secondary discharge inception along with propagating leader from the plug.

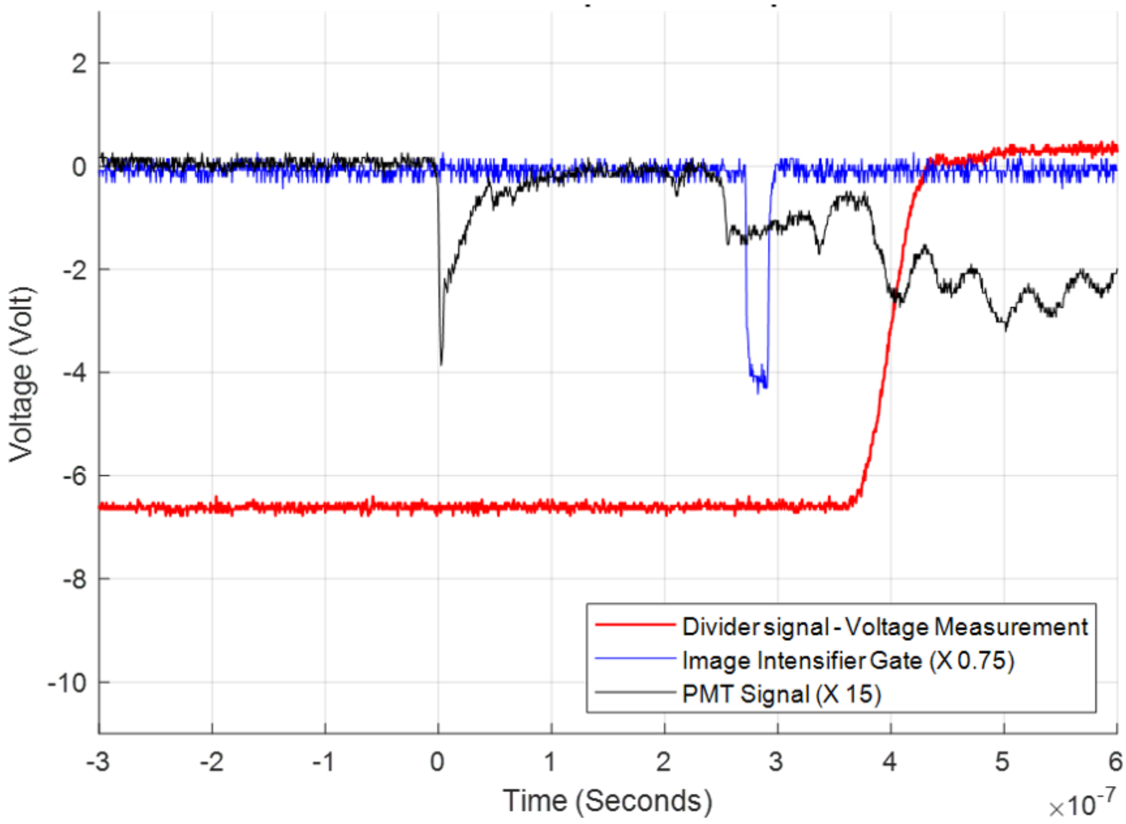


(a) Data recorded by LeCroy scope with signals obtained from PMT, Image-intensifier gate and voltage divider.

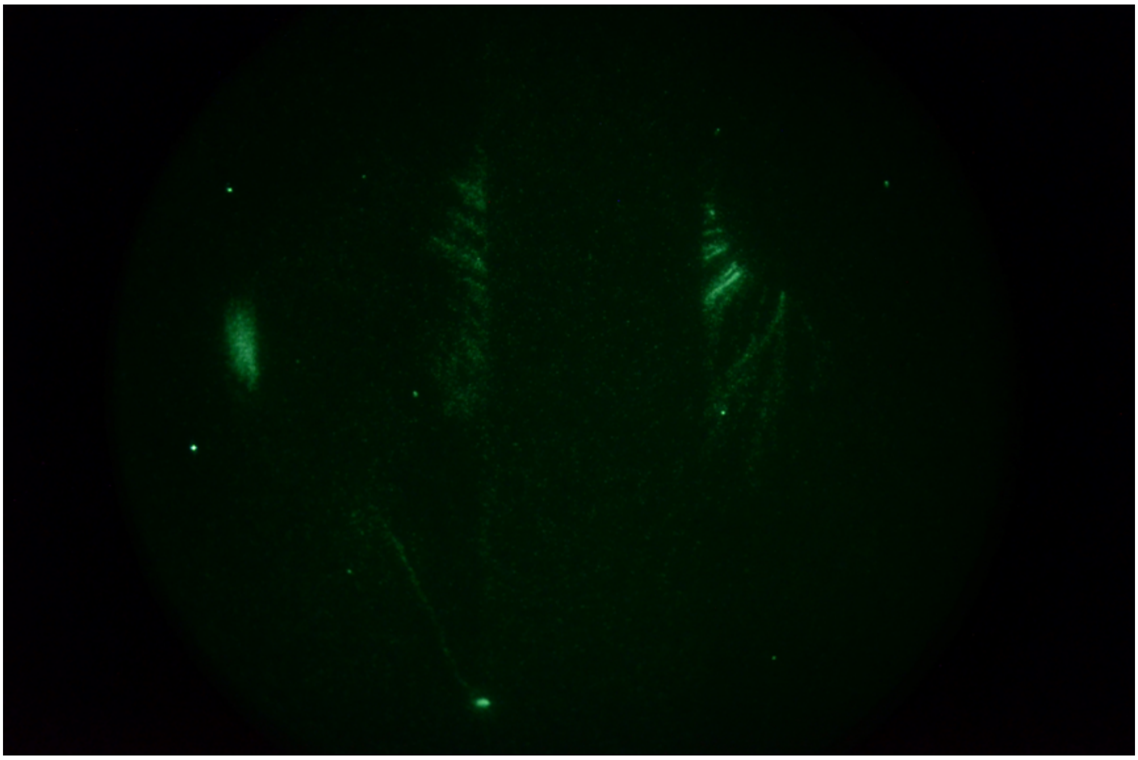

(b) Intensified image captured when gate time = 20ns

Figure 5.16: Optical diagnostic results obtained from experiment in Test object-1 with when $CO_2/O_2$ was filled at $0.2MPa$. Test voltage applied was $195kV$. Time lag readings of the primary discharge was $t_s = 12.5\mu s$ and $t_f = 370ns$. The captured image shows secondary discharge inception from the plug.

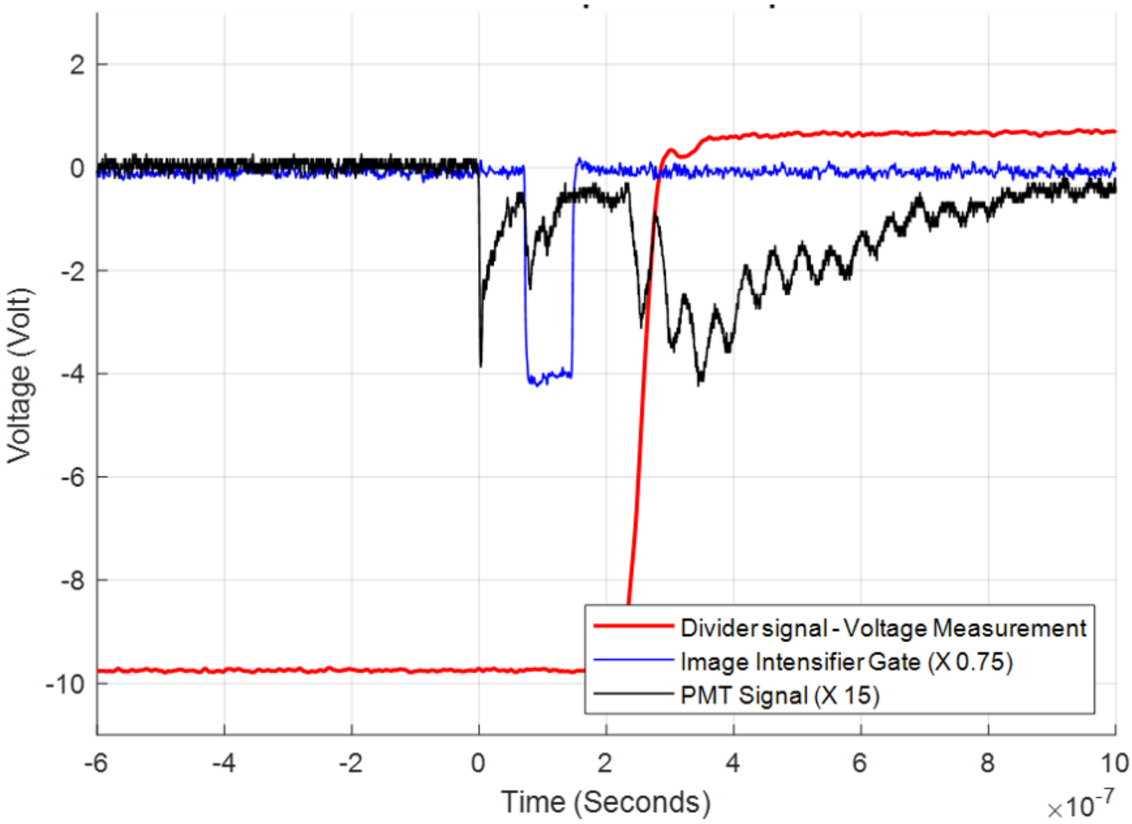


(a) Data recorded by LeCroy scope with signals obtained from PMT, Image-intensifier gate and voltage divider.

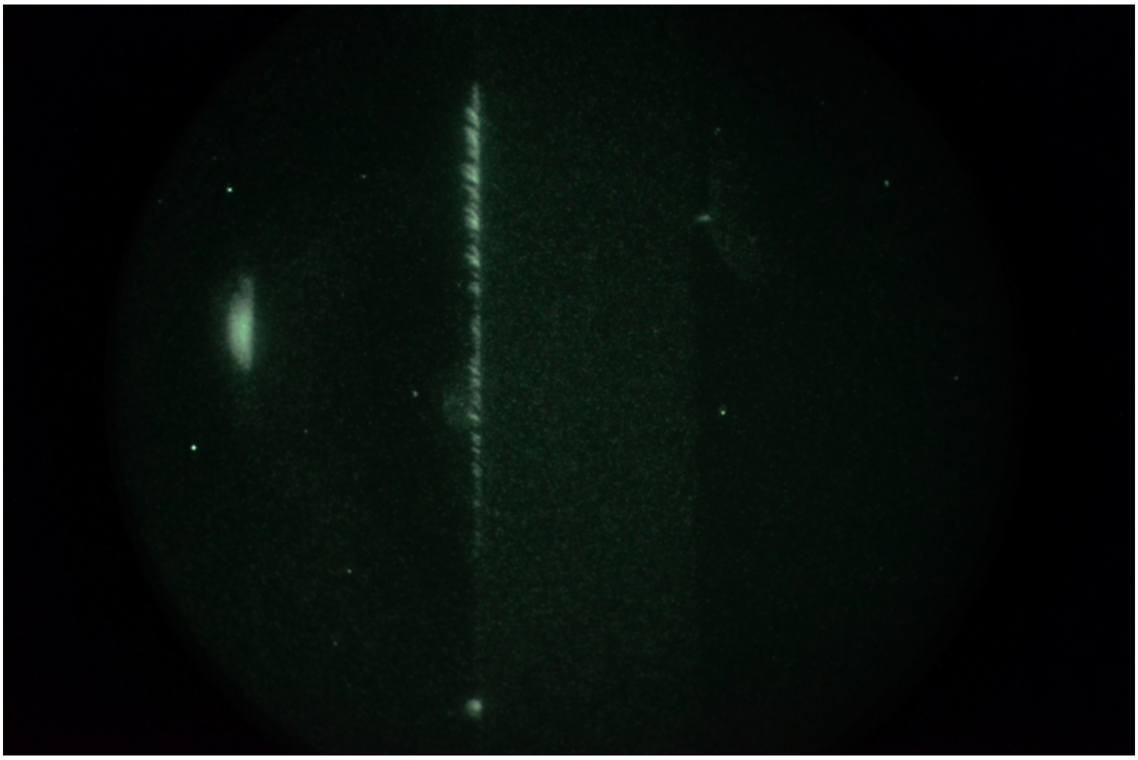

(b) Intensified image captured when gate time = 75ns

Figure 5.17: Optical diagnostic results obtained from experiment in Test object-1 with when $SF_6$ was filled at $0.2MPa$. Test voltage applied was $294kV$. Time lag readings of the primary discharge was $t_s = 60\mu s$ and $t_f = 230ns$. The captured image shows secondary discharge inception from the plug.

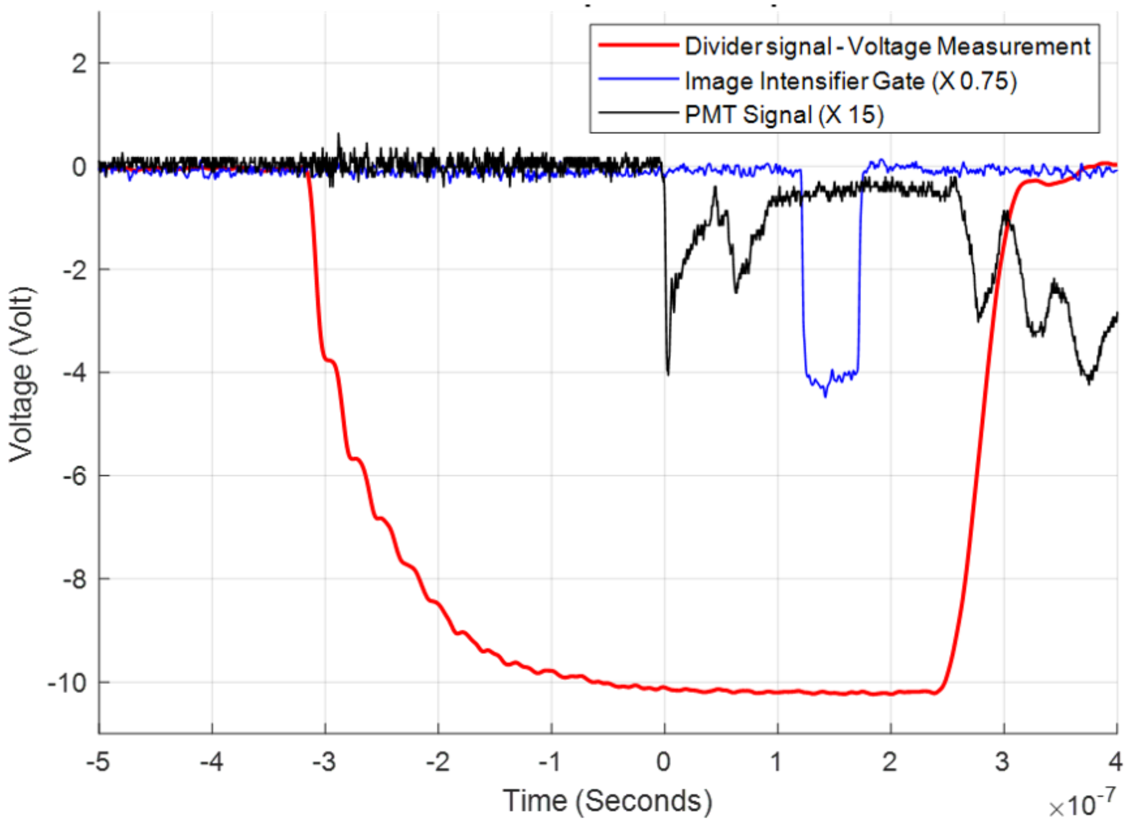


(a) Data recorded by scope with signals obtained from PMT, Image-intensifier gate and voltage divider.

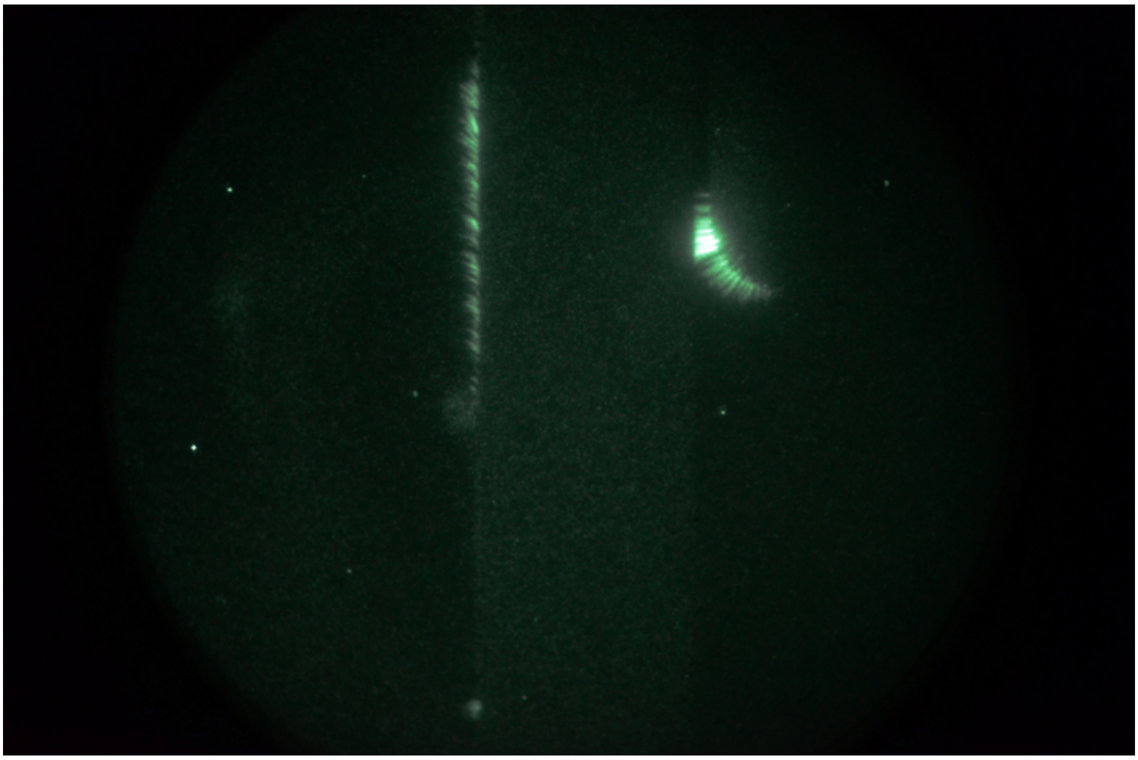

(b) Intensified image captured when gate time = 50ns

Figure 5.18: Optical diagnostic results obtained from experiment in Test object-1 with when $SF_6$ was filled at $0.2MPa$. Test voltage applied was $296kV$. Time lag readings of the primary discharge was $t_s = 300ns$ and $t_f = 250ns$. The captured image shows secondary discharge inception from the plug.

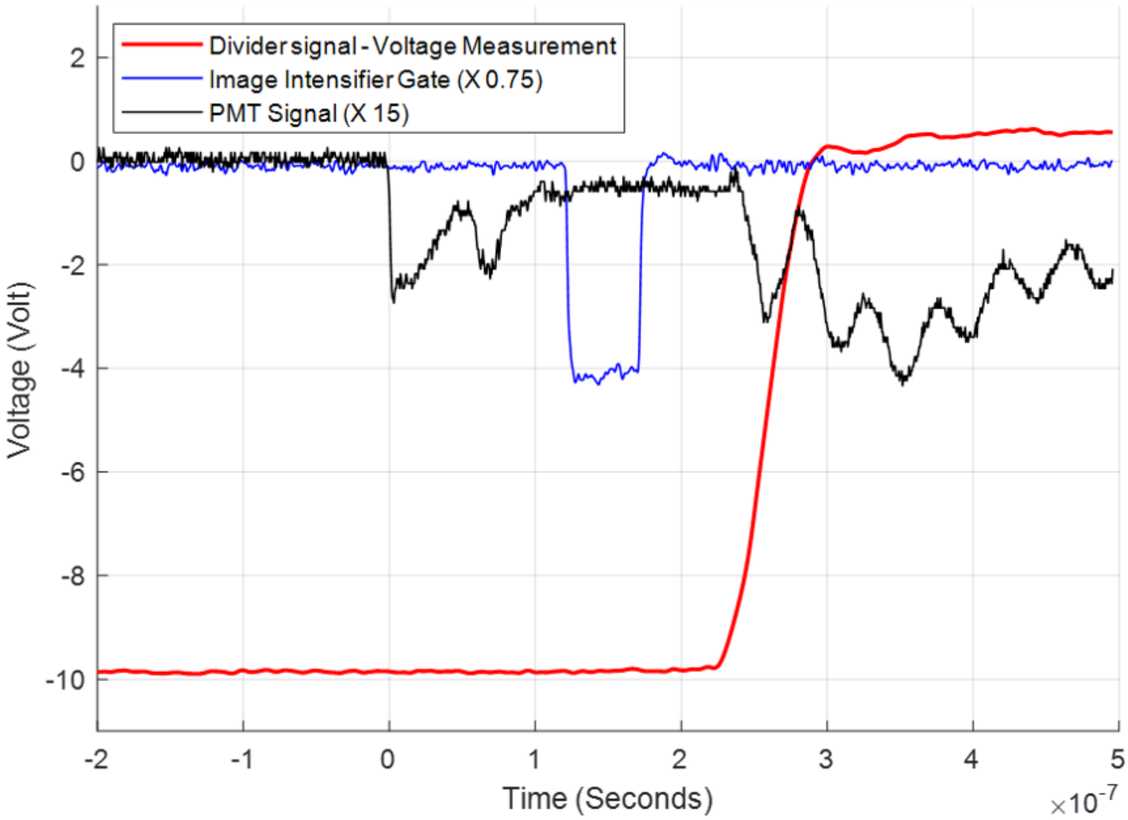


(a) Data recorded by LeCroy scope with signals obtained from PMT, Image-intensifier gate and voltage divider.

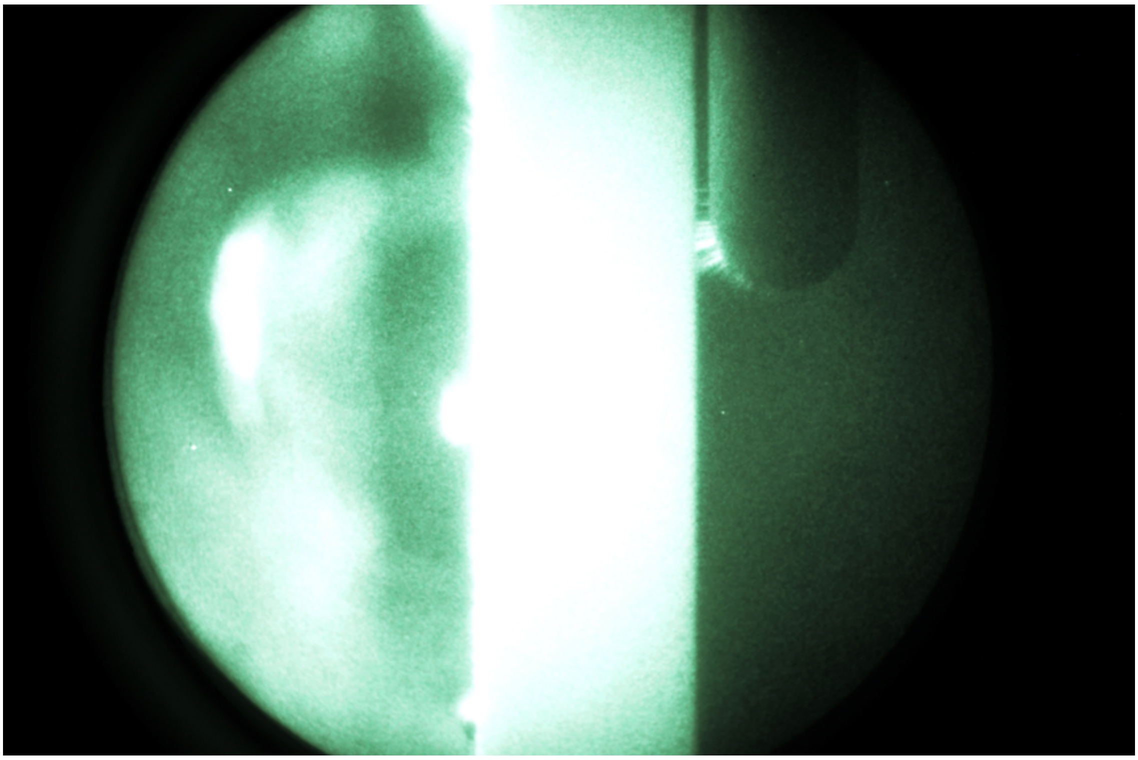

(b) Intensified image captured when gate time = 50ns

Figure 5.19: Optical diagnostic results obtained from experiment in Test object-1 with when $SF_6$ was filled at $0.2MPa$. Test voltage applied was $296kV$. Time lag readings of the primary discharge was $t_s = 30\mu s$ and $t_f = 250ns$. The captured image shows secondary discharge inception from the plug.

The **Figure 5.13a** illustrates the following. The scope is triggered as soon as the PMT signal detects a large pulse (light from the first streamer corona). This in turn triggers the gate of the image intensifier to open it for a predetermined amount of time, following the intrinsic time delay $\approx 75ns$ delay. In this instance, the applied voltage is $222kV$. The formative time lag for $CO_2/O_2$ at $2ba$r were typically in the range of $200ns$ (see **Figure 5.9b**). Therefore, to ensure that the gate time does not fall in the breakdown region, the gate time of the image intensifier is comfortably set to $50ns$. The rest of the captures were conducted the same way (**Figures 5.14a**-**5.19a**).

**Figure 5.13b** shows a nice image of the primary discharge progressing across the gap causing breakdown (left side) and discharge inception in the plug at the same time. The statistical time lag ($t_s$) and the formative time lag($t_f$) of the main discharge recorded are $42\mu s$ and $180ns$ respectively. It is important to understand that, the plug was exposed to field stress only for $\approx (ts + tf)$ time duration (which is $42\mu s + 180ns$). Under the same background conditions, we must examine the plug's inception without propagating discharge and check whether the plug can initiate inception after a similar time lag. Performing such a comparison can reveal whether or not inception at the plug is actually caused by the enhanced field resulting from the discharge from the rod. The same applies to all detect ions observed in **Figures 5.13-5.19**.

It is expected that the formative time lag ($t_f$) for $CO_2/O_2$ at $0.4MPa$ is between $100ns$ and $300ns$ (**Figure 5.10**). It was found that the formative time lag was as small as $100-120ns$ at higher voltages, where secondary discharges are expected to occur. Due to the same reasons explained above, it was not possible to set the gate time in the image intensifier properly in this case. Besides, optical investigation until $240kV$, didn't show any evidence of secondary inception.

## 5.6. Time delay measurement of Test object-2

During the optical investigation tests conducted on Test object-1, we have observed numerous instances in which discharge inception can be seen on the plug. It is, however, yet to be proved that this is the result of propagating discharge from the rod causing local field enhancement of the plug. In order to investigate this issue, Test object-2 is also subjected to voltage application under the same conditions. In **Section 4.2.1** (see **Figure 5.5b**), it was established that the electric field at the surface of the plug in Test object-1 and Test object-2 is almost the same. An investigation of discharge inception at plug in Test object-2 will, accordingly, provide more insight about when discharge inception happens from plug in Test object-1 if propagation from rod is absent. **Figure 5.20** shows that the statistical time lag ($t_s$) of the plug (in both $CO_2/O_2$ at $0.2MPa$ and $SF_6$ at $0.2MPa$) is in the range of $10^{-1}$-$10^{-2}s$.

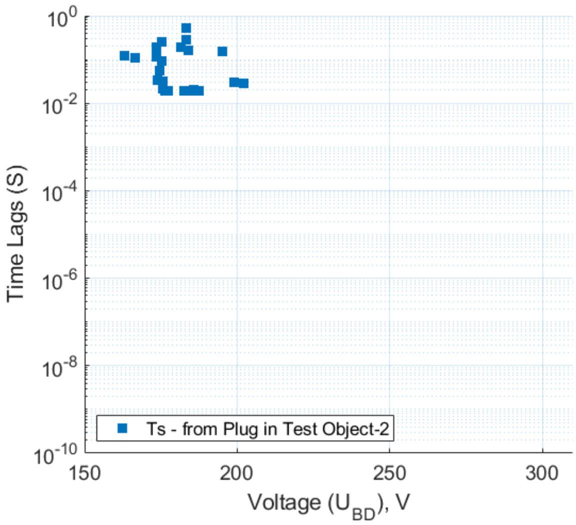


(a) $CO_2/O_2$ at 0.2MPa

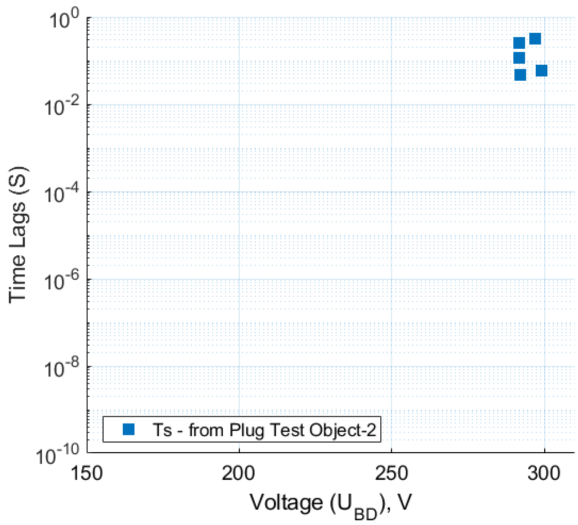


(b) $SF_6$ at 0.2MPa

Figure 5.20: Statistical time lag ($t_s$) recorded from plug in Test setup-2.

The testing of 'SF$_6$ at $0.2MPa$' was very much limited due to high inception voltage(≈$300kV$). Statistical time lag at various voltage ranges couldn't be obtained. This is because maximum voltage that can be generated in the VdG machine at that time was limited to ≈$310kV$.

# 6
# Discussion

The main research question behind this study is whether or not a transient field enhancement caused by propagating streamers or leaders can ignite secondary discharges in another location. We investigated the answer to this question in both $CO_2$ and $SF_6$. In the beginning, a pressure range of $0.2 - 0.6MPa$ was planned for the experiments. Unfortunately, due to test limitations, we were not able to test $0.4MPa$ and $0.6MPa$ cases of all gases. In this chapter, we discuss the results obtained for $CO_2/O_2$ at 0.2MPa and $SF_6$ at $0.2MPa$. Additionally, it discusses other operating conductions by extrapolating the results.

## 6.1. Reduction in statistical time lag($t_s$)

Simultaneous observation of discharges on a scale of few $ns$ strongly indicates or even proofs that these discharges are correlated. Due to this influence the statistical time lags get significantly reduced, see **Figure 6.1**. The correlation of the discharges cannot be due to *UV photons* since they cannot pass the *PTFE* wall. So the only influence is the field enhancement due to the field increase of the rod discharge we reached inception at the plug, i.e. reducing statistical time lag and even leader inception could be seen (for e.g. **Figures 5.14** and **5.15**). However, time was not sufficient to produce a complete bridging of the gap. This is probably also related to the remaining length of the rod discharge to bridge the gap and the leader propagation velocities, which are probably lower for the plug breakdown. Tests with reversed polarity would be interesting to give more insight to this.

A comparison of the results obtained from experiments that determined the inception time lag of the rod in Test object-1 and the plug in Test object-2 is presented. The $blue$ circles in **Figure 6.1** show the main discharge from the rod in Test object-1. In more detail, these data pertain to the statistical time lag ($ts$) plotted against the respective voltage applied. When the voltage exceeded a certain level (marked in $grey$), there were also discharges detected from the plug, within the gate time of the image intensifier, i.e. discharges from the plug which occurred simultaneously to the rod discharge. It is reasonable to attribute these statistical time lag values to secondary discharges from the plug as well. In Test object-2, the $black$ circles are the statistical time lag ($ts$) values for discharges from plugs. As explained in the previous paragraph, this represents how the plug in Test object-1 will behave in the absence of a propagating discharge nearby.

As can be seen in **Figure 6.1**, the statistical time lag of the discharge from the plug has been reduced significantly in both cases ($CO_2/O_2$ at $0.2MPa$ and $SF_6$ at $0.2MPa$). In Test object-2, it shows that the $ts$ of the plug is in the range of $10^{-1} - 10^{-2}s$, whereas it has reduced to the range of $10^{-5} - 10^{-7}s$ in presence of discharge from the rod.

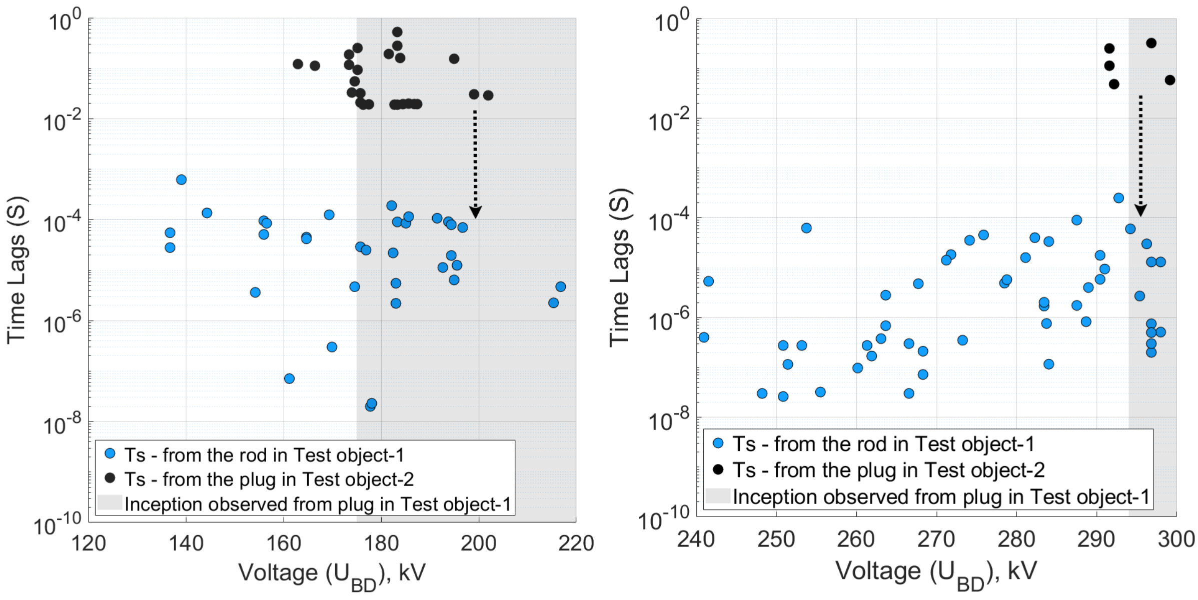


(a) $CO_2/O_2$ at 0.2MPa (b) $SF_6$ at 0.2MPa

Figure 6.1: Statistical time lag ($t_s$) recorded from plug in Test setup-2 in comparison with that obtained from the primary discharge event from the rod in Test setup-1. In Test object -1, in the $grey$ highlighted region, secondary discharges from the plug were also observed and hence this $t_s$ can me assumed to be equal to that of plug as well.

However, it is also important to note that the statistics obtained for tests in Test object-2 were limited. It happened because the VdG test set had a maximum test voltage for application. In $SF_6$ at $0.2MPa$, the inception voltage was $290kV$, and we could only increase the voltage by a few $kV$'s until we reached the maximum test voltage. In the case of $CO_2/O_2$ at $0.2MPa$, inception voltage for discharge from the plug couldn't be obtained due to inception of discharges from other areas.

## 6.2. First electron calculation

The plug is at negative polarity. The surface of an electrode is assumed to deliver the start electron at negative polarity. The *Fowler-Nordheim equation*[50, 53], which gives the rate of electron emission from a surface exposed to an electric field due to tunneling of electrons out of the surface. The negative polarity discharge is then associated with statistical time lags $t_s$ given by **Equation.6.1**.

$$t_s = \left[A_{eff}.10^{\frac{4.52}{\sqrt{\Phi}}}.(1.54).10^{-6}.\frac{(\beta.E_b)}{\Phi}.\exp\left(-\frac{\Phi^{1.5}.2.84.10^9}{\beta.E_b}\right)/e\right]^{-1} \quad [s] \tag{6.1}$$

where $\Phi \approx 4.5eV$ is the work function for steel, $e$ the elementary charge, $\beta$=$(2+l/r).\beta2$, is the field enhancement factor at the protrusion tip, while $\beta2$ is the field enhancement factor due to micro surface roughness. $A_{eff}$ the effective electron emitting area.

Using **Equation 6.1**, statistical time lags from the plug can be analytically estimated and fit with experimental values. MATLAB scripts based on above equation is used to calculated the time to first electron and the the result is plotted together with experimental values in **Figure 6.2** & **6.3**. For $SF_6$ values for $\beta2$ and $A_{eff}$ were taken from the fits in[53] with and using $\beta2$ =30 and $A_{eff}$ = $10^{-16}m^2$ . In the case $ts$ of the plug without field enhancement, a maximum field of $70V/m$ (when $1V$ appled) is used in the calculation. In the case the plug with field enhancement, a maximum field of $138V/m$ (when $1V$ appled) is used. Both these values are obtained from field calculations given in **Figure 5.3**.

The rod, since it is under positive field stress, generates its first electron in front of the field enhanced electrode. Electrons provided by the inter-electrode gas space are mainly detached electrons from negative ions. Collision field detachment is strongly field-dependently for negative ions. A determination of the electron production rate ($\dot{N}_e$) is made by multiplying the detachment rate coefficient $k_d$ by the concentration of negative ions $\bar{n}$ and dividing it by the time and volume of electron detachment[53, 54].

$$\begin{aligned} \dot{N}_e &= k_d.\bar{n} \quad [1/s] \\ t_s &= \dot{N}_e^{\,-1} \quad [s] \end{aligned} \tag{6.2}$$

The size of the critical volume and the electron production rate within the critical volume determines the statistical time lag at positive polarity. As well as, the streamer inception need to be fulfilled in such critical volume. The values of all quantities are dependent on the distribution of electric fields, and thus the electrode arrangement[53]. MATLAB scripts based on above equations are used to calculate the statistical time lag for the rod for both $CO_2/O_2$ at $0.2MPa$ and $SF_6$ at $0.2MPa$.

$CO_2$ was studied using the same approach and models as $SF_6$, but with $CO_2$ specific adaptations for some of the relevant parameters. This was necessary since only little information is so far available for CO2. It includes the field-dependent electron detachment rate and the equilibrium negative ion concentration. The parameters in the *Fowler-Nordheim* equation were adapted in agreement with experimental data from [53]. The field enhancement parameter $\beta2$ in **Equation 6.1** was set to $50$ and the $A_{eff}$ to $10^{-24}m^2$. The small value of $A_{eff}$ is nonphysical and must be seen as a fit parameter to obtain good agreement with measurements in [50, 53].For positive polarity, the best agreement was achieved empirically using equilibrium concentrations of $10^4\ ions/m^3$ at $0.1MPa$, according to [16], as well as field dependence of the electron detachment rate coefficient of $\delta$, as given in **Equation 6.3**. The critical electric field of $CO_2$ at pressure $p$ is $E_{cr}$ = $p.(E/p)_{cr,0}$ with $(E/p)_{cr,0}$ = $21.5V/(m.Pa)$[53].

$$\delta = 10.\left(\frac{E}{E_{cr}}\right)^{13} \quad [1/s] \tag{6.3}$$

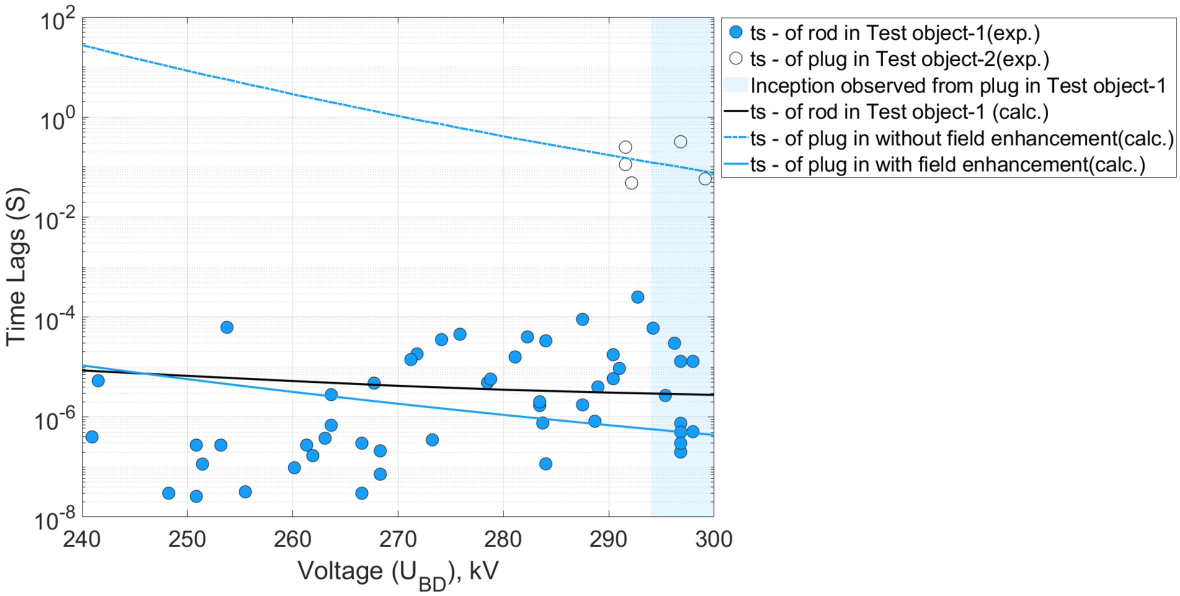


Figure 6.2: Comparison of statistical time lag from plug with and without propagating discharge from the rod at 0.2MPa $SF_6$

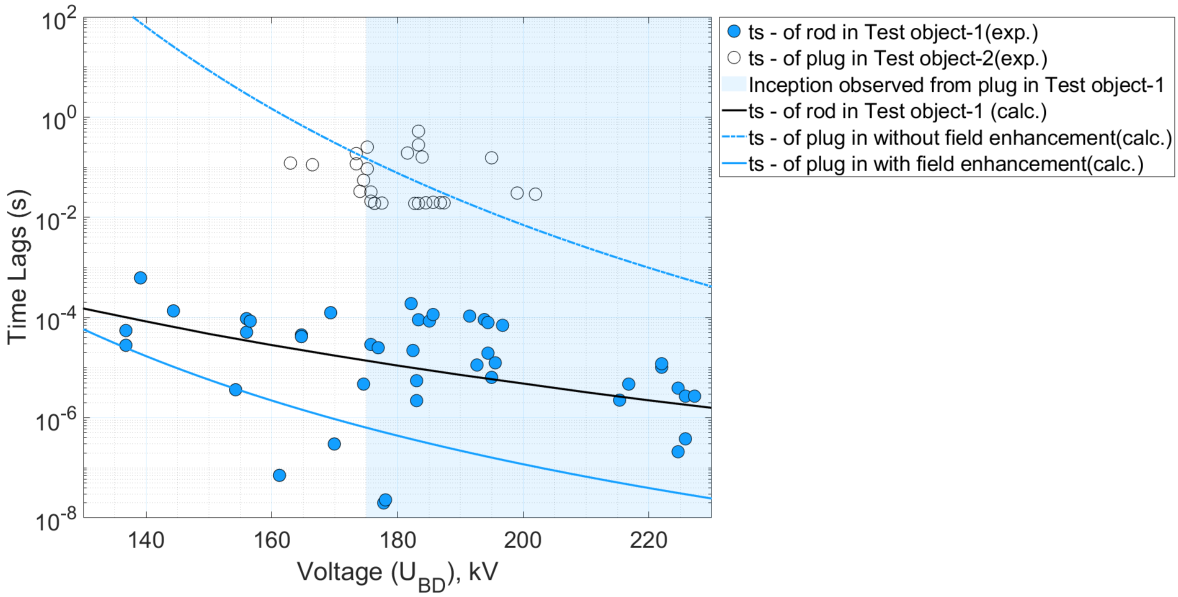


Figure 6.3: Comparison of statistical time lag from plug with and without propagating discharge from the rod at 2 bat $CO_2$

In **Figure 6.2** & **6.3**, the experimental results of the statistical time lag of the plug without field enhancement (*blue dotted line*) are shown with the calculations of **Equa-**

**tion 6.1**. The same parameters are also used to calculate the statistical time lag when the local field at the plug is enhanced (*blue line*) due to the discharge from the plug.

One has to remember that, according to the hypothesis presented in the thesis, the extra field enhancement at the plug exists only for a short duration of time. Because it is caused by a transient field distortion due to the propagating discharge. During this period, the discharge begins from the rod and ends when it reaches the opposite electrode, leading to voltage collapse.The duration of this field enhancement corresponds to the formative time lag of the rod discharge. The plug field enhancement during this period is then, not constant since it is caused by travelling charges. In order to simplify, we assume that there is a constant enhancement during this whole formative period.

$SF_6$ at $0.2MPa$ case is shown in **Figure 6.2**. When the field enhancement occurs at the plug, the statistical time lag for the discharge from the plug has reduced to the same range (or slightly less) as the primary discharge from the rod. Thus, the calculations can explain the higher values without field distortion and the reduction of statistical time lag due to the presence of the rod discharge as well. The formative time lag for this case is shown in **Figure 5.11b**. It from $250ns$ at higher voltages, where we saw secondary discharges, to $550ns$ at lower voltages. When field enhancement is present, the *blue curve* representing the statistical time lag of the plug is already reaching this range, explaining why secondary discharges are observed there.

**Figure 6.3** explains $CO_2$ at $0.2MPa$ case. We can see how statistical time lag has reduced to few nanoseconds at a higher voltage when there is field enhancement (*blue curve*). From **Figure 5.9b**, it is clear that the formative time ling, in this case, is somewhere between a few microseconds at lower voltage and $200ns$ at higher voltages. As shown in **Figure 6.3**, these nanoseconds are sufficient to initiate the inception at the plug when a field enhancement is present. As a result, this explains the cause of secondary discharge inception in this case.

Based on the above observation, we can confirm that our time to first electron model explained the secondary discharge when the plug was stressed with negative polarity.

## 6.3. Influence of surface charge

Since the discharge propagates along the surface of a PTFE plate installed between two electrode tips, it is very likely that surface charges will be deposited on the PTFE. During the optical investigation, many such observations (**Figure 6.4**, for example) were noticed and further examined. Figures shows that charges of same polarity is located only in the area close to the rod, which leads to starting of the discharge away from surface but reattach to the surface later. The majority of such charges were neutralized after the testing object was grounded. This is verified using camera as the neutralizing discharges were recorded in the camera during grounding.

The plug inception was the main focus and there were no traces of surface charge deposition on the plug side. Discharges from the plug side are always interpreted as propagation or attempt to propagate along the PTFE surface.

As (**Figure 6.4** indicates, due to possible restriction of surface charges to the vicinity of the rod, the influence on the plug is field is expected to be low. Also, in the case the field distortion by the charges on the PTFE surface, there be no time correlation of the discharge from the rod and that from the plug. So in the present investigation we can neglect probably the influence of surface charges on the results.

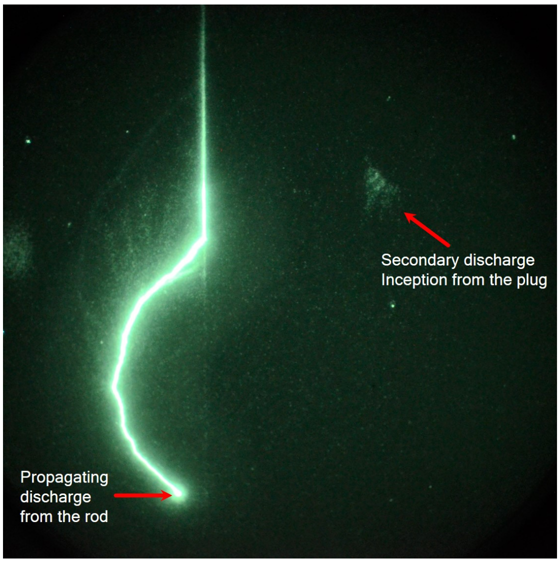


(a) Optical diagnostic results obtained from experiment in Test object-1 when $CO_2/O_2$ was filled at $0.2MPa$. Test voltage applied was $173kV$. The statistical time lag and formative time lag of the discharge from the rod was $t_s = 5.6\mu s$ and $t_f = 570ns$. The captured image shows secondary discharge inception from the plug. The image intensifier gate time was set at $150ns$ with a $150ns$ delay

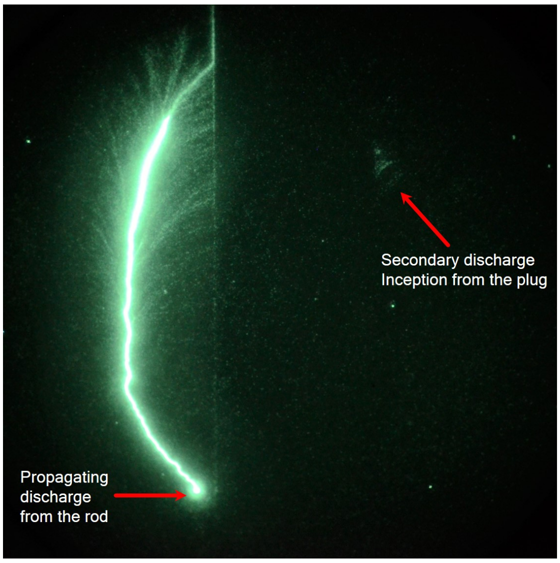


(b) Optical diagnostic results obtained from experiment in Test object-1 when CO2/O2 was filled at $0.2MPa$. Test voltage applied was $175kV$. The statistical time lag and formative time lag of the discharge from the rod was $t_s = 597ns$ and $t_f = 585ns$. The captured image shows possible secondary discharge inception from the plug. The image intensifier gate time was set at $150ns$ with a $150ns$ delay

Figure 6.4: Leader repelling away from the surface of PTFE indicate influence of surface charges in the vicinity of the propagation positive streamer/leader propagation

## 6.4. Recommendations for future research

On the basis of the experience gained from conducting this project, a number of suggestions and recommendations are made to strengthen the research on the same topic in the future.

1. The VdG test injection set used in this experiment is rated only up to $400kV$. In practice, the maximum voltage attainable was limited to some $330kV$. The electrode gap and dimensions of the rod and plug were chosen in the expectation that, we can clearly record the images of the discharges using optical diagnostics. It is highly recommended in future works that, the test injection set and test objects shall are chosen in such a way, the inception test of the plug (or position where secondary discharge is expected) shall be able to do for all pressure range.

2. In this project, the polarity of the plug was set to negative, and that was the only possible configuration at that time with the test injection set. In the case of an

extended version of this project, it is highly recommended that you also conduct experiments with the plug polarity set to positive. It has been established that both polarities behave differently in non-uniform fields, and it will be intriguing to see the experimental evidence for how they behave differently in the case of secondary discharges.

3. Because there are two possible inception sources, it is important to understand each inception separately. Test object-1 in the current project records breakdown information from the rod and the optical image of the discharge detection from plug and rod when it is being tested. An inception voltage is recorded when a discharge is detected optically from both parts. However, the statistical time lag information of the inception from the plug is not recorded. In this project only one PMT is used that focuses to the tip of the rod to set the trigger of the scope. It is recommended to use one more PMT which is focusing towards the tip of the plug simultaneously so that the statistical time lag of the inception from the plug can also be determined. Another option would be to use a high-frequency current transformer (HFCT) to detect discharge current from the plug. An arrangement similar to this can be seen in [55]. Experimentally determined statistical time lags of the plug with and without primary discharge can provide a easy firm conclusion to the research question.

4. It is also recommended that statistical time lags be represented as a distribution function as shown in [52]. Then we can pay extra attention to extremely low probabilities. In order to achieve this, the discharge inception voltages of the plug shall be recorded for sufficient number of attempts in each pressure range so that we can make a distribution out of it.

5. As explained above, inception and statistical time lag of the plug shall be experimentally determined at each pressure range. For this we need sufficient voltage at higher pressures. We could decrease the statistical time lag further by increasing the size of the electrode (plug), then even with short formative time lags from the rod we should be able to see inception from the plug.

# 7 Conclusion

Experiments have primarily been conducted to investigate whether or not secondary discharge inception due to field enhancement caused by streamer or leader propagation is possible in the investigated geometry. At three different pressure ranges, $SF_6$ and $CO_2/O_2$ are selected as the insulation mediums. Practical limitations, however, limited testing to $0.2MPa$ cases.

The experiments using optical diagnostics at $0.2MPa$ in $CO_2/O_2$ and SF6 revealed images of discharge inception from a second location (plug) at negative polarity, triggered by the the discharges from the positive polarity rod. Analyzing the time lag of the discharges from the plug with and without a primary discharge could explain the secondary inception. As a result of a possible additional field enhancement at the plug, the statistical time lag of discharge from the plug appears to have been reduced considerably when a primary discharge is sufficiently close. This could be explained by statistical time lag model as well.

Despite that, it is realized that the extra field enhancement at the plug can exist only for a short time because it is caused by a transient field distortion due to the propagating discharge. As the discharge proceeds toward the opposite electrode, the voltage collapses to zero, leading to the discharge end. It is known as the formative period of the discharge. An examination of the formative time lag recorded during experiments revealed that at low pressures ($0.2MPa$), the formative time lag of the primary discharge is sufficient time to initiate the first electron (statistical time lag) at the plug when it is exposed to the enhanced field. This is the reason for the secondary discharge detection at the plug.

# Bibliography


[1] M. Rabie and C. M. Franck. Assessment of Eco-friendly Gases for Electrical Insulation to Replace the Most Potent Industrial Greenhouse Gas SF6. *Environmental Science & Technology*, 52(2):369–380, 2018. doi: 10.1021/acs.est.7b03465. URL https://doi.org/10.1021/acs.est.7b03465. PMID: 29236468.

[2] M. T. Rodine and R. G. Herb. Effect of CCl4 Vapor on the Dielectric Strength of Air. *Phys. Rev.*, 51:508–511, Mar 1937. doi: 10.1103/PhysRev.51.508. URL https://link.aps.org/doi/10.1103/PhysRev.51.508.

[3] N. R. McCormick and J. D. Craggs. Some measurements of the relative dielectric strength of gases. *British Journal of Applied Physics*, 5(5):171–173, may 1954. doi: 10.1088/0508-3443/5/5/303. URL https://doi.org/10.1088/0508-3443/5/5/303.

[4] J. G. Owens. Greenhouse gas emission reductions through use of a sustainable alternative to SF6. pages 535–538, 2016. doi: 10.1109/EIC.2016.7548658. URL https://10.1109/EIC.2016.7548658.

[5] A. Küchler. High Voltage Engineering Fundamentals-Technology-Applications. *Text book*, pages 141–157, 2011.

[6] J. M. Meek and J. D. Craggs. Electrical breakdown of gases. *Wiley series in Plasma Physics, NY, USA*, 1978. URL https://inis.iaea.org/search/search.aspx?orig_q=RN:10485622.

[7] M. Maiss and C. Brenninkmeijer. Atmospheric SF6: Trends, sources and prospects. *Environmental Science Technology*, 32:3077–3086, 1998. URL https://doi-org.tudelft.idm.oclc.org/10.1021/es9802807.

[8] M Seeger. Perspectives on Research on High Voltage Gas Circuit Breakers. *Plasma Chem Plasma Process*, 1(35):527–541, 2014. URL https://doi-org.tudelft.idm.oclc.org/10.1007/s11090-014-9595-4.

[9] Westinghouse Research and PA (USA) Development Center, Pittsburgh. Gases superior to SF6 for insulation and interruption. Final report. *U.S. Department of Energy Office of Scientific and Technical Information*, (EPRI-EL-2620 ON: DE83900518), 9 1982.

[10] X. Li, H. Zhao, and A. Murphy. SF6-alternative gases for application in Gas-Insulated Switchgear. *Journal of Physics D: Applied Physics*, 51, 03 2018. doi: 10.1088/1361-6463/aab314. URL https://doi.org/10.1088/1361-6463/aab314.

[11] Task Force WG B3.45. Application of non-SF6 gases or gas-mixtures in medium and high voltage Gas-Insulated Switchgear. *TECHNICAL BROCHURE 802*, 1 (1), 2020.

[12] P. Simka, U. Straumann, and C. M. Franck. SF6 high voltage Circuit Breaker contact systems under Lightning Impulse and Very Fast Transient voltage stress. *IEEE Transactions on Dielectrics and Electrical Insulation*, 19(3):855–864, 2012. doi: 10.1109/TDEI.2012.6215088. URL https://doi.org/10.1109/TDEI.2012.6215088.

[13] I. Gallimberti and N. Wiegart. Streamer and leader formation in SF6 and SF6mixtures under positive impulse conditions. II. Streamer to leader transition. *Journal of Physics D: Applied Physics*, 19(12):2363–2379, dec 1986. doi: 10.1088/0022-3727/19/12/016. URL https://doi.org/10.1088/0022-3727/19/12/016.

[14] I. Gallimberti. Breakdown mechanisms in electronegative gases. pages 61–80, 1987. doi: https://doi.org/10.1016/B978-0-08-034693-9.50013-7. URL https://www.sciencedirect.com/science/article/pii/B9780080346939500137.

[15] L. Niemeyer, L. Ullrich, and N. Wiegart. The mechanism of leader breakdown in electronegative gases. *IEEE Transactions on Electrical Insulation*, 24(2):309–324, 1989. doi: 10.1109/14.90289. URL https://doi.org/10.1109/14.90289.

[16] M Seeger, L Niemeyer, and M Bujotzek. Partial discharges and breakdown at protrusions in uniform background fields in SF6. *Journal of Physics D: Applied Physics*, 41(18):185204, aug 2008. doi: 10.1088/0022-3727/41/18/185204. URL https://doi.org/10.1088/0022-3727/41/18/185204.

[17] M Seeger and M Clemen. Partial discharges and breakdown in SF6in the pressure range 25–150 kPa in non-uniform background fields. *Journal of Physics D: Applied Physics*, 47(2):025202, dec 2013. doi: 10.1088/0022-3727/47/2/025202. URL https://doi.org/10.1088/0022-3727/47/2/025202.

[18] M Seeger, L Niemeyer, and M Bujotzek. Leader propagation in uniform background fields in SF6. *Journal of Physics D: Applied Physics*, 42(18):185205, sep 2009. doi: 10.1088/0022-3727/42/18/185205. URL https://doi.org/10.1088/0022-3727/42/18/185205.

[19] M Seeger, J Avaheden, S Pancheshnyi, and T Votteler. Streamer parameters and breakdown in CO2. *Journal of Physics D: Applied Physics*, 50(1):015207, Nov 2016. doi: 10.1088/1361-6463/50/1/015207. URL https://doi.org/10.1088/1361-6463/50/1/015207.

[20] Y. Kieffel, F. Biquez, P. Ponchon, and T. Irwin. SF6 alternative development for high voltage Switchgears. pages 1–5, 2015. doi: 10.1109/PESGM.2015.7286096. URL https://doi.org/10.1109/PESGM.2015.7286096.

[21] D. H. Peng, Z. Y. Li, and J. M. K. MacAlpine. The Combined Effect of Moisture, Temperature and Conducting Particles on the Discharge Behaviour of Sulphur Hexafluoride. *HKIE Transactions*, 8(2):55–57, 2001. doi: 10.1080/1023697X.2001.10667849. URL https://doi.org/10.1080/1023697X.2001.10667849.

[22] P. C. Stoller, M. Seeger, A. A. Iordanidis, and G. V. Naidis. CO2 as an Arc Interruption Medium in Gas Circuit Breakers. *IEEE Transactions on Plasma Science*, 41(8):2359–2369, 2013. doi: 10.1109/TPS.2013.2259183. URL https://doi.org/10.1109/TPS.2013.2259183.

[23] M. Shiiki, M. Sato, M. Hanai, and K. Suzuki. Dielectric Performance of CO2 Gas Compared with N2 Gas. pages 365–370, 2001. doi: 10.1007/978-1-4615-0583-9_51. URL https://doi.org/10.1007/978-1-4615-0583-9_51.

[24] D. R. Young. Electric breakdown in co2 from low pressures to the liquid state. *Journal of Applied Physics*, 21(3):222–231, 1950. doi: 10.1063/1.1699638. URL https://doi.org/10.1063/1.1699638.

[25] K. P Brand and J. Kopainsky. Breakdown field strength of unitary attaching gases and gas mixtures. *Applied physics*, 18(4):321–333, 1979. URL https://doi-org.tudelft.idm.oclc.org/10.1007/BF00899684.

[26] T. Uchii, Y. Hoshina, T. Mori, H. Kawano, T. Nakamoto, and H. Mizoguchi. Investigations on sf6-free gas circuit breaker adopting co2 gas as an alternative arc-quenching and insulating medium. pages 205–210, 2004. doi: 10.1007/978-1-4419-8979-6_28. URL https://doi.org/10.1007/978-1-4419-8979-6_28.

[27] E. Kynast and K. Juhre. *N2 and N2/CO2 Mixture in Gas Insulated Compartments under High Pressure*, pages 211–216. Springer US, Boston, MA, 2004. ISBN 978-1-4419-8979-6. doi: 10.1007/978-1-4419-8979-6_29. URL https://doi.org/10.1007/978-1-4419-8979-6_29.

[28] S. Meijer, J.J. Smit, and A. Girodet. Comparison of the Breakdown Strength of N2, CO2 and SF6 using the Extended Up-and-Down Method. In *2006 IEEE 8th International Conference on Properties applications of Dielectric Materials*, pages 653–656, 2006. doi: 10.1109/ICPADM.2006.284262. URL https://doi.org/10.1109/ICPADM.2006.284262.

[29] T. Liu, I. V. Timoshkin, S. J. MacGregor, M. P. Wilson, M. J. Given, N. Bonifaci, and R. Hanna. Field-Time Breakdown Characteristics of Air, N2, CO2, and SF6. *IEEE Transactions on Plasma Science*, 48(10):3321–3331, 2020. doi: 10.1109/TPS.2020.2991860. URL https://doi.org/10.1109/TPS.2020.2991860.

[30] M. Seeger, T. Votteler, J. Ekeberg, S. Pancheshnyi, and L. Sánchez. Streamer and leader breakdown in Air at atmospheric pressure in strongly non-uniform fields in gaps less than one metre. *IEEE Transactions on Dielectrics and Electrical*

*Insulation*, 25(6):2147–2156, 2018. doi: 10.1109/TDEI.2018.007246. URL http://doi.org/10.1109/TDEI.2018.007246.

[31] M. Seeger, P. Stoller, and A. Garyfallos. Breakdown fields in synthetic air, CO2, CO2/O2 mixture, and CF4 in the pressure range 0.5–10 MPa. *IEEE Transactions on Dielectrics and Electrical Insulation*, 24(3):1582–1591, 2017. doi: 10.1109/TDEI.2017.006517. URL https://doi.org/10.1109/TDEI.2017.006517.

[32] S. Kumar, T. Huiskamp, A. J. M. Pemen, M. Seeger, J. Pachin, and C. M. Franck. Breakdown Study in CO2 and CO2/O2 Mixtures in AC, DC and Pulsed Electric Fields at 0.1–1 MPa Pressure. *IEEE Transactions on Dielectrics and Electrical Insulation*, 28(1):158–166, 2021. doi: 10.1109/TDEI.2020.009115. URL https://doi.org/10.1109/TDEI.2020.009115.

[33] V. Cooray. An Introduction to Lightning. *Text book*, 2014.

[34] H. Raether. Electron avalanches and breakdown in gases. *Text book*, 1964.

[35] E. Marode, F. Bastien, and M. Bakker. A model of the streamer□induced spark formation based on neutral dynamics. *Journal of Applied Physics*, 50(1):140–146, 1979. doi: 10.1063/1.325697. URL https://doi.org/10.1063/1.325697.

[36] M. S. Bhalla and J. D. Craggs. Measurement of Ionization and Attachment Coefficients in Carbon Dioxide in Uniform Fields, journal = Proceedings of the Physical Society. 76(3):369–377, sep 1960. doi: 10.1088/0370-1328/76/3/307. URL https://doi.org/10.1088/0370-1328/76/3/307.

[37] T. Uchii, Y. Hoshina, H. Kawano, K. Suzuki, T. Nakamoto, and M. Toyoda. Fundamental research on SF6-free gas insulated switchgear adopting CO2 gas and its mixtures. *ISETS07*, 2007. URL http://www-eng.lbl.gov/~shuman/NEXT/MATERIALS&COMPONENTS/HV/1333Uchii.pdf.

[38] W. Wang and A. Bogaerts. Effective ionisation coefficients and critical breakdown electric field of CO2at elevated temperature: effect of excited states and ion kinetics. *Plasma Sources Science and Technology*, 25(5):055025, sep 2016. doi: 10.1088/0963-0252/25/5/055025. URL https://doi.org/10.1088/0963-0252/25/5/055025.

[39] R. Arora and W. Mosch. *High Voltage and Electrical Insulation Engineering*, volume 69. John Wiley and Sons, 2011.

[40] R. J. Van de Graaff. A 1,500,000 Volt Electrostatic Generator. *Phys. Rev*, 38:1919, 1931. URL http://web.ihep.su/dbserv/compas/src/van%20de%20graaff31/eng.pdf.

[41] J. G. Trump, F. H. Merrill, and F. J. Safford. Van de Graaff Generator for General Laboratory Use. *Review of Scientific Instruments*, 9(12):398–403, 1938. doi: 10.1063/1.1752376. URL https://doi.org/10.1063/1.1752376.

[42] Hamamatsu Photonics K. K. Photomultiplier tubes; Basics and applications. *PMT Handbook by HAMAMATSU*, 3(1):13–21, 2007. URL https://www.hamamatsu.com/eu/en/product/optical-sensors/pmt/index.html.

[43] W. S. Zaengl and K. Petcharaks. Application of Streamer Breakdown Criterion for In-homogeneous Fields in Dry Air and SF6. *Gaseous Dielectrics VII*, pages 153–159, 1994. doi: 10.1007/978-1-4899-1295-4_28. URL https://doi.org/10.1007/978-1-4899-1295-4_28.

[44] R. Morrow. Properties of streamers and streamer channels in SF6. *Phys. Rev. A*, 35:1778–1785, Feb 1987. doi: 10.1103/PhysRevA.35.1778. URL https://link.aps.org/doi/10.1103/PhysRevA.35.1778.

[45] M Seeger, M Schwinne, R Bini, N Mahdizadeh, and T Votteler. Dielectric recovery in a high-voltage circuit breaker in SF6. *Journal of Physics D: Applied Physics*, 45(39):395204, sep 2012. doi: 10.1088/0022-3727/45/39/395204. URL https://doi.org/10.1088/0022-3727/45/39/395204.

[46] B. W. Turnbull. Nonparametric Estimation of a Survivorship Function with Doubly Censored Data. *Journal of the American Statistical Association*, 69(345):169–173, 1974. URL http://www.jstor.org/stable/2285518.

[47] S. R. Giolo. Turnbull's Non-parametric Estimator for Interval-Censored Data. *Department of Statistics, Federal University of Parana, Technical Report*, 2004. doi: 10.13140/RG.2.1.4034.8648. URL http://doi.org/10.13140/RG.2.1.4034.8648.

[48] T. Kiyan, T. Ihara, S. Kameda, T. Furusato, M. Hara, and H. Akiyama. Weibull Statistical Analysis of Pulsed Breakdown Voltages in High-Pressure Carbon Dioxide Including Supercritical Phase. *IEEE Transactions on Plasma Science*, 39(8):1729–1735, 2011. doi: 10.1109/TPS.2011.2159135. URL https://doi.org/10.1109/TPS.2011.2159135.

[49] M. Finkel, W. Boeck, and E. Kynast. Statistical determination of minimum breakdown voltage for GIL and GIS. 1:401–404 vol.1, 2000. doi: 10.1109/CEIDP.2000.885310. URL https://doi.org/10.1109/CEIDP.2000.885310.

[50] C. Feet, O, M. Seeger, D. Over, K. Niayesh, and F. Mauseth. Breakdown at Multiple Protrusions in SF6 and CO2. *Energies*, 13(17), 2020. ISSN 1996-1073. URL https://www.mdpi.com/1996-1073/13/17/4449.

[51] I. Pobočíková and Z. Sedliačková. Comparison of four methods for estimating the Weibull distribution parameters. *Applied Mathematical Sciences*, 8 (83):4137–4149, 2014. URL http://www.m-hikari.com/ams/ams-2014/ams-81-84-2014/sedliackovaAMS81-84-2014.pdf.

[52] N. Wiegart, L. Niemeyer, F. Pinnekamp, W. Boeck, J. Kindersberger, R. Morrow, W. Zaengl, M. Zwicky, I. Gallimberti, and S.A. Boggs. In-homogeneous field breakdown in GIS; the prediction of breakdown probabilities and voltages. II. Ion

density and statistical time lag. *IEEE Transactions on Power Delivery*, 3(3):931–938, 1988. doi: 10.1109/61.193870. URL https://doi.org/10.1109/61.193870.

[53] M. Bujotzek and M. Seeger. Parameter dependence of gaseous insulation in SF6. *IEEE Transactions on Dielectrics and Electrical Insulation*, 20(3):845–855, 2013. doi: 10.1109/TDEI.2013.6518954. URL https://doi.org/10.1109/TDEI.2013.6518954.

[54] X. Xu, S. Jayaram, and S.A. Boggs. Prediction of breakdown in SF6 under impulse conditions. pages 149–152, 1995. doi: 10.1109/CEIDP.1995.483598. URL https://doi.org/10.1109/CEIDP.1995.483598.

[55] N. Hayakawa, K. Hatta, S. Okabe, and H. Okubo. Streamer and leader discharge propagation characteristics leading to breakdown in electronegative gases. *IEEE Transactions on Dielectrics and Electrical Insulation*, 13(4):842–849, 2006. doi: 10.1109/TDEI.2006.1667744. URL https://doi.org/10.1109/TDEI.2006.1667744.